
Theoretical and Experimental Study of Flow-Control Devices for Inlets of Indraft Wind Tunnels

James C. Ross

September 1989

(NASA-TM-100050) THEORETICAL AND
EXPERIMENTAL STUDY OF FLOW-CONTROL DEVICES
FOR INLETS OF INDRAFT WIND TUNNELS (NASA)
74 p CSCL 148

N90-21778

Unclas

G3/09 0279954



National Aeronautics and
Space Administration



Theoretical and Experimental Study of Flow-Control Devices for Inlets of Indraft Wind Tunnels

James C. Ross, Ames Research Center, Moffett Field, California

September 1989

NASA

National Aeronautics and
Space Administration

Ames Research Center
Moffett Field, California 94035

TABLE OF CONTENTS

	<u>Page</u>
NOMENCLATURE.....	v
SUMMARY.....	vii
CHAPTER 1. INTRODUCTION.....	1
Review of Previous Work.....	1
Problem Statement.....	4
CHAPTER 2. TWO-DIMENSIONAL SCREEN/INLET EXPERIMENT.....	5
Experimental Apparatus.....	5
Inlet geometry definition.....	5
Tunnel description.....	6
Experimental Results.....	10
Flow separation.....	10
Test section flow uniformity.....	10
CHAPTER 3. SCREEN ANALYSIS METHOD.....	16
Computational Method.....	16
Governing equations.....	16
Finite difference representation.....	20
Boundary conditions.....	21
Determination of total pressure.....	21
Actuator disk model.....	21
Computational grid.....	23
Solution procedure.....	23
Code Verification.....	25
CHAPTER 4. PARAMETRIC STUDY OF SCREEN EFFECTS.....	31
Effect of Screen Loss Coefficient.....	31
Variable Loss Coefficient.....	34
Geometric Variations.....	38
Contraction ratio.....	38
Constant width duct.....	39
Match point.....	43
Contraction length.....	43
CHAPTER 5. INLET CASCADE.....	45
Cascade Analysis.....	46
Potential flow cascade calculation.....	47
Total pressure determination.....	47
Simulation of screen turning.....	48
Effect of Kutta condition.....	49
Sample calculations.....	50
Inlet Cascade Experiment.....	52

	<u>Page</u>
Comparison of Predictions and Experiment.....	54
Extension to Three-Dimensions.....	59
CHAPTER 6. CONCLUDING REMARKS	60
REFERENCES	62
APPENDIX A: DESCRIPTION OF DATA ACQUISITION SYSTEM	66

NOMENCLATURE

A_1, A_2, A_3	metrics of coordinate transformation from physical plane to computational plane.
c	contraction ratio, w_i/w_e .
C_p	static pressure coefficient, $C_p = \frac{p - p_{ts}}{q_{CL}}$.
d	screen wire diameter.
D	drag force acting on a screen.
j	index associated with grid stations in the x- (or ξ -) direction.
J	Jacobian of coordinate transformation from physical plane to computational plane.
k	index associated with grid levels in the y- (or η -) direction.
k_o	pressure loss coefficient of a screen for normal incident flow, $k_o = D/q$.
k_θ	pressure loss coefficient of a screen for incident flow at angle θ relative to the screen normal.
L	length of contracting section of inlet.
L_d	length of constant width upstream duct.
p	static pressure.
p_o	total pressure.
p_{ts}	reference static pressure, wall static pressure in test section.
q	dynamic pressure, $q = 1/2 \rho V^2 = p_o - p$.
q_{CL}	reference dynamic pressure, dynamic pressure at centerline of test section.
Re_β	modified Reynolds number, $Re_\beta = \frac{dV}{\beta \nu}$.
u	x-component of velocity.
v	y-component of velocity.
\bar{V}	velocity vector, $[u, v]$.
V	magnitude of the velocity, $\sqrt{u^2 + v^2}$.

w	width of duct.
x	physical coordinate in direction of tunnel axis.
x_m	x-location of the match point of the two cubic curves defining the contraction shape measured from the start of the contraction.
x_s	x-location of the screen in the upstream duct measured from the upstream end of the duct.
y	physical coordinate perpendicular to tunnel axis.
β	porosity of a screen, ratio of open area to total area.
∂	differential operator.
∇	del operator.
θ	flow onset angle relative to screen normal.
ϕ	flow exit angle from screen relative to downstream normal.
ν	kinematic viscosity of the fluid.
ρ	fluid density.
Ψ	stream function.
ω	vorticity, $\omega = \nabla \times \bar{V}$.
ξ	streamwise coordinate in computational domain.
η	transverse coordinate in computational domain.

subscripts:

ts	test section.
i	inlet or start of contracting section.
e	exit of contraction.
CL	wind tunnel centerline.
1	upstream of screen.
2	downstream of screen.
x, y, ξ , η	derivative with respect to the variable.

SUMMARY

The design of closed-circuit wind tunnels has historically been performed using "rules of thumb" which have evolved over the years into a body of useful guidelines. The development of indraft wind tunnels however, has not been as well documented. The design of indraft wind tunnels is therefore generally performed using a more intuitive approach, often resulting in a facility with disappointing performance. The primary problem is a lack of understanding of the flow in the inlet as it passes through the required anti-turbulence treatment. For wind tunnels which employ large-contraction-ratio inlets, this lack of understanding is not serious since the relatively low velocity of the flow through the inlet treatment reduces the sensitivity of the flow to improper inlet design. Unfortunately, large contraction ratio inlets are expensive and often violate budgetary and size constraints for new facilities, particularly when a large test section is desired. A large body of literature concerning the performance of various flow control devices to reduce test-section turbulence is available. The influence of these devices on the test-section flow uniformity, however, has not received any detailed study. The effect is particularly strong for short, low-contraction ratio inlets. The present study was undertaken to examine the effect of anti-turbulence devices on test-section velocity uniformity and to find ways of designing low-contraction ratio inlets with antiturbulence treatments which produce uniform test-section flow. The most common antiturbulence treatment is a set of screens located at the front of the inlet. Therefore, a two-dimensional analysis method capable of predicting the effect of such screens on the test-section flow uniformity was developed. The analysis showed that screen turning plays a large role in modifying the inlet flow distribution. The amount of turning is determined by the pressure drop of the screen, the angle of onset, and the velocity variation of the flow passing through the screen. Further analyses were performed to examine the effect of geometric variations on the test-section flow uniformity. The test-section flow distribution provided by a given inlet geometry and screen combination can be accurately calculated using the computational method, however, designing a small inlet for uniform flow is still a formidable problem because of the strong interaction between the inlet geometry and the screen characteristics. A more straightforward design approach was therefore examined in which a cascade was placed in the inlet to provide a more controllable mechanism for flow redistribution. By properly tailoring the angles of the individual vanes, uniform test-section velocity can be obtained. An analysis method based on existing potential flow methods and an empirical screen pressure drop calculation was developed to demonstrate the utility of the inlet cascade. Descriptions of both the screen and cascade analysis methods are presented. The accuracy of the computations was demonstrated using experimental data from tests of a two-dimensional indraft wind tunnel. The predictions are in very good agreement with the experimental data in all cases. Extension of the results for the inlet cascade to three-dimensions is demonstrated and a successful wind tunnel design is presented.



CHAPTER 1. INTRODUCTION

Review of Previous Work

The design of closed-circuit wind tunnels has historically been performed using "rules of thumb" which have evolved over the years into a body of useful guidelines (refs. 1-3). The development of indraft wind tunnels, however, has not been as well documented. The design of indraft wind tunnels is therefore performed using a more intuitive approach, which can result in a facility with disappointing performance. This is particularly true of large wind tunnels which are often affected by a lack of sufficient space and/or funds required to construct a high-performance tunnel using conservative design rules. The result of this conflict is usually a facility which does not produce the desired flow quality. Expensive retrofitted modifications may then be necessary to make the tunnel useful. Indraft wind tunnels are notorious for this type of design fault, some of which have been reported in the literature (refs. 4-6).

The required flow quality of a wind tunnel is strongly dependent on the type of testing which will be performed in it. In general, the test-section flow must have uniform velocity, small flow angularity, and low turbulence. Quantitative limits for these parameters vary widely for the various types of testing performed in wind tunnels. For studying natural laminar flow, for example, the turbulence intensity and flow angle variations must be kept as small as possible so as not to prematurely trip the boundary layer (rms turbulence intensity $< 0.05\%$). In contrast, large-scale testing of configurations over which the boundary layer is predominantly turbulent does not require the same restriction on turbulence intensity. In nearly all types of testing, however, the spatial variation of the test-section velocity should be as small as possible. The present research was directed at this particular problem; development of short, low-contraction ratio inlet designs which can provide uniform test-section velocity in low-speed, indraft wind tunnels.

A general description of the traditional design philosophy of both indraft wind tunnel inlets and the contraction section of closed-return wind tunnels is a good introduction to the inlet design problem. An important function of a contracting section in a wind tunnel is to reduce the power consumption of the flow conditioning devices. Flow conditioning devices such as screens and honeycombs are placed upstream of the contraction in a region of low velocity. The drag of these devices varies with the square of the velocity of the flow passing through them. Increasing the contraction ratio reduces the velocity of the flow through the screen. A large contraction ratio is therefore desirable to reduce the power required (or increase the attainable test-section velocity). The contraction also reduces the relative magnitudes of the mean and fluctuating velocity variations compared to the average test-section velocity. The amount of reduction as a function of contraction ratio, c (defined as the ratio of the inlet area to exit area of the contraction) summarized by Mehta and Bradshaw (ref. 2) from Batchelor (ref. 7) are:

spacial variations in axial velocity: $\frac{1}{c^2}$

axial component of rms turbulence intensity: $\frac{\sqrt{3(\ln 4c^3 - 1)}}{2c^2}$

transverse component of rms turbulence intensity: $\sqrt{\frac{3}{4c}}$

The reduction factors presented were derived using a linearized theory in which the contraction takes place over an infinitesimal distance which clearly does not occur in practical wind tunnels. Nevertheless, the

trends given by these expressions are in agreement with the observed flow quality in wind tunnels. Increasing the contraction ratio then improves the test-section flow quality. Care must be taken, however, in designing a nozzle with a large contraction ratio so as to avoid boundary layer separation at both the inlet and exit planes of the contracting section.

A large number of reports have been presented which address the particular problem of contraction design. The earlier works made use of hodograph methods in which a velocity distribution along the wall or centerline of the contraction is specified and the wall shape required to attain that distribution is solved for (refs. 8-13). The utility of these methods is limited in that the resulting contractions must be infinitely long. A novel approach is presented by Rouse and Hassan (ref. 14) in which an electrical analogy is used to obtain the potential field for specific inlet shapes. In their work, an electric potential field is generated by proper placement of electrodes on an insulating table to simulate the velocity potential of a contraction. This approach had limited practical application because of the complexity of setting up the inlet geometry.

The first truly useful work on the subject is that of Morel (refs. 15, 16). In these reports, design charts are presented for a family of contraction shapes which relate the geometry of the contraction to such features of the flow field as wall pressure gradients and flow uniformity at the inlet and exit of the nozzle. A finite difference solution of the Laplace equation for the given wall shapes was obtained for both two-dimensional (2-D) and axisymmetric contractions. The wall shapes examined were obtained from two cubic curves joined at the so called match point. Using this family of curves the effects of contraction ratio, contraction length, and match point location were examined individually. The turbulent Stratford (ref. 17) separation criterion was used to define limits on the amount of flow nonuniformity at both the inlet and exit which can be tolerated. By just avoiding separation at both ends of the contraction, Morel maintains, the minimum exit boundary layer thickness is obtained. Whether or not this is the case, the reports provided useful design information for contraction shapes.

It is apparent from the results of Morel (refs. 15, 16) that separation is most easily avoided by using a long contraction. Several reports can be found in the literature which address the "optimum" solution to the contraction problem. In the reports of Chmielewski (ref. 18), Borger (ref. 19), and Mikhail (ref. 20), the optimum contraction is defined as the one which provides the required flow quality with minimum length. The desired flow quality determines the required contraction ratio. The minimum length contraction which does not exhibit flow separation is then optimum. These three works are very similar in that a potential flow solution is obtained for a given contraction which is subsequently used in either a Stratford separation prediction (ref. 18) or in an integral boundary layer calculation (refs. 19, 20). Different families of wall shapes are used in the three reports so the results cannot be directly compared but minimum contraction lengths are defined for the different shapes and the analyses are in good agreement with the experimental results presented.

In all of the work described, the contractions examined were axisymmetric or 2-D. Most wind tunnels, however, have contractions which are three-dimensional (3-D). Downie et al. (ref. 21) presented 3-D solutions to the Laplace equation for contractions with square cross-section. No boundary-layer calculations were performed in this work but the parametric variations of the inlet geometry reported indicate that contractions with large maximum slope provide more uniform inlet and exit velocity profiles than those with shallower maximum slope.

With the exception of the work by Rouse and Hassan (ref. 14), all of the work described previously have addressed only the contraction problem as it relates to closed-return wind tunnels. That is, the analyses were all for contracting ducts. The flow into an inlet is somewhat more complicated and has not been examined in much detail, at least for wind tunnel applications. Batill and Hoffmann (ref. 22) and

Batill et al. (ref. 23) present a 3-D solution to the inlet problem using a finite difference solution to Laplace's equation. Preliminary design charts are presented to show the effects of contraction ratio, contraction length, and match point on the flow uniformity at the inlet and exit. While these results are interesting, the grid generation problem prevents the accurate modelling of the large cowls which are invariably present on wind-tunnel inlets to reduce the tendency for the flow to separate which would occur if only the sharp edge of the contraction were present. Panel codes which model potential flow using superposition of sources and doublets should be capable of accurately calculating inlet flow in the absence of flow separation. Complex geometries are easier to simulate using panel codes since only surface points must be specified rather than points throughout the flow field (refs. 24-26). Batill and Hoffmann (ref. 22) found that unsatisfactory results are obtained when the surface is represented by use of source singularities alone. This was attributed to the "leakage" allowed by the calculation. Leakage is caused by the fact that the flow tangency condition is enforced only at the control points of the panels. Fluid is not prevented from passing through the panels at other points. Leakage greater than 5% of the volume flow rate through the tunnel in the calculation is sufficient to invalidate a solution.

Results of a more advanced panel method, VSAERO (ref. 26), are presented by Ross et al. (ref. 4). This method uses source and doublet panels to represent the surface and imposes different boundary conditions resulting in much lower leakage (on the order of 1-2%). Very good agreement with experimental data for the flow into a rectangular indraft wind tunnel was obtained. Both the wall pressure distribution and velocity distribution at the inlet were accurately calculated. The boundary-layer development along surface streamlines was calculated using an integral, 2-D method. The estimated separation lines determined from the calculations are in good agreement with the observed separation in the experiment.

The mean flow characteristics of indraft wind tunnel inlets can be accurately predicted, in the absence of separated flow, using existing computational methods (refs. 4, 22-27). Unfortunately, real wind tunnels operate in a much more hostile environment than can be simulated by the inviscid, steady analyses presented to date. In many instances, indraft wind tunnels are located outdoors so that they must operate in the presence of atmospheric winds. These winds can be steady or very gusty and can also generate thick boundary layers. The inlet must be able to isolate the test section from the effects of wind under as many conditions as possible. Even for tunnels located indoors, the exhaust of the fan can induce unsteady flow around the tunnel which, again, must be conditioned by the inlet to provide good test-section flow quality.

A good deal of research has been performed with the goal of reducing the effect of external flow conditions on the test-section flow quality of indraft wind tunnels (refs. 5, 6, 28-33). Nonetheless, many of the facilities built as a result of these studies required modifications to meet the flow quality goals (refs. 4-6, 28). These modifications ranged from the simple addition more screens (ref. 5) to constructing elaborate isolation devices upstream of the inlet (ref. 28). One of the more imaginative proposals was to use a grove of large trees planted surrounding the inlet to isolate a large facility from the wind (ref. 29). This aesthetically pleasing approach has, unfortunately, never been implemented.

Many of the design rules developed for closed-return tunnels should also apply to indraft facilities. In particular, large contraction ratio inlets have been shown to provide very steady and uniform test-section flow when several screens are placed in the inlet (ref. 33). Transverse external velocities are typically attenuated using honeycomb. This high-loss approach works very well for small facilities where space is not a major concern. For the large facilities (refs. 4-6, 28-31) the inlet must often be made smaller than would be desired from a strictly aerodynamic standpoint to fit into the available space.

A small-contraction-ratio inlet has been shown to generate more flow nonuniformity at both the entrance and exit planes than does a larger contraction-ratio inlet of the same length to diameter ratio (refs. 15, 16). If the wind isolation devices (i.e., screens and/or honeycomb) are placed in this nonuniform flow the result is a large velocity variation in the test section. The velocity variation is caused simply by the pressure drop experienced by the flow passing through the treatment. The pressure drop through a screen or honeycomb depends primarily on the local dynamic pressure of the flow (ref. 34). Since the dynamic pressure is proportional to the square of the velocity, a nonuniform velocity distribution passing through a screen results in a large variation in the total pressure downstream of the screen. This total pressure distribution is convected downstream to the test section since there is no mechanism for further changes in total pressure. The static pressure is constant in the test section once the streamlines are aligned with the tunnel axis. The result is a variation in the test-section dynamic pressure, equal in magnitude to the total pressure variation just downstream of the screen. For this reason most modifications to existing facilities are in the form of high-loss devices located as far upstream of the inlet as possible (e.g., refs. 6, 28-30).

Problem Statement

If the wind isolation devices could be placed in a short inlet without generating large velocity gradients in the test section, the overall size of the facility could be reduced. To design such an inlet, the behavior of the nonuniform velocity field generated by a wind-tunnel inlet, passing through a screen must be better understood. To this end, an experimental study of the effect of inlet screens on the test-section velocity distribution of a 2-D indraft wind tunnel was performed. The effect of the number of screens in the inlet was the primary focus of the experiment. The experimental apparatus and results are presented in Chapter 2. A computational method capable of predicting this type of flow in 2-D was also developed to further study the problem. Details of the analysis method are presented in Chapter 3. Comparisons with the experimental results are also presented. The computational method was used to perform parametric variations of inlet geometry and screen loss coefficient. The results of those calculations provide some insight as to the interaction of the inlet geometry and screen characteristics and the resulting flow distributions. These results are summarized in Chapter 4.

The understanding gained in performing the study of the flow into inlets with screens resulted in the development of the concept of the inlet cascade (ref. 4). In this inlet design, a set of vanes is located immediately upstream of the anti-turbulence screens. The individual vanes in the cascade are adjusted so that the resulting test-section flow has uniform velocity. This inlet design proved to be very effective in the model tests described in references 4, 35, and 36. A prediction method was developed which could be used to determine the required vane angles without extensive model testing. The details of the prediction method are presented in Chapter 5. Once again, experimental data were obtained to validate the prediction method and to demonstrate the effectiveness of the cascade. The experimental data and comparisons with the calculated results are given in Chapter 6. The dissertation concludes with a discussion of the applicability of the prediction methods to other problems and with a description of a simple extension to 3-D.

CHAPTER 2. TWO-DIMENSIONAL SCREEN/INLET EXPERIMENT

An experimental investigation was performed to examine the effect of screens located in the inlet of a 2-D indraft wind tunnel on the test-section flow uniformity. The data from the experiment were intended for use in validation of the computational prediction method which will be presented in Chapter 3. A 2-D experiment was chosen for two reasons. Most importantly, the computational method can then be 2-D. This simplifies the computational effort tremendously. The other reason is the relative simplicity of a 2-D test over a similar 3-D test. A 2-D inlet is much easier to define since the contraction takes place in only one plane. In a 3-D test decisions must be made as to the cross-sectional shape of the tunnel as well as whether the inlet is located near the ground or not. A 2-D test avoids these complications. In addition, the results are more easily interpreted since unexpected 3-D effects are minimized. The instrumentation for a 2-D test is also much simpler than for a 3-D test. With a 3-D tunnel the entire test section must be surveyed to completely determine the flow uniformity. In 2-D a single line of measurements is usually sufficient. The number of static pressure taps is also much lower for a 2-D test since only the side wall must be instrumented rather than the entire periphery as in the 3-D case.

Experimental Apparatus

Inlet geometry definition

The shape of an inlet, or contraction in a closed circuit tunnel, has a large influence on the performance of a wind tunnel. In much of the previous work on contraction design a matched cubic wall shape was employed. Using this type of wall description the geometry can be completely defined by three parameters: contraction ratio, length to width ratio, and position of the point of inflection (or match point of the two cubic curves). A parametric geometry definition allows easy variation of the inlet shape for analytical studies. Since the data from the experiment will be used as part of an analytical study, the matched cubic contraction geometry was adopted. There is no evidence, however, which indicates that the matched cubic shape is in any way "optimum." The particular formula used to determine the wall shape was obtained from Batill and Hoffman (ref. 22):

$$\begin{aligned} y &= y_e + (y_i - y_e) \left[1 - \frac{x^3}{x_m^2 L^3} \right], & x \leq x_m; \\ y &= y_e + (y_i - y_e) \frac{[1 - x/L]^3}{[1 - x_m/L]^2}, & x \geq x_m. \end{aligned} \tag{1}$$

The geometry of the inlet and variable definitions are shown in Fig. 1.

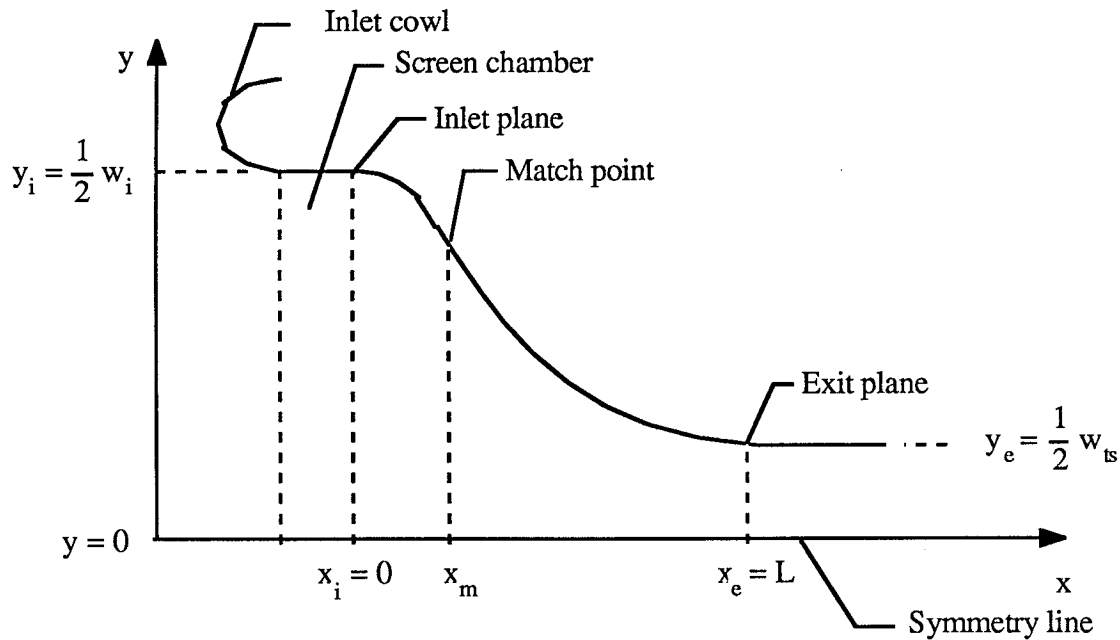


Figure 1. Inlet geometry definitions

The shape of the inlet was designed to demonstrate two aspects of inlet flows. The primary interest was in documenting the effect of screens on test-section flow uniformity. To examine this effect, the velocity variation across the inlet at the screen location should be as large as possible. The second aspect was the effect that screens have on any flow separation at the entrance to the inlet which may exist when screens are not present. The inlet used was designed to have both a large velocity variation at the screen location and flow separation on the side walls at the entrance so that both of the flow problems could be examined using a single inlet.

The design process was aided by use of the 3-D panel code VSAERO (ref. 26). This program can calculate the potential flow around arbitrary bodies to provide both surface pressure distributions and velocities at arbitrary points in the flow field. A 2-D, integral boundary layer calculation performed along surface streamlines was used to predict separation locations. Since the flow-field calculation is 3-D it was also used to determine the required size of the upstream floor and ceiling plates which confine the flow to motion in 2-D before entering the inlet. The panelled representation of the experimental tunnel is shown in figure 2. Projections of the velocity vectors in the inlet plane are also shown in figure 2. It is apparent that the velocity is confined to 2-D motion by the upstream plates. Boundary-layer separation was indicated in the calculation at the junction of the inlet cowl and the screen chamber (see figure 1).

Tunnel description

The inlet selected for the experimental investigation has a contraction ratio of 4 and a length to width ratio of 0.5. The match point for the two cubic sections is located at $x_m/L = 0.2$. A screen chamber is located immediately upstream of the contraction (shown in fig. 1) providing space for up to 12 screens. The screens are mounted in individual frames to keep them from bowing and to maintain spacing between the screens. Semicircular cowls are located at the entrance to the screen chamber.

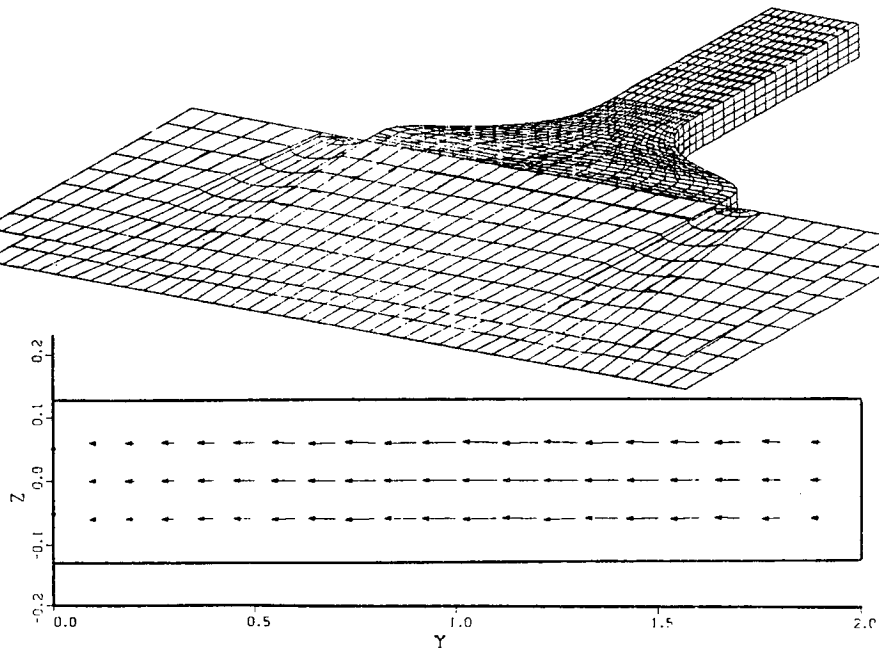


Figure 2. Paneled representation of test facility for a 3-D panel code (VSAERO) and the projected velocity vectors in the inlet plane

The layout of the experimental facility is shown in figure 3. The inlet opening measures 4 ft wide by 4 in. high and the test section measures 1 ft by 4 in. The flow entering the inlet is constrained to travel in only two dimensions by the 4 by 8 ft floor and ceiling planes upstream of the inlet. The tunnel is driven by a 5-hp centrifugal blower. A large plenum chamber is located between the test section and the blower.

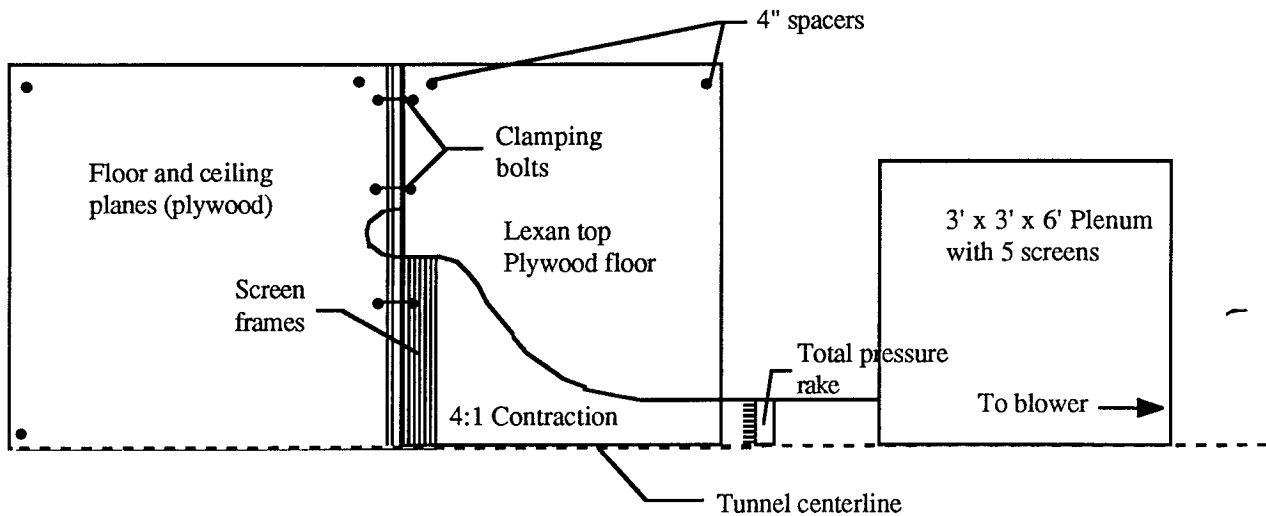


Figure 3. Layout of the 2-D wind tunnel test facility

Five screens were placed in the plenum chamber to increase the steadiness of the flow. The blower can be operated at either 1200 or 2000 rpm and provides a maximum test section velocity of 140 ft/sec when no screens are placed in the inlet.

A total pressure rake was used to measure the variation in test-section dynamic pressure. The static pressure is assumed to be constant across the test section and was measured by mechanically averaging the static pressure on the four walls of the test section. The reference dynamic pressure was taken to be that at the center of the test section. The pressures were measured using a Scani-Valve™ pressure scanning device made by Scani-Valve, Inc. A Zenith PC-100 computer with an analog to digital converter performed both the data acquisition and data reduction. A description of both the hardware and software used in the test may be found in Appendix A.

Various views of the tunnel are presented in figures 4-7. Figure 4 is an overhead view of the tunnel showing the basic layout of the tunnel. The top of the tunnel is made of 0.5 in. plexiglass to allow viewing of the tufts located on one wall of the inlet. The tufts are visible in the photo on the wall furthest from the camera. Pressure taps are located on the other wall. The screen frames are also visible at the front end of the inlet. Upstream of the screen frames is the plywood sheet used as a ceiling plane. The large box at the right of the photograph is the plenum. The Scani-Valve™ is located on top of the test section. The floor of the tunnel is painted black to contrast with the white walls. A water manometer was used to calibrate the pressure transducer before each run. The exhaust from the blower is directed out a door in the lab (fig. 5). This was done to prevent reingestion of fan exhaust by the tunnel inlet. The total pressure rake, shown in figure 6, completely spans the test section. It was made as thin as possible to minimize the blockage. The maximum thickness is approximately 7% of the test section height. The test section static pressure taps are located 3 in. in front of the main body of the rake at the same streamwise location as the total pressure tubes.

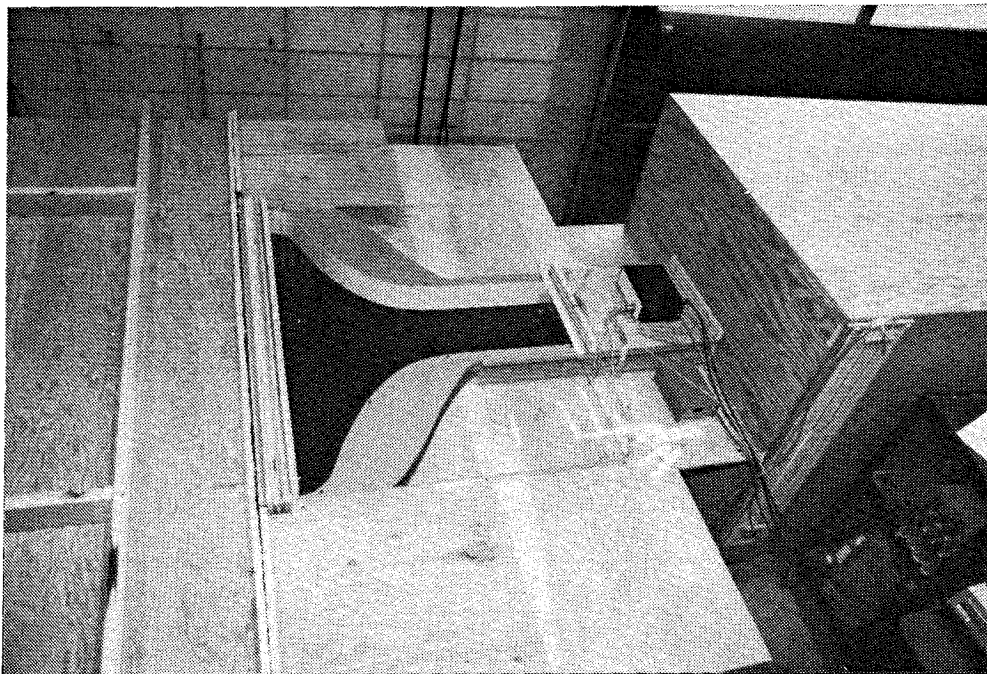


Figure 4. Overhead view of the 2-D wind tunnel

ORIGINAL PAGE
BLACK AND WHITE PHOTOGRAPH

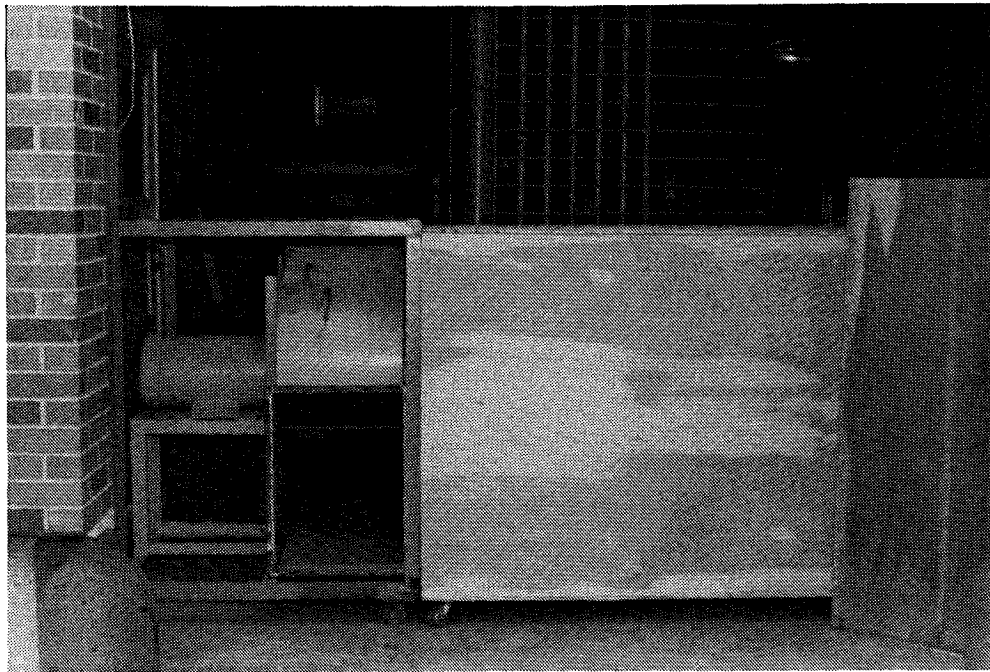


Figure 5. Plenum chamber and centrifugal blower exhaust

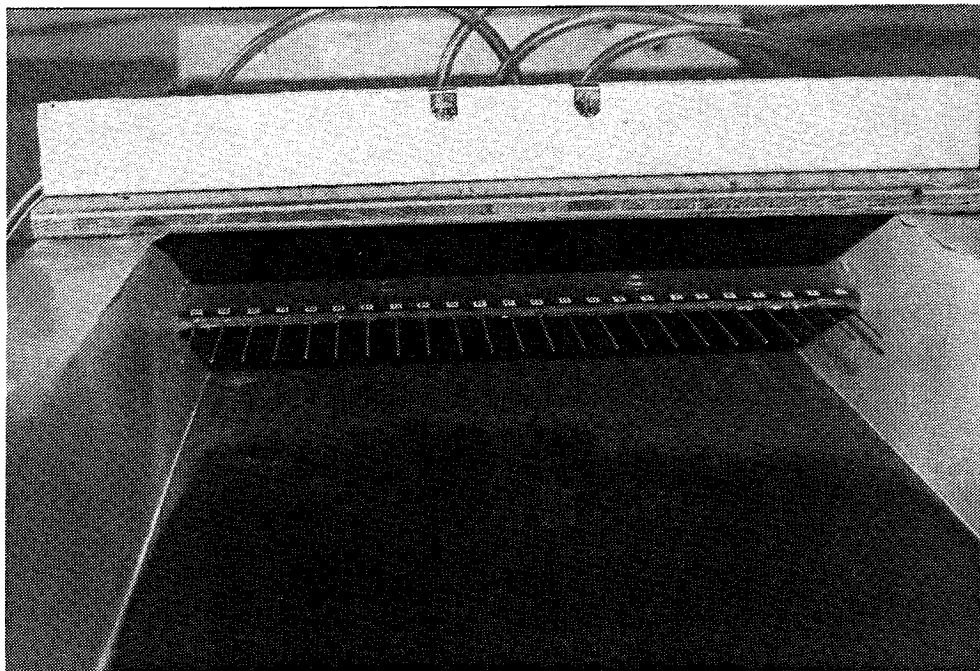


Figure 6. Total pressure rake mounted in the test section, viewed from upstream

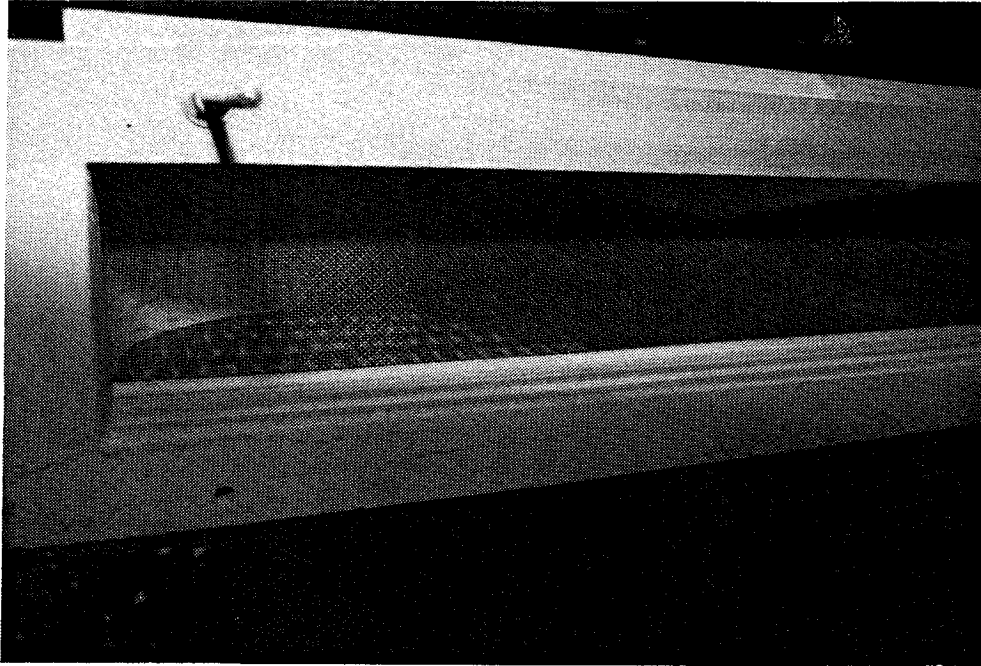


Figure 7. Single screen mounted in the screen chamber, viewed from upstream. The thread tufts are visible on the tunnel floor and wall behind the screen

Up to 12 screens can be mounted in the inlet by clamping them between the frames in the screen chamber. A single screen is shown mounted in figure 7. In this view, the upstream floor and ceiling planes have been removed.

Experimental Results

Flow separation

The tunnel was run without screens to observe the flow separation that was predicted during the design process. A sketch of the separated region is shown in figure 8. When a single screen was positioned as shown in the figure, the tufts indicated that the flow separation was eliminated. This particular effect of screens on boundary layer flow has been noted by other researchers. Mehta (ref. 37) terms the effect of screens on the boundary layer as giving it "a new lease on life." A screen can be used to clean up a separated inlet, therefore eliminating the need for reshaping the walls as long as flow uniformity constraints are not violated. This phenomenon was not examined in the present study but it does merit further investigation.

Test-section flow uniformity

The primary focus of the present study is the effect of screens on test-section flow uniformity. The most straightforward method of measuring the dynamic pressure distribution is to determine the total pressure distribution. The variation in total pressure in the test section is equivalent to the dynamic pressure variation since the static pressure is constant. The dynamic pressure is determined by subtracting the test-section static pressure from the total pressure measured by the rake. To facilitate comparisons of the

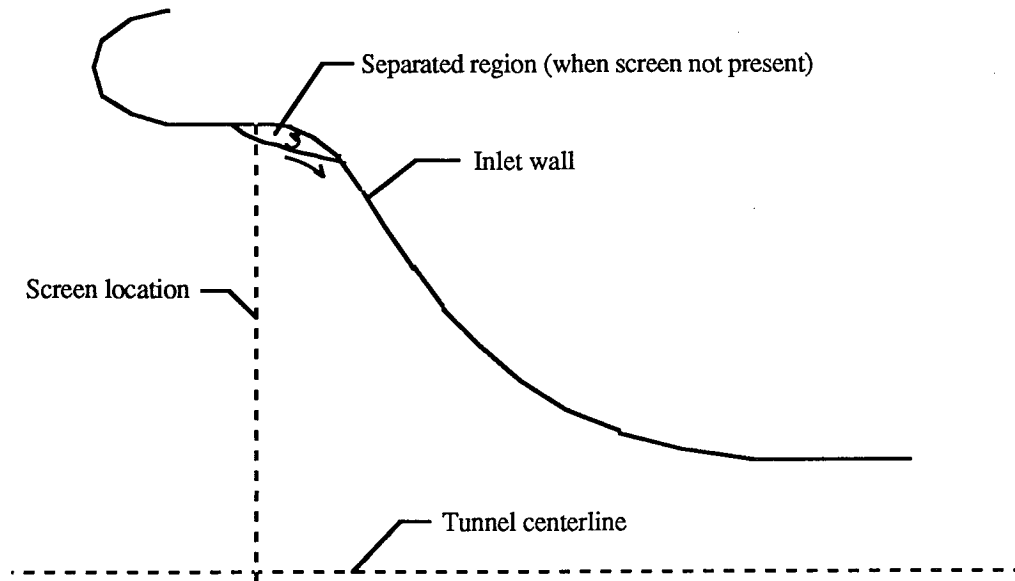


Figure 8. Sketch of the separated flow region present on the inlet wall when no screens are present

distributions obtained in the various inlet configurations, the dynamic pressure is normalized by that measured in the center of the test section. This procedure eliminates the problem of comparing data obtained for different configurations which may have been run with different mass flows. The plots of the dynamic pressure distribution which will be presented show the value of q/q_{CL} plotted against the lateral position in the test section normalized by the test-section width, y/w_{TS} .

Two dynamic pressure distributions are shown in figure 9 for the tunnel operated with no screens in the inlet. Operated in this manner, there should be very little dynamic pressure variation across the test section except for that introduced by the separated flow in the inlet (see fig. 8) and by the side-wall boundary layers. These two effects should only be apparent near the test-section walls. Because of space limitations in the laboratory, the tunnel was placed near a wall (see fig. 4). The exhaust from the fan was directed at a door located in this wall. During the winter months in Iowa, it is very desirable to run experiments with this door closed. Unfortunately when operated in this manner, the fan exhaust is reingested by the inlet. This is apparent in the differences in the two curves in figure 9, particularly on the right-hand side. This was the side closest to the laboratory wall. This sensitivity to reingestion required that all of the subsequent testing be done with the exhaust door open as shown in figure 5.

The repeatability of the test-section dynamic pressure measurements is shown in figures 10a and 10b. Figure 10a shows four distributions measured with two screens present while figure 10b is the same comparison with 12 screens present. The measurements were made in separate runs with the curves in each figure obtained at two different test-section velocities, as indicated. From these two figures, it is apparent both that the normalized dynamic pressure distribution is not sensitive to tunnel speed and that the data are repeatable. The 90% confidence band is ± 0.02 (q/q_{CL}) for the two-screen case and ± 0.012 for the 12-screen case. The stated confidence bands are for the measurements made between $y/w_{TS} = -0.4$ and $+0.4$. Much more scatter is evident in the data outside of this region. The boundary layer is apparent in the figures as a rapid decrease in the dynamic pressure near the test-section walls located at $y/w_{TS} = \pm 0.5$.

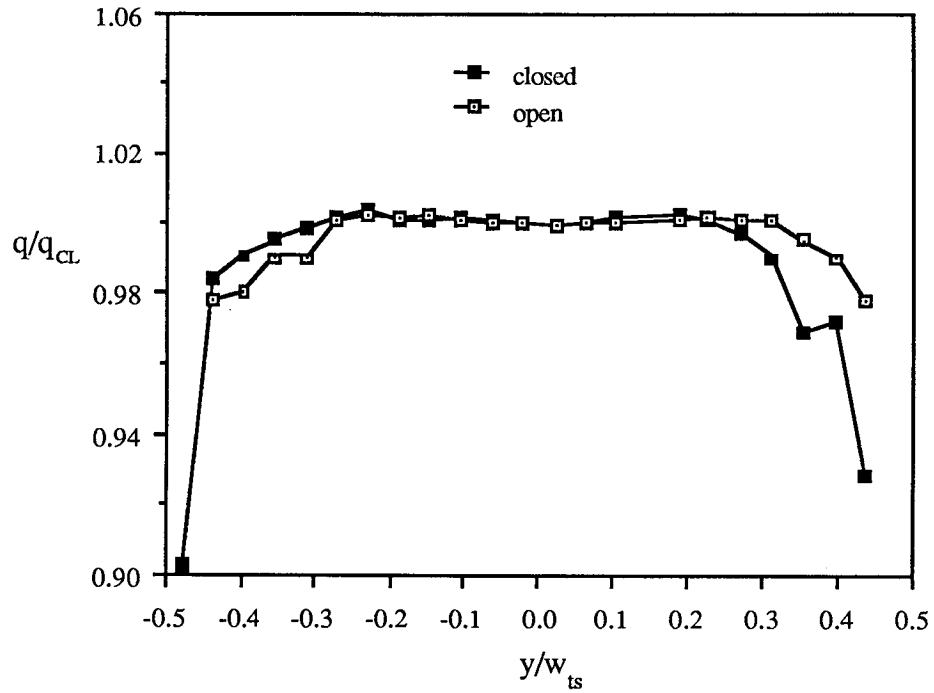


Figure 9. The effect of exhaust reingestion on the test-section dynamic pressure distribution. No screens present

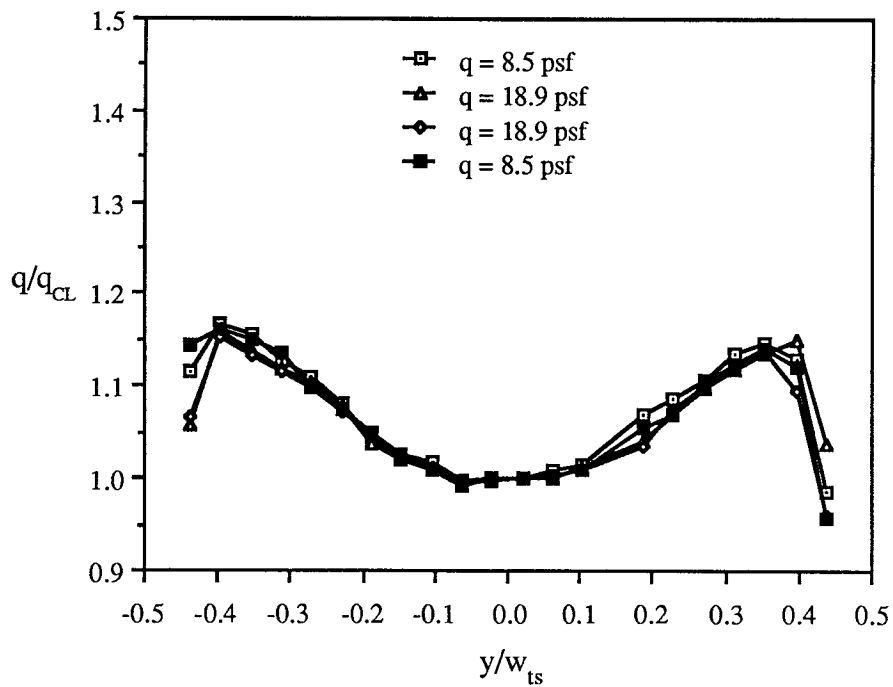


Figure 10a. Repeatability of the test-section dynamic pressure distribution measurements with two screens

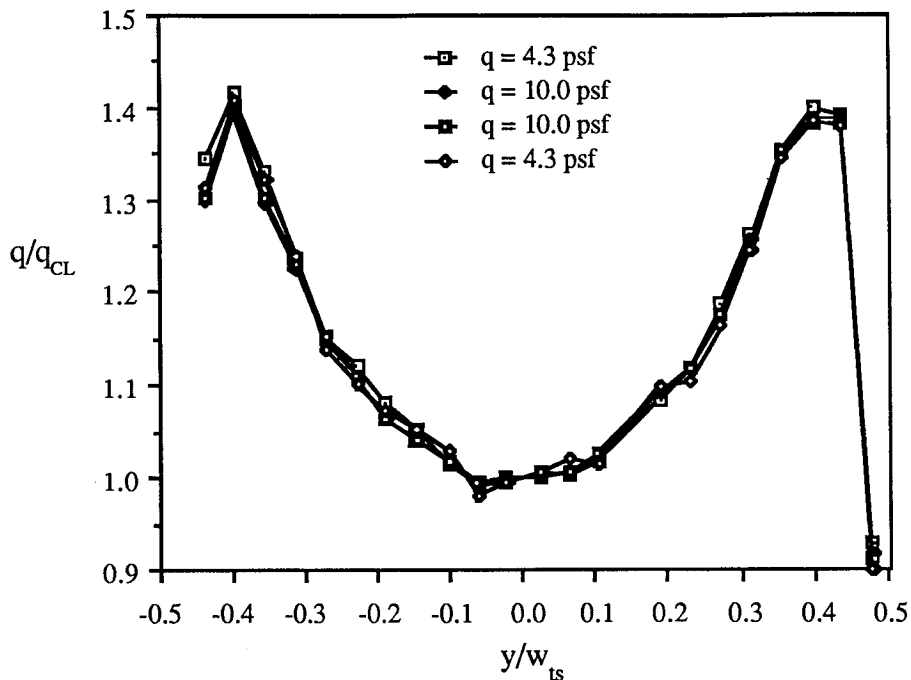


Figure 10b. Repeatability of the test-section dynamic pressure distribution measurements for 12 screens

The shape of the curves in figures 10a and 10b are a result of the velocity distribution across the width of the inlet. The shape of the inlet was designed to produce very nonuniform inlet flow with the velocity at the center much higher than near the sides. The air passing through the center portion of the screen experiences a larger drop in total pressure than the air near the sides. As this total pressure distribution is convected into the test section, the result is that the velocity in the center is lower than toward the sides.

As the number of screens is increased the magnitude of the dynamic pressure nonuniformity also increases. Figure 11 shows the dynamic pressure distributions for one, three, five, seven, and nine screens. The increase in nonuniformity with number of screens is quite apparent. The amount of increase with each additional screen, however, decreases as the number of screens increases. In fact, adding more than nine screens has almost no effect on the distribution. The distributions for 9, 10, 11, and 12 screens are shown in figure 12, and the variations between these curves are comparable to those in repeat runs of the same configuration.

Another way of examining the effect of multiple screens on the test-section flow nonuniformity is to plot some measure of the flow distortion versus the number of screens in the inlet. The maximum variation of q/q_{CL} across the center 80% of the test section ($-0.4 \leq y/w_{ts} \leq 0.4$) was used as this measure. Outside of this region the effect of the wall boundary layers is noticeable. This measure of distortion versus the number of screens is plotted in figure 13. The magnitude of the distortion reaches a maximum at about 10 screens. Adding more screens has no effect on the amount of variation. This was an unexpected result and the mechanism for this behavior was fully understood until examined using the analysis method presented in the next chapter.

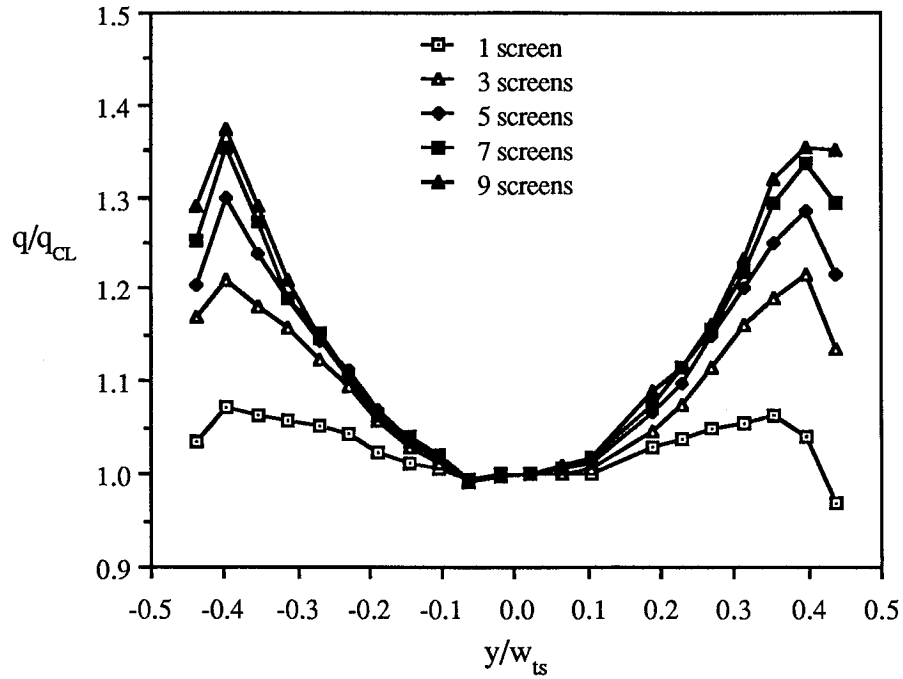


Figure 11. Test-section dynamic pressure distributions for different numbers of screens in the inlet (up to 9 screens)

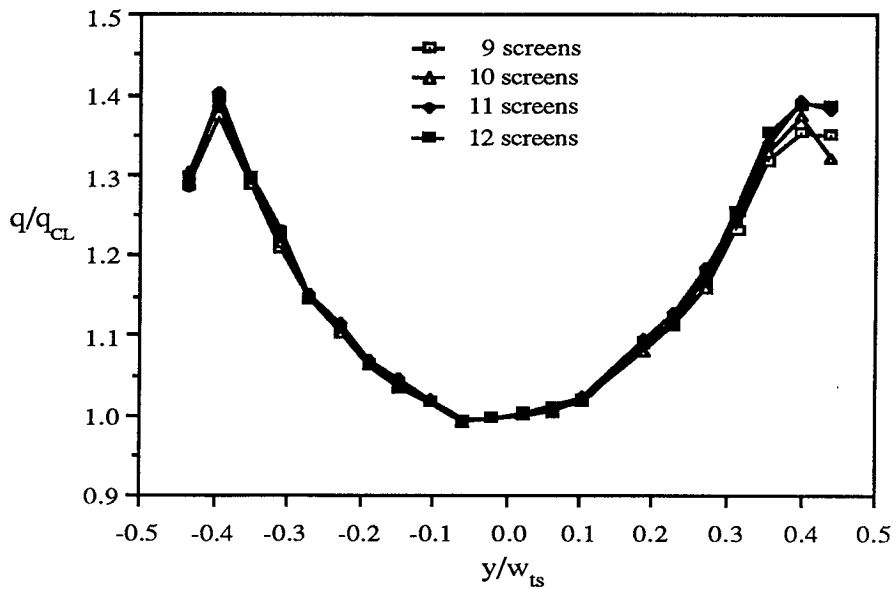


Figure 12. Insensitivity of the dynamic pressure distribution to more than 9 screens

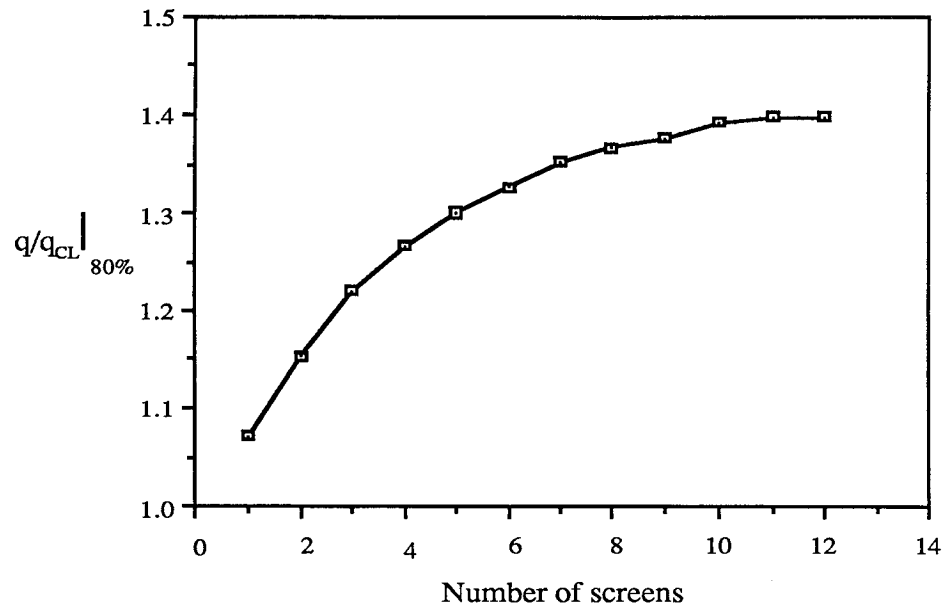


Figure 13. Effect of the number of screens on the magnitude of the test-section dynamic pressure nonuniformity

CHAPTER 3. SCREEN ANALYSIS METHOD

While perfectly feasible, a completely experimental investigation of the effects of screens on the test-section flow uniformity of indraft wind tunnels would be extremely time consuming and expensive. The extent of such a study would, therefore, be limited in scope. To perform a detailed study of the screen effects an analysis method was developed which could properly predict inlet flows including the pressure drop induced by the screen. Use of a computational method allows the effects of many inlet design parameters to be examined individually over a wide range of values. For this purpose, a 2-D prediction method was developed. A 2-D method was chosen to gain an understanding of screen effects without the increased complication and computational effort of a 3-D analysis.

Computational Method

Governing equations

When modeling fluid dynamics problems on the computer it is best to solve the least complicated set of equations which contain the important physics of the problem of interest. Flow through a screen involves viscous drag and the resulting generation of vorticity. The Navier-Stokes equations contain all of the physics of continuum fluid dynamics. These equations could be solved for the entire flowfield for the inlet flow problem including the screens. This approach is not very practical because of the large number of computational grid points which would be required to properly resolve the flow through the screen. Some of the physics of the problem is also sacrificed to achieve closure by using a turbulence model which is required in the current Navier-Stokes solution methods. Fortunately, the details of the flow through the screen and the boundary-layer development along the walls of the tunnel are not of primary interest in the present study. By ignoring the viscous terms, the governing equation can be reduced to the Euler equation. In using this equation of fluid motion, the screens are modelled as actuator disks across which the total pressure is discontinuous.

In making the simplification to an inviscid flow solution some approximations are made. The major approximation is the lack of viscous forces in the equation. This limits the region of accurate flow modelling to areas outside of the shear layers and separated flow. The wall boundary layer in a wind tunnel is relatively thin compared to the width of the test section so this assumption should not affect the accuracy of the calculations over most of the flowfield as long as there are no large regions of separated flow. Modelling the screen as an actuator disk entails additional approximation. This type of analysis of the flow through screens has been shown to work well for some simple flows (ref. 34) such as flow at an angle through a screen and flow through a bowed screen. It is a straightforward way of including the pressure drop produced by a screen into the inviscid flowfield solution.

If the flow velocity is limited to the incompressible range (i.e., Mach number less than 0.2) the momentum equation may be written as:

$$\nabla \cdot \nabla \bar{v} = \frac{-\nabla p}{\rho}$$

$$\text{or} \quad uu_x + vu_y = \frac{-1}{\rho} p_x \quad (2)$$

$$uv_x + vv_y = \frac{-1}{\rho} p_y .$$

In this equation, V is the velocity vector, p is the static pressure, and ρ is the fluid density. In the present problem, it is more convenient to solve for the total pressure rather than the static pressure. Rewriting the static pressure in terms of the velocity and total pressure gives:

$$p = p_o - \frac{1}{2} \rho V^2 = p_o - \frac{1}{2} \rho (u^2 + v^2)$$

$$p_x = p_{o_x} - \rho (uu_x + vv_x) \quad (3)$$

$$p_y = p_{o_y} - \rho (uu_y + vv_y) .$$

Substituting the expressions for p_x and p_y from equations (3) into (2) gives:

$$uu_x + vu_y = \frac{-1}{\rho} p_{o_x} + (uu_x + vv_x) \quad (4)$$

$$uv_x + vv_y = \frac{-1}{\rho} p_{o_y} + (uu_y + vv_y) .$$

Equation (4) may be rewritten as:

$$-v(v_x - u_y) = \frac{-1}{\rho} p_{o_x} \quad (5)$$

$$u(v_x - u_y) = \frac{-1}{\rho} p_{o_y} .$$

Multiplying the first of (5) by v and subtracting from u times the second, gives the single equation:

$$v_x - u_y = \frac{1}{\rho V^2} (up_{o_y} - vp_{o_x}) . \quad (6)$$

The right-hand side of (6) may be recognized as an expression for the vorticity, ω , in terms of total pressure gradients. The velocity derivatives may be written in terms of the stream function as:

$$u_y = \Psi_{yy} \quad \text{and} \quad v_x = -\Psi_{xx}.$$

Equation (6) may then be written in the more familiar form of the Poisson equation:

$$\nabla^2 \Psi = -\omega .$$

A more convenient form of (6) is obtained by writing the velocities on the right-hand side in terms of the stream function:

$$\nabla^2 \Psi = \frac{-1}{\rho V^2} \left[\Psi_y p_{o_y} + \Psi_x p_{o_x} \right]. \quad (7)$$

Equation (7) contains two unknowns, namely the stream function and the total pressure (the velocity is specified by the stream function). The convection equation for the total pressure is used to achieve closure:

$$\bar{\nabla} \cdot \nabla p_o = 0$$

or, in terms of stream function:

$$\Psi_y p_{o_x} - \Psi_x p_{o_y} = 0 . \quad (8)$$

Equations (7) and (8) must be solved over the computational domain.

To solve these equations for arbitrary geometries the equations are written in generalized coordinates. The solution grid is mapped from the x-y plane into the rectangular ξ, η plane. The momentum equation (7) must then be rewritten in terms of ξ and η . Looking first at the $\nabla^2 \Psi$ term:

$$\begin{aligned} \Psi_{xx} + \Psi_{yy} &= \partial_x \Psi_x + \partial_y \Psi_y \\ &= \partial_x (\Psi_\xi \xi_x + \Psi_\eta \eta_x) + \partial_y (\Psi_\xi \xi_y + \Psi_\eta \eta_y) \\ &= \partial_\xi (\Psi_\xi \xi_x + \Psi_\eta \eta_x) \xi_x + \partial_\eta (\Psi_\xi \xi_x + \Psi_\eta \eta_x) \eta_x \\ &\quad + \partial_\xi (\Psi_\xi \xi_y + \Psi_\eta \eta_y) \xi_y + \partial_\eta (\Psi_\xi \xi_y + \Psi_\eta \eta_y) \eta_y . \end{aligned} \quad (9)$$

Collecting the derivatives with respect to ξ and η individually gives:

$$\begin{aligned} \nabla^2 \Psi &= \partial_\xi (\Psi_\xi \xi_x^2 + \Psi_\eta \eta_x \xi_x + \Psi_\eta \eta_y \xi_y + \Psi_\xi \xi_y^2) \\ &\quad + \partial_\eta (\Psi_\eta \eta_x^2 + \Psi_\xi \xi_x \eta_x + \Psi_\xi \xi_y \eta_y + \Psi_\eta \eta_y^2) . \end{aligned} \quad (10)$$

Continuing to collect terms and simplifying:

$$\begin{aligned} \nabla^2 \Psi = & \partial_{\xi} \left[(\nabla \xi \cdot \nabla \xi) \Psi_{\xi} + (\nabla \xi \cdot \nabla \eta) \Psi_{\eta} \right] \\ & + \partial_{\eta} \left[(\nabla \xi \cdot \nabla \eta) \Psi_{\xi} + (\nabla \eta \cdot \nabla \eta) \Psi_{\eta} \right]. \end{aligned} \quad (11)$$

Dividing both sides by the Jacobian of the coordinate transformation gives the desired form:

$$\nabla^2 \Psi = \partial_{\xi} \left[A_1 \Psi_{\xi} + A_2 \Psi_{\eta} \right] + \partial_{\eta} \left[A_2 \Psi_{\xi} + A_3 \Psi_{\eta} \right] \quad (12)$$

where:

$$\begin{aligned} A_1 &= \frac{\nabla \xi \cdot \nabla \xi}{J} \\ A_2 &= \frac{\nabla \xi \cdot \nabla \eta}{J} \\ A_3 &= \frac{\nabla \eta \cdot \nabla \eta}{J}. \end{aligned} \quad (13)$$

J is the Jacobian of the transformation defined by:

$$\begin{aligned} J &\equiv \left| \frac{\partial(\xi, \eta)}{\partial(x, y)} \right| \\ &= \xi_x \eta_y - \xi_y \eta_x. \end{aligned} \quad (14)$$

Performing a similar set of operations on the right-hand side of (7) gives the final form of the momentum equation in generalized coordinates:

$$\begin{aligned} \partial_{\xi} \left[A_1 \Psi_{\xi} + A_2 \Psi_{\eta} \right] + \partial_{\eta} \left[A_2 \Psi_{\xi} + A_3 \Psi_{\eta} \right] = \\ \frac{1}{\rho V^2 J} \left[(u \xi_y - v \xi_x) p_{o_{\xi}} + (u \eta_y - v \eta_x) p_{o_{\eta}} \right]. \end{aligned} \quad (15)$$

The velocities u and v , and the magnitude, V , in (15) remain in the physical coordinate system. This is convenient since the equation, as written, is nonlinear since the velocity is a function of the stream function. The equation is linearized by lagging the velocity so it can be considered to be a known in the above derivation. The velocity is obtained from the stream function as:

$$\begin{aligned}
V^2 &= u^2 + v^2 = \Psi_y^2 + \Psi_x^2 \\
&= (\Psi_\xi \xi_y + \Psi_\eta \eta_y)^2 + (\Psi_\xi \xi_x + \Psi_\eta \eta_x)^2
\end{aligned} \tag{16}$$

Finite Difference Representation

The alternating direction implicit (ADI) approximate factorization scheme presented by Chaderjian (ref. 34) and Chaderjian and Steger (ref. 39) was used to solve for the stream function. The compressible dual potential code developed by Chaderjian was modified to solve only for the stream function. The original derivation of the dual potential method used Crocco's equation which expresses the pressure gradients in terms of entropy gradients. Therefore, the program was also modified to retain total pressure as one of the variables. The ADI approximate factorization algorithm used in solving for the stream function is:

$$\left[1 - h \nabla_\eta A_{3_{k+1/2}} \Delta_\eta \right] \left[1 - h \nabla_\xi A_{1_{j+1/2}} \Delta_\xi \right] \Delta \Psi^n = hr \Psi_R^n \tag{17}$$

where:

$$\begin{aligned}
\Psi_R &= \nabla_\xi A_{1_{j+1/2}} \Delta_\xi \Psi + \nabla_\eta A_{3_{k+1/2}} \Delta_\eta \Psi + \delta_\xi (A_2 \delta_\eta \Psi) + \delta_\eta (A_2 \delta_\xi \Psi) \\
&\quad - \frac{1}{\rho V^2} \left[(A_1 \delta_\xi \Psi + A_2 \delta_\eta \Psi) \delta_\xi p_o + (A_2 \delta_\xi \Psi + A_3 \delta_\eta \Psi) \delta_\eta p_o \right].
\end{aligned} \tag{18}$$

The difference operators in the above equation are given by:

$$\begin{aligned}
\Delta_\xi &= \frac{(\)_{j+1} - (\)_j}{\Delta \xi} \\
\nabla_\xi &= \frac{(\)_j - (\)_{j-1}}{\Delta \xi} \\
\delta_\xi &= \frac{(\)_{j+1} - (\)_{j-1}}{2 \Delta \xi}
\end{aligned}$$

The η -differences are defined in the same manner. Recall that $\Delta \xi$ and $\Delta \eta$ have been set to 1. The h and r terms on the right-hand side of (17) are relaxation parameters (refs. 38, 39) which accelerate the convergence of the scheme and n refers to an iteration level. The total pressure is treated as a known in the above formulation and is obtained from the previous iteration level.

Boundary conditions

Boundary conditions must be supplied both on the far-field boundaries and on the solid walls of the tunnel. The walls themselves must correspond to streamlines in order for the zero-normal velocity condition to be met. The walls therefore have a prescribed value of stream function. The mass flow through the tunnel is proportional to the difference in stream function between the two walls. At the downstream end of the test section, the streamwise gradient of the stream function is set to zero. This specifies zero transverse velocity. The far-field boundaries are assigned values of stream function such that the normal velocity (tangential gradient in Ψ) is the same at every point on the boundary. The gradient in Ψ is set such that the mass flow into the computational domain through the far-field boundary is equal to the mass flow exiting the test section. This is a very simple, if somewhat arbitrary, boundary condition. It was found, however, that if the far-field boundary is placed far enough from the region of interest (the inlet) that it has very little effect on the solution. A sufficient distance was found to be approximately 1 inlet width in both the upstream and lateral directions. In the present study all calculations were performed with the boundaries placed at least 2 inlet widths from the inlet.

Determination of total pressure

So far, the solution procedure for finding the stream function has been described with the total pressure treated as a known throughout the flowfield. This is not the case as it is the total pressure distribution downstream of the screen which is the unknown of primary interest. Before passing through the screen, the flow is irrotational, that is, the total pressure is uniform. The screen is modelled as an actuator disk across which the total pressure is discontinuous. The total pressure drop is a function of both the dynamic pressure and onset angle of the flow at each point on the screen. Using the actuator disk model described in the next section, the total pressure at each grid point immediately downstream of the screen is calculated. The total pressure is then convected downstream in accordance with (8).

Total pressure is convected by specifying that it remain constant along streamlines. This is equivalent to solving the convection equation. The total pressure distribution immediately downstream of the screen is determined using the actuator disk model. This distribution defines a relationship between the stream function and the total pressure. At grid points further downstream of the screen (inside the tunnel) the total pressure is obtained by linear interpolation; that is the total pressure is set equal to the total pressure corresponding to the same value of stream function at the first grid station past the screen. A higher order interpolation scheme or finite difference solution of the convection equation could be used at the expense of additional complication but the results obtained using the scheme described are quite accurate.

Actuator disk model

The pressure drop caused by a screen in the inlet is modeled by use of a simple actuator disk representation. The static pressure-loss coefficient for flow perpendicular to a screen depends on the physical characteristics of the screen; porosity, Reynolds number of the flow based on wire diameter, and the details of the weave among others. The loss coefficient for normal flow is defined as:

$$k_o \equiv \frac{D}{\frac{1}{2}\rho V^2} = \frac{P_1 - P_2}{\frac{1}{2}\rho V^2} \quad (19)$$

where D is the drag force per unit area acting on the screen and the subscripts 1 and 2 refer to upstream and downstream of the screen, respectively. The value of k_0 is a function of Re (for low values of Re). When the onset flow is not perpendicular to the screen, the loss coefficient has been found to vary as:

$$k_{\theta} = k_0 \cos^m \theta \quad (20)$$

where θ is the angle between the onset flow and the normal to the screen (ref. 37). The value of m in (20) varies between 1.0 and 1.4 depending on the porosity of the screen.

A large body of literature can be found describing the loss characteristics of many types of screens (refs. 34, 37, 40-48). Some of these reports present empirical methods for determining the value of k_0 based on the porosity and wire diameter (refs. 43-48). None of these methods is entirely satisfactory, however, the formula presented by Wieghardt (ref. 44) appears to be the most accurate based on the measurements of Smith, Olson, and McMahon (NASA TM to be published). Those measurements were made for a screen which is identical to that used in the experimental investigations of the present study. The exponent, m , in (20) for this screen is given in Smith et al. as 1.1. The formula used to determine the loss coefficient at each point across the width of the screen for use in the actuator disk model is:

$$k_{\theta} = 5.5 \frac{1-\beta}{\beta^2} Re_{\beta}^{-.33} \cos^{1.1} \theta . \quad (21)$$

β is the porosity of the screen which is defined as the ratio of the open area of the screen to the total area. The parameter Re_{β} is the modified Reynolds number defined by:

$$Re_{\beta} = \frac{dV}{\beta\nu} \quad (22)$$

where d is the wire diameter, V is the onset flow velocity, and ν is the kinematic viscosity of the fluid. The value of Re_{β} ranges from 60 to 600 in (21). For values greater than 600, Re_{β} is set equal to 600 in this formula.

Figure 14 shows a comparison of the predicted and measured (Smith et al.) pressure loss coefficient for a 20-mesh screen with a porosity of 0.46 and wire diameter of 0.016 in. Results for onset angles of 0 and 40° are presented. The predicted values are in good agreement with the experimental data especially for velocities greater than 20 ft/sec. The pressure drop at each point on the screen is then given by:

$$p_{o2} = p_{o1} - k_{\theta} \frac{1}{2} \rho V^2 \quad (23)$$

where k_{θ} is determined by (21) using the local flow velocity and its angle of onset relative to the screen.

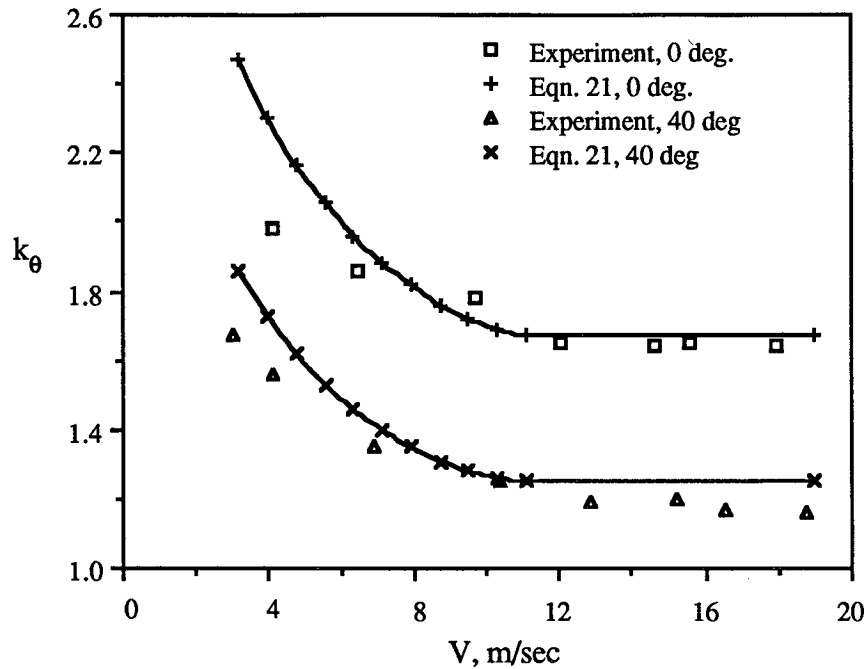


Figure 14. Comparison of the predicted and measured pressure loss coefficient for 20-mesh stainless steel screen. Wire diameter = 0.06 in., $\beta = 0.46$. (The data are from Smith et al.)

Computational Grid

The grid used in the calculations is shown in figures 15a and 15b. Grid points are distributed on lines of constant x . The wall shape is generated using the matched cubic formula presented in chapter 2. Points are clustered near the walls of the tunnel and in regions of rapid area changes. Since the inlet is of the indraft variety, a small cowl was added at the end of each wall. The large amount of grid skewness near this cowl causes some small inaccuracies in the local solution but the perturbations are much smaller than are present without the cowl. An orthogonal grid around the cowl would eliminate the problems with skewness but the simplicity of the present grid outweighs the small, localized inaccuracy which it induces. The simple grid also simplifies the screen modelling since the screen can be simulated at a single grid line. A close-up of the grid in the cowl region is shown in figure 15b. The wall of the tunnel has finite thickness and is represented by two grid points. These points are not used in the solution of the finite difference equations. The value of the stream function at each point on the walls is supplied as part of the boundary conditions.

Solution procedure

The solution procedure is as follows:

- 1) First an initial guess for the stream function and total pressure is made at every grid point.
- 2) Equation (17) is solved iteratively using the ADI scheme with the right-hand side set equal to zero. This gives the potential flow solution (i.e., no screen present).

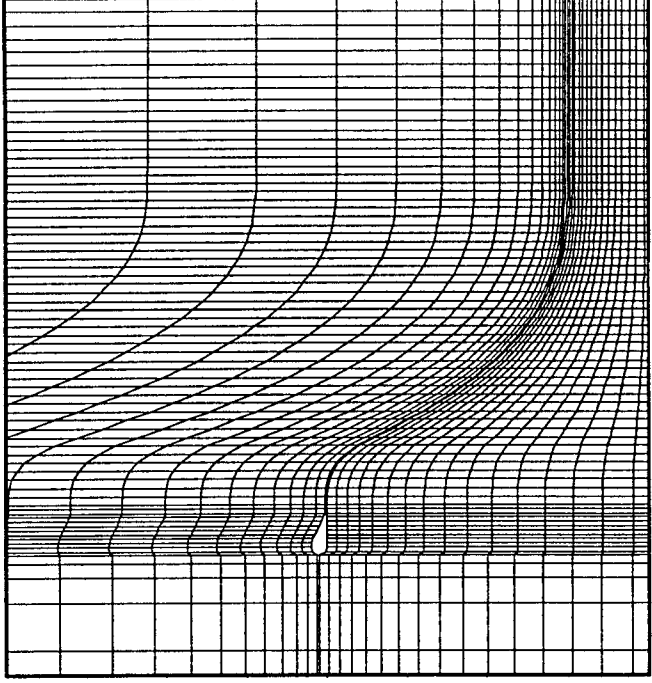


Figure 15a. Computational grid in physical space for the screen analysis

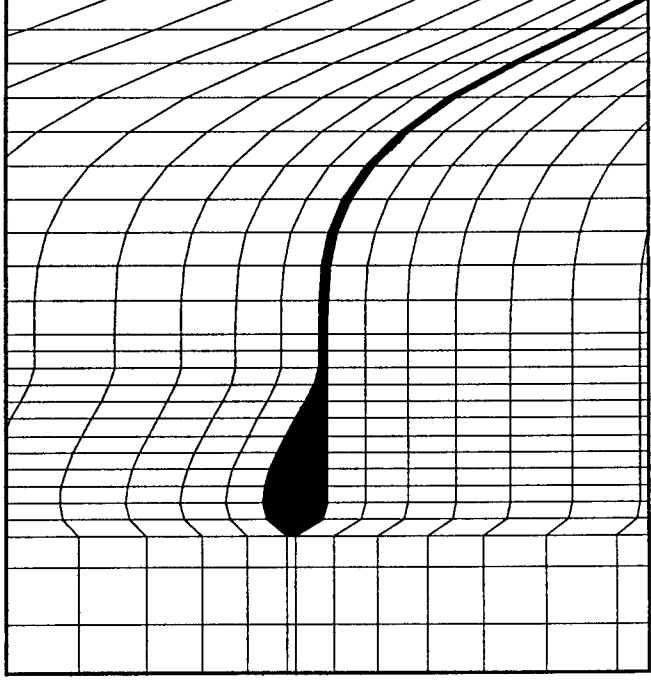


Figure 15b. Detail of the grid around the inlet cowl. The wall is the shaded region

- 3) The pressure drop at the screen is calculated using (23).
- 4) The total pressure downstream of the screen is determined by interpolation using the current solution for the stream function.

5) The solution for Ψ is updated in (17) by a complete cycle of the ADI scheme with the right-hand side as shown in the equation.

- 6) Repeat steps 3 - 6 until the solution for Ψ is converged.

The program can solve cases with more than one screen by simply multiplying the pressure drop determined in (23) by the number of screens desired in the simulation. When a large number of screens was used in the simulation the solution procedure as described above sometimes became unstable. By gradually increasing the loss coefficient used in the screen simulation the instability was avoided. The procedure was to obtain converged solutions first for no screens, then for one screen, two screens, etc., until the desired number of screens was reached.

Code Verification

The predicted wall static pressure coefficient is plotted in figure 16 for an inlet with a contraction ratio of 4, length to width ratio of 0.5, and a match point of 0.2. The calculation did not include a screen and therefore should be identical with potential flow results. Results from a potential flow calculation are also shown in the figure. The potential flow results were obtained using the program HILIFT (ref. 25). Except for the cowl region, the two codes give nearly identical results. The large suction spike in the

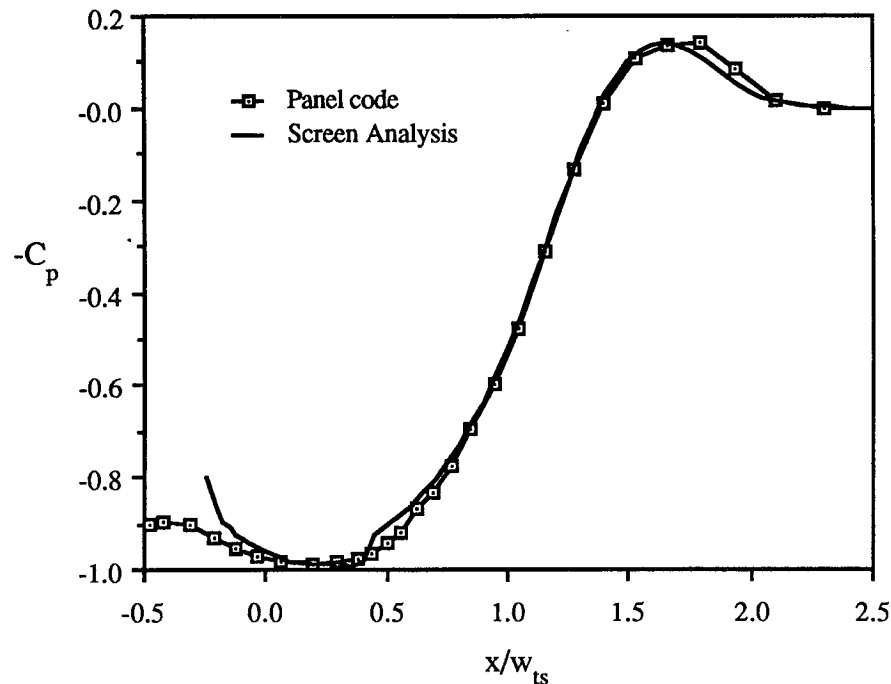


Figure 16. Comparison of the calculated wall static pressure distributions from a panel code and from the screen analysis

pressure distribution near the cowl in the present solution is very likely due to the skewness of the grid in that region. An interesting point to note is the small wiggle in the present prediction at $x/w_{ts} = 0.4$. This is the location of the match point and the glitch is due to the discontinuous curvature of the wall at that point. The formula used to define the wall shape generates a shape with continuous first derivatives so the present method is able to resolve discontinuous changes in curvature.

The screen analysis was applied to the same configurations tested in the experiment which was described in chapter 2. Comparisons of the calculated and measured dynamic pressure distributions for the inlet with 1, 5, 9, and 12 screens are shown in figures 17a-d. The agreement between the predictions and data is very good except near the walls where the boundary layer significantly reduces the dynamic pressure. A small asymmetry in the experimental results is apparent in the figures. The asymmetry was found to be caused by a slight misalignment of the inlet with respect to the wind tunnel centerline. Keeping these differences in mind the results of the analysis are in good agreement with the data over the center 80% of the test-section span.

A useful measure of the flow uniformity in a wind tunnel is the magnitude of the dynamic pressure variation over the useful portion of the test section. In most situations no more than 75% of the test section width is occupied by a model caused by excessive wall interference or blockage effects for larger models. In fact, most wind tunnel models occupy a much smaller portion of the test section. As introduced in chapter 2, the maximum dynamic pressure variation over the center 80% of the test-section width was used as a measure of the flow uniformity. In figure 18 the test-section flow uniformity is plotted against the number of screens for both the experiment and calculations. The agreement is again good, with the predictions within about 3.5% of the measured values for all the configurations studied. The

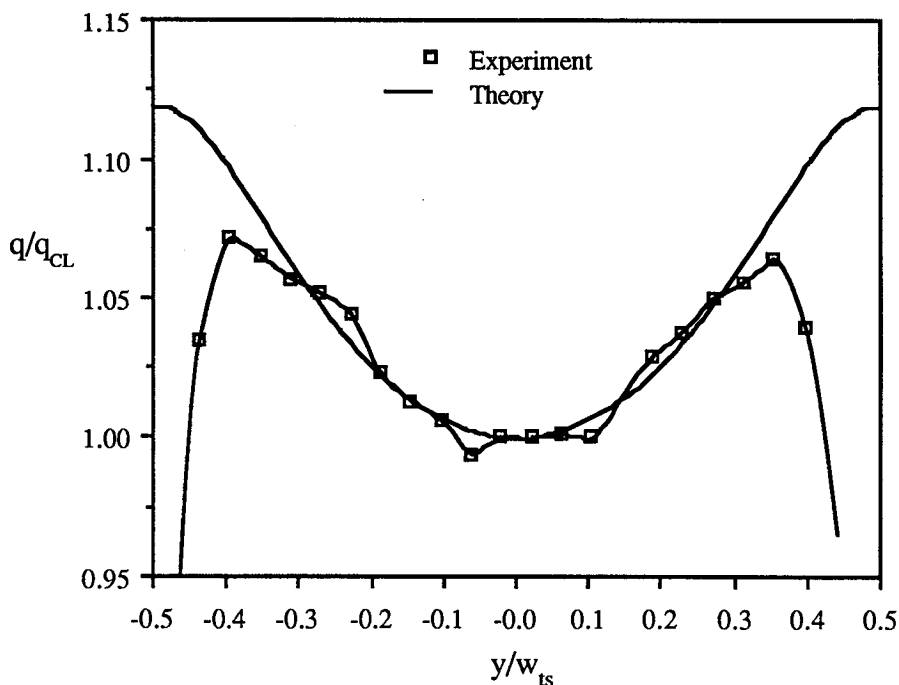


Figure 17a. Comparison of the predicted and measured test-section dynamic pressure distributions for the case of one screen in the inlet

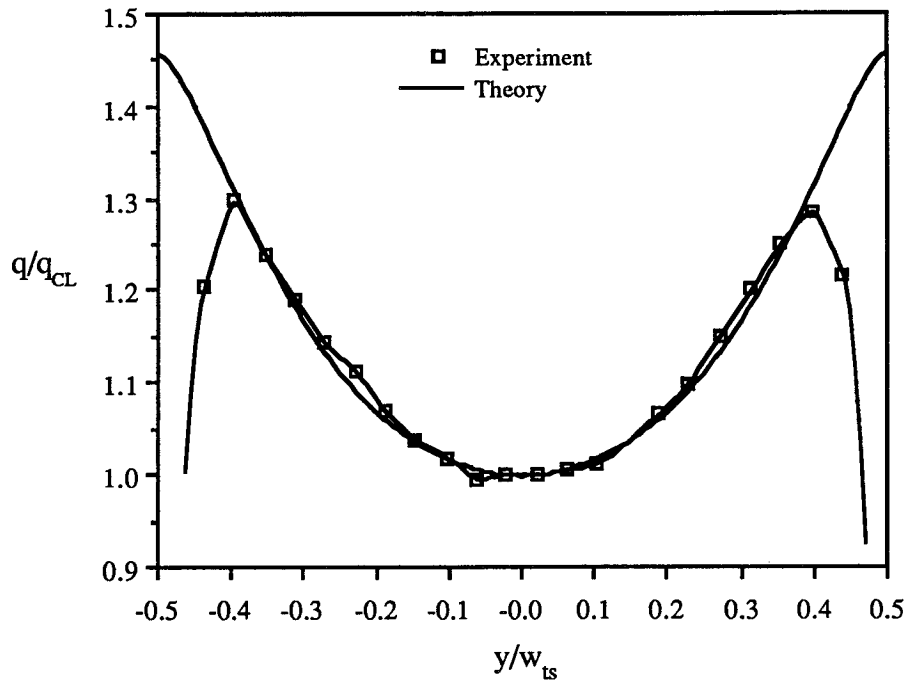


Figure 17b. Comparison of the predicted and measured test-section dynamic pressure distributions for the case of five screens in the inlet

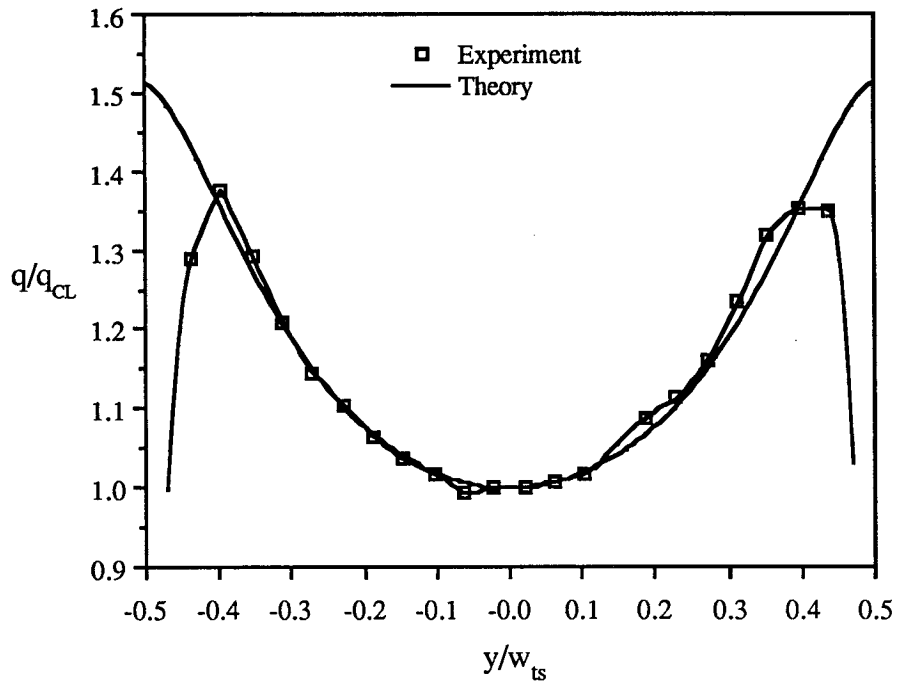


Figure 17c. Comparison of the predicted and measured test-section dynamic pressure distributions for the case of nine screens in the inlet

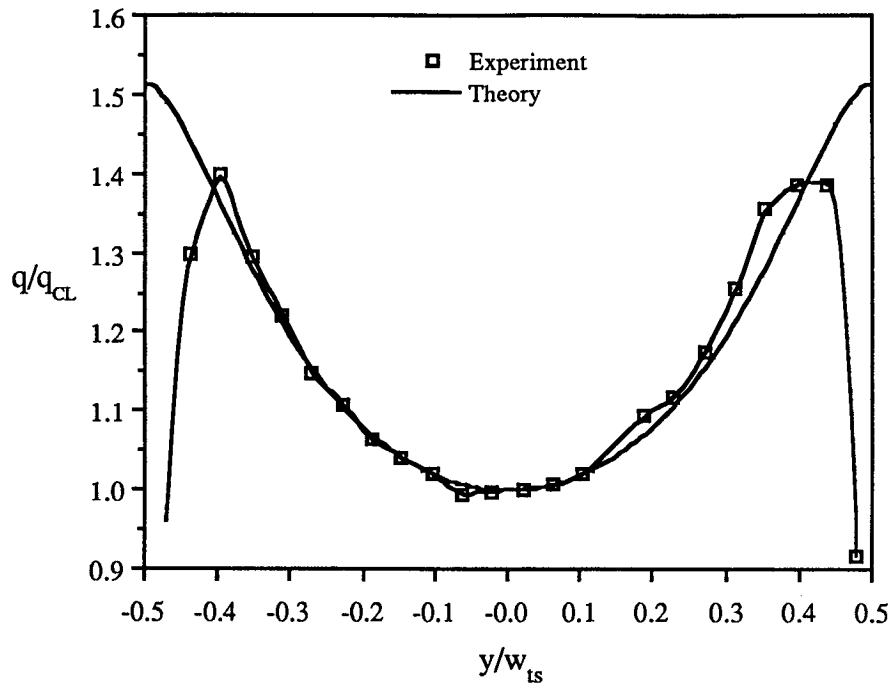


Figure 17d. Comparison of the predicted and measured test-section dynamic pressure distributions for the case of 12 screens in the inlet

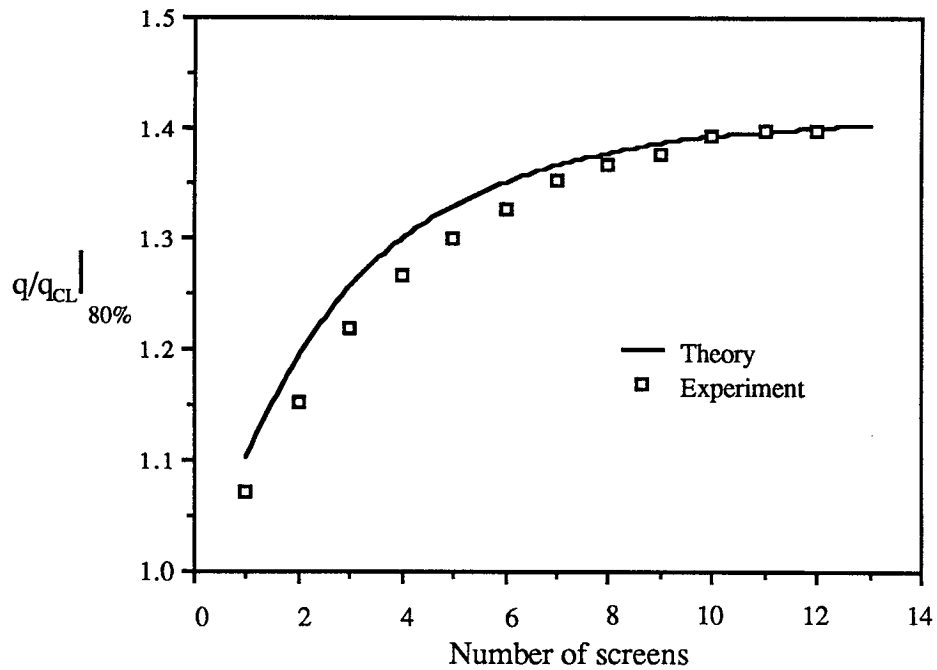


Figure 18. Comparison of the predicted and measured test-section dynamic pressure non-uniformity as a function of the number of screens in the inlet

flattening of the curve at about 10 screens is also predicted, indicating that the analysis may be used to determine the cause of this behavior.

The wall static pressure distribution is also accurately calculated by the analysis. Figure 19 shows a comparison between the predicted and measured static pressure-coefficient distributions for the case of no screens in the inlet. A similar comparison was shown previously between the present analysis and a panel method calculation. The agreement with the panel method was nearly exact while there are some differences between the present method and the data. The most significant difference is in the region where separated flow was indicated by the tuft and smoke flow visualizations of the experiment. The slightly lower pressures measured in this region is consistent with the displacement effect of a separated bubble just downstream of the inlet cowl.

If the difference is indeed due to the separation in the experiment, the comparison should be better for cases which did not exhibit flow separation. The predictions and measurements for a single screen case are shown in figure 20. The agreement is better in this case but the experimental pressure data still appears to indicate separation in spite of the tuft observations. This may not be separated flow but rather caused by the displacement effect of a thick boundary layer in the upstream portion of the inlet resulting in lower pressure than indicated by the theory.

The calculation shows a possible mechanism for the elimination of the separation when a screen is added. As the air passes through the screen it experiences a drop in total pressure. An identical drop in static pressure must also occur in order to satisfy continuity. Therefore, the screen induces a favorable pressure gradient to the flow through the screen. It is possible that this results in the elimination of the separation. Mehta (ref. 37) reported that a screen has a rejuvenating effect on turbulent boundary layers, reducing the thickness and turbulent fluctuations relative to the upstream values. The turning of the flow passing through the screen may also be responsible for the cleaning up of the flow at the inlet in the experiment.

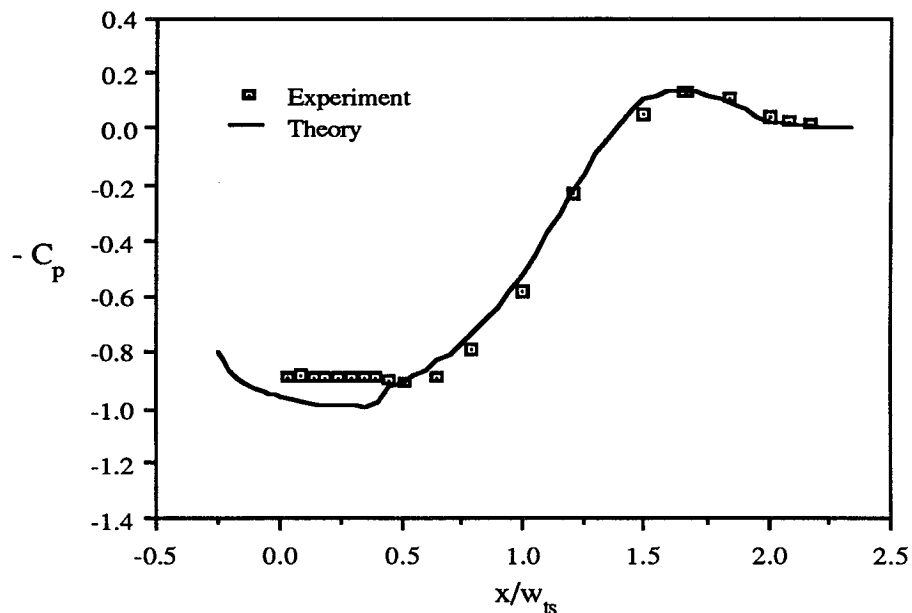


Figure 19. Comparison of the predicted and measured wall static pressure coefficient distributions for the case of no screens in the inlet

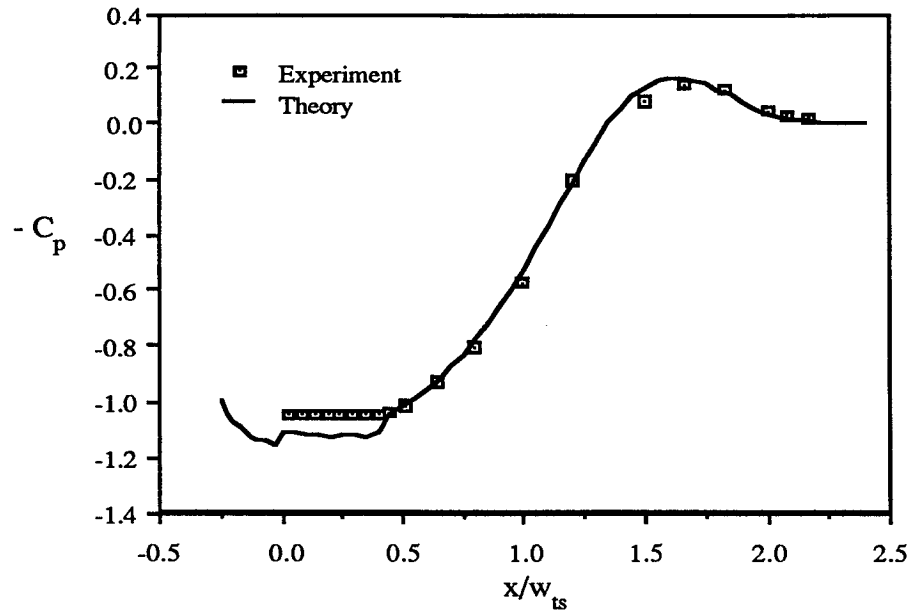


Figure 20. Comparison of the calculated and measured wall static pressure coefficient distributions for the case of 1 screen

CHAPTER 4. PARAMETRIC STUDY OF SCREEN EFFECTS

Experience does not ever err, it is only your judgment that errs in promising itself results which are not caused by your experiments.

- Leonardo Da Vinci (c.1510)

To obtain an understanding of the effect of screens on flow uniformity, several parametric variations of inlet geometry and screen loss coefficient were performed. Calculations were performed for various screen loss coefficients to observe the effect on flow uniformity. The use of nonuniform screen loss coefficient was also examined as a possible method of achieving uniform test-section velocity. The geometric variations examined include contraction ratio, length to inlet width ratio, match point to inlet length ratio, length of the upstream constant width section, and the screen position in the constant width section.

Effect of Screen Loss Coefficient

One surprising result of the experimental study of screen effects was that adding more screens in front of the inlet did not improve the test-section flow uniformity. The author, as well as some associates, felt that high enough losses at the inlet would result in uniform test-section flow. The argument was that the large drag in the center of the screens, where the flow is the fastest, would cause more air to be drawn through the outer portions of the screens where the flow was originally slower and hence had less drag. Redistribution of the flow, as the logic went, would result in a situation with uniform drag and, hence, uniform test-section flow. The experimental data, however, did not support this conclusion. As seen in chapter 2, the flow uniformity was insensitive to additional screens once 10 screens were in place. Since only 12 screens could be installed in the experimental tunnel one possible conclusion is that 12 screens were simply not sufficient to produce the expected effect. The fallacy of the expected result was not discovered until the prediction code was applied to the problem.

Figure 21 shows the magnitude of the test-section flow nonuniformity across 80% of the test section as a function of the number of screens. While it is obviously not possible to physically place as many as 80 screens in the inlet, the number of screens can be interpreted as a multiple of the screen loss coefficient of a single screen. Above about 12 screens, there is very little change in the magnitude of the nonuniformity even up to 80 screens. In fact, the dynamic pressure distributions are nearly identical for the 12- and 40-screen cases as shown in figure 22. Clearly, some mechanism other than the drag of the screens is responsible for redistributing the flow.

The transverse or lift force generated by the screens has a large effect on the velocity distribution of the flow passing through the screens. The velocity distribution in the test section is, therefore, also affected. The effect of the screen turning is apparent in the calculated streamline plots shown in figure 23. The dashed streamlines are for the case of no screens while the solid lines indicate the streamlines for the 12-screen case. The turning induced by the screen is quite apparent at the screen location. The flow exits the screen nearly perpendicular to the screen when 12 screens are present. The exit angle of a flow passing through a screen has been shown to approach 90° as the loss coefficient of the screen is increased (ref. 47). Therefore, once the flow is made to exit normal to the screens adding more screens cannot increase the screen turning and, hence, does not change the distribution of the flow passing through the screen. This is evident in the streamline patterns shown in figure 24 for the cases of 12 and 40 screens in

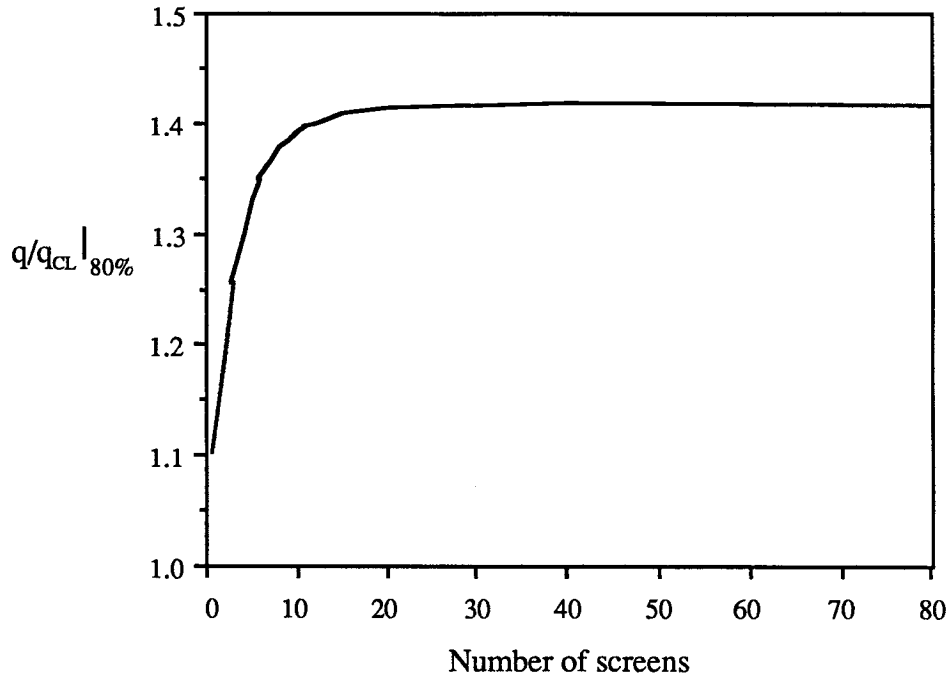


Figure 21. The predicted effect of the number of screens on the magnitude of the test-section dynamic pressure nonuniformity. $c = 4$; $L/w_1 = 0.5$; $x_m/L = 0.2$

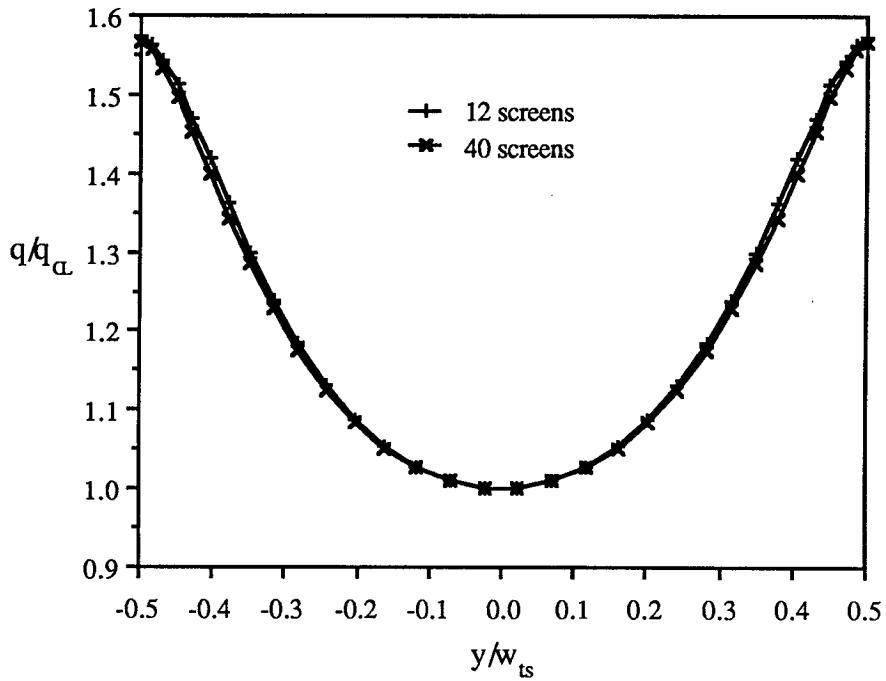


Figure 22. Comparison of the calculated test-section dynamic pressure distributions for 12 and 40 screens in the inlet

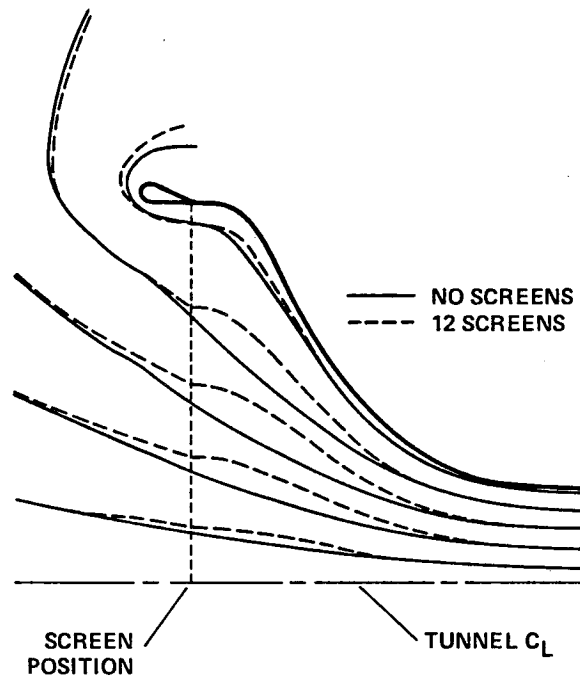


Figure 23. Predicted streamline paths for the case of no screens and 12 screens

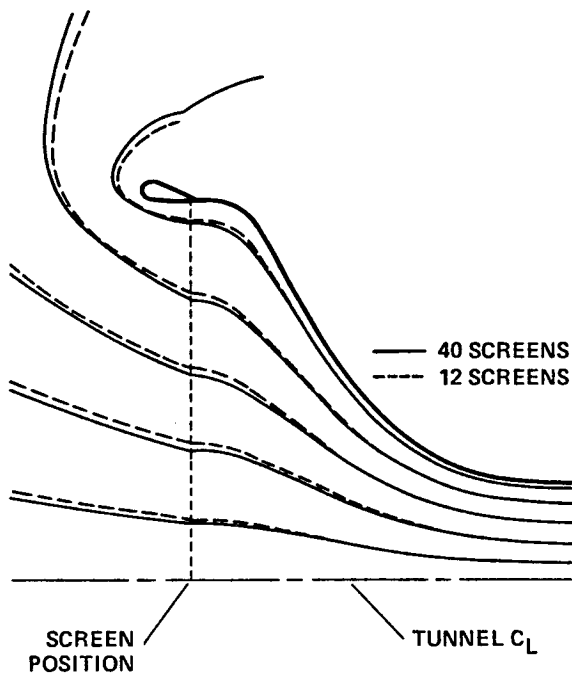


Figure 24. Predicted streamline paths for the case of 12 and 40 screens in the inlet

the inlet. Once the flow distribution at the screen is made insensitive to the presence of additional screen loss the amount of flow distortion in the test section will also not change with the addition of more screens.

Screen turning is a result of the vorticity generated by the pressure drop induced by the screen. Recall that the vorticity is given by:

$$\omega = \frac{1}{\rho V^2} (u p_{o_y} - v p_{o_x}) .$$

Both of the total pressure gradients are nonzero along the screen. The y-derivative is nonzero because of the nonuniform velocity distribution passing through the screen and the x-derivative because of the drop in pressure across the screen. The resulting vorticity generates the lift force which turns the flow. Capturing the screen turning was very important in accurately calculating the flow through the screens.

Variable Loss Coefficient

Since the velocity of the air passing through the screen varies across the width of the inlet it should be theoretically possible to vary the loss coefficient of the screen in such a way as to achieve uniform test section flow. A simple approach would be to determine from a no screen calculation (potential flow) the required loss coefficient at every point at the screen location necessary to obtain uniform pressure drop across the width of the inlet equal in magnitude to that produced by a single screen at the inlet centerline. In performing such an analysis, both the magnitude and onset angle of the flow relative to the screen normal must be taken into account (see eq. 21). The loss coefficient distribution (k_o as a function of the lateral position in the inlet) determined in this manner is shown in figure 25. The required loss coefficient varies from 1.6 (the loss of a single screen) at the center of the inlet to 4.5 near the side walls. When this loss distribution was used in a calculation the result was a reduction in the magnitude of the dynamic pressure nonuniformity from 10% to 6% (over the center 80% of the test section). The dynamic pressure distributions for the two cases are shown in figure 26. While the trend is in the right direction the remaining distortion is still too large for most wind tunnel applications. The problem is that the inlet flow is redistributed by the screen and is no longer the same as when no screen was present. A simple estimate such as this is not adequate to produce uniform test-section flow.

A somewhat more sophisticated adaptive method was then used to find the required loss coefficient distribution. In this procedure, the centerline value of screen loss is increased in small steps to the final value of 1.6 (the single screen value). At each step a converged solution is obtained. The velocity distribution thus obtained is used to determine the screen-loss distribution necessary to generate constant pressure drop across the width of the inlet with the centerline value incremented to the next step. A new solution is then obtained using this loss distribution and the process is repeated until the desired centerline loss coefficient is reached. By taking small enough steps the correct distribution can be found. Taking 100 steps resulted in only 0.06% variation in dynamic pressure over the center 80% of the test section. The dynamic pressure variation for this case is shown in figure 27 along with the distributions for constant loss coefficient and for the simple estimate. The loss coefficient distribution required for uniform flow is shown in figure 28. The simple estimate is also shown in figure 28 for comparison. The optimized distribution is very different than the first estimate, requiring a loss coefficient of more than 70 near the walls (considerably larger than the scale of the figure) compared with only about 4.5 for the simple estimate.

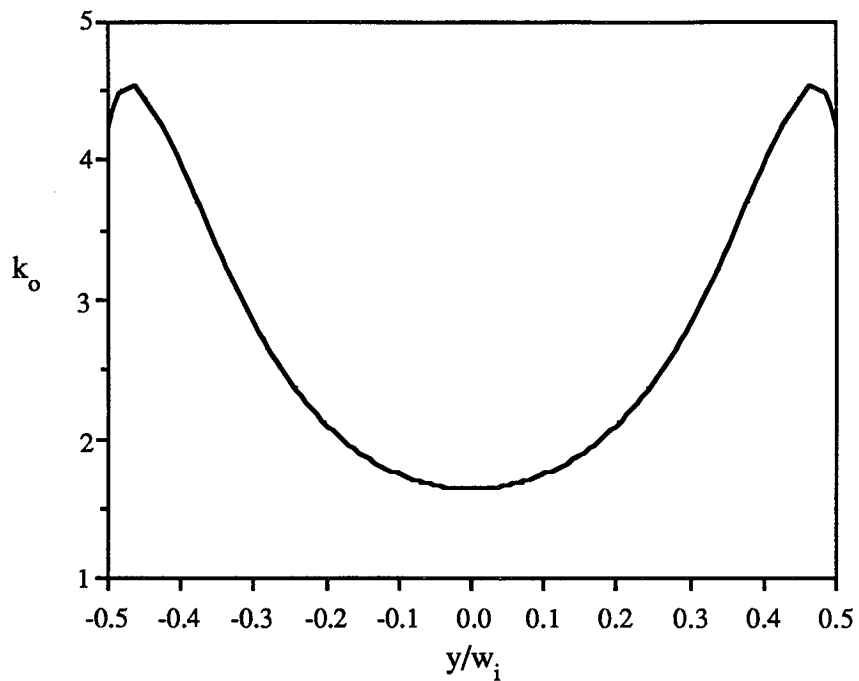


Figure 25. Simple estimate of the loss coefficient distribution necessary to provide uniform test-section dynamic pressure

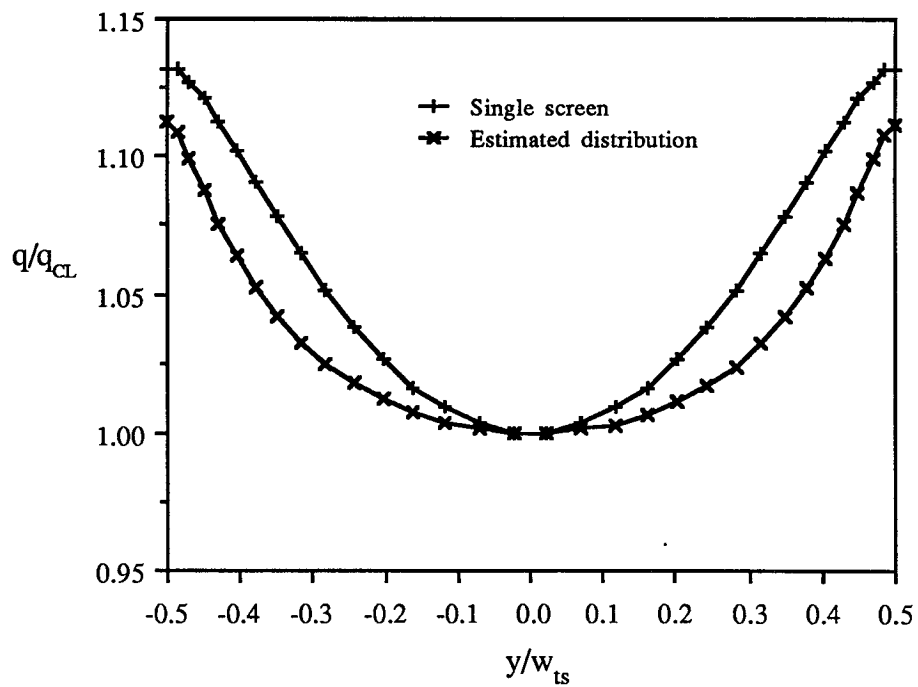


Figure 26. Comparison of the calculated test-section dynamic pressure distributions for a uniform single screen and for the estimated variable loss coefficient distribution

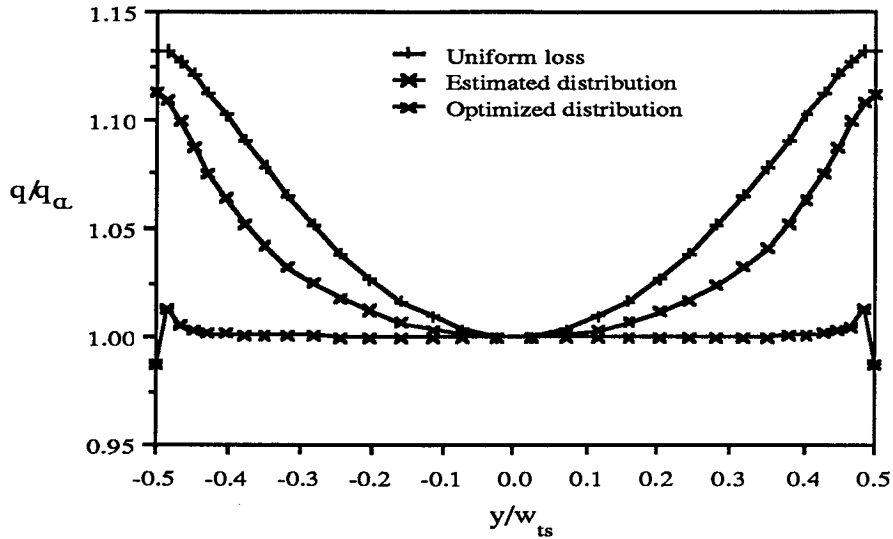


Figure 27. Comparison of the calculated test-section dynamic pressure distributions for a uniform single screen, the estimated variable loss coefficient distribution, and the "optimized" loss distribution

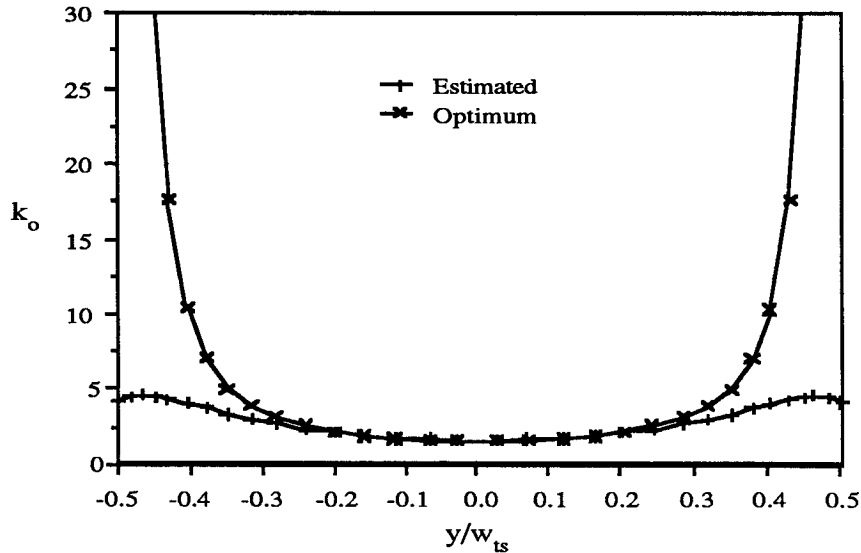


Figure 28. Comparison of the loss coefficient distributions necessary to produce uniform test-section dynamic pressure as determined by a simple estimate and by "optimization"

A continuously variable screen loss (not to mention a loss coefficient of 70) is not easily achieved in practice. Therefore, a calculation was made using stepwise increments in the loss coefficient. This type of loss coefficient distribution could be achieved by adding more layers of screen toward the walls of the inlet. One such stepwise distribution is shown in figure 29 along with the optimized distribution. The resulting test-section dynamic pressure distribution is shown in figure 30 in comparison with the distributions for the optimized screen and the simple estimate. The stepwise loss distribution results in a very jagged dynamic pressure distribution. The general character of the distribution, however, is fairly flat. It

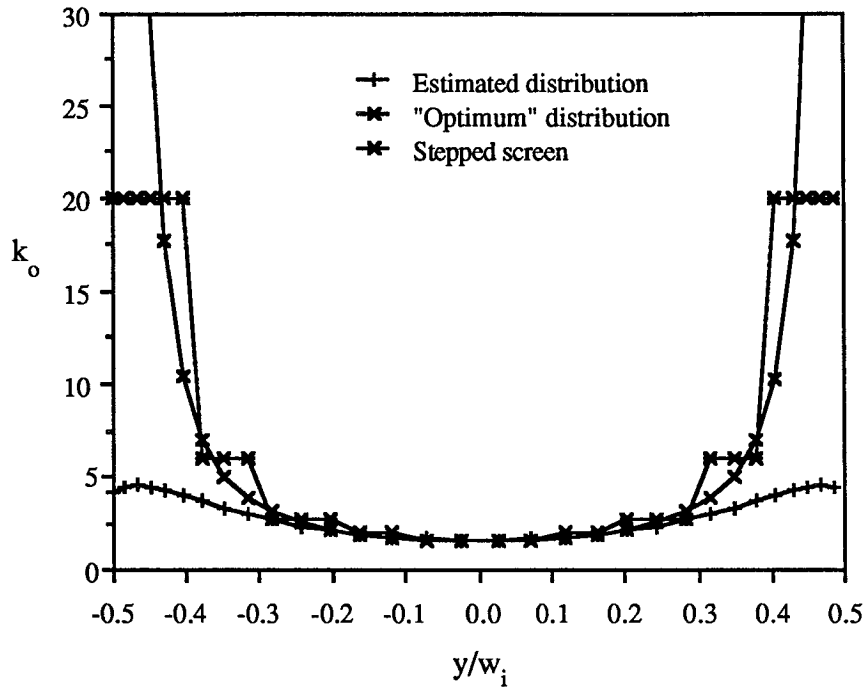


Figure 29. Comparison of the "optimum", estimated, and stepped loss coefficient distributions designed to provide uniform test-section dynamic pressure

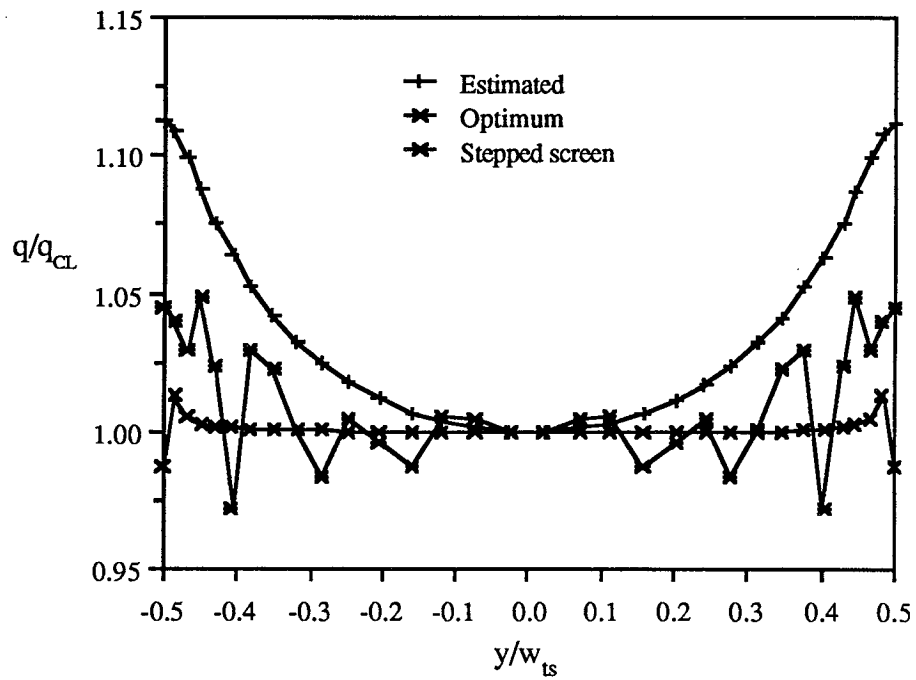


Figure 30. Comparison of the calculated test-section dynamic pressure distributions for the "optimized", estimated, and stepped loss coefficient distributions

should be possible, therefore, to achieve uniform test section flow if the loss coefficient distribution can be made sufficiently smooth. This method of obtaining uniform flow may be particularly useful for cases in which the screen is placed in a region of more uniform flow than was examined in the present study.

A method of producing uniform flow which, at first glance, seems to have merit is to locate the screen along a line of constant velocity. Unfortunately, the pressure drop through the screen depends not only on the flow velocity but also on the angle of onset relative to the screen normal. Determining the curve along which the screen produces uniform pressure drop is therefore a difficult task. In practice it is also much more difficult to install a screen along a curve than it is to hang it in a straight line.

Geometric Variations

The effects of various geometric parameters on the flow uniformity at the inlet plane of 2-D and axisymmetric contractions in ducts were calculated by Morel (refs. 15, 16). The parameters examined in these studies were contraction ratio, match point, and the length of the contraction. The same geometric variations were performed in the present study. In addition, the effect of a straight duct between the inlet cowl and the start of the contraction was studied. The purpose of this part of the study is to show some of the effects of these variations on test section flow uniformity when screens are present in the inlet. The intent of this report is not to provide detailed design charts, but rather to show general trends. The analysis method could, however, be used as part of the design process of wind tunnel inlets to demonstrate trade-offs for a particular design.

Contraction ratio

The contraction ratio of an inlet can have a large influence on the flow uniformity in the test section for a given screen loss coefficient and screen location. The effect of the contraction ratio on test-section flow uniformity is shown in figure 31. The contraction shape for these calculations was a matched cubic with the match point at 0.2 times the inlet width from the start of the contraction ($x_m/L = 0.2$) and a length of 0.5 times the inlet width ($L/w_i = 0.5$). The effect of contraction ratio is quite dramatic with a maximum flow distortion produced by $c = 2$. The $q/q_{c1}|_{80\%}$ parameter plotted in the figure is simply the maximum variation of the dynamic pressure across the center 80% of the test section divided by the dynamic pressure at the centerline. For $c > 2$, the dynamic pressure distortion decreases rapidly from the peak of 1.64 for $c = 2$ to 1.1 for $c = 8$.

This result is consistent with references 15 and 16 which state that a large contraction ratio provides more uniform velocity distributions at the both the inlet and exit than does a small contraction ratio. Since large inlets are expensive to fabricate, compromises are usually made in the design of large wind tunnels which general result in a smaller than desired contraction ratio. In figure 31, it is apparent that there is diminishing return for increasing c . The improvement in uniformity is much more rapid from $c = 2$ to 4 than from 4 to 8. The length of the contraction also has an effect on this behavior. Other factors may also dictate a large contraction ratio for a given facility, for example, low-turbulence-intensity requirements for the types of testing to be done and low power consumption by the inlet treatment to increase the maximum test section velocity for a given drive system.

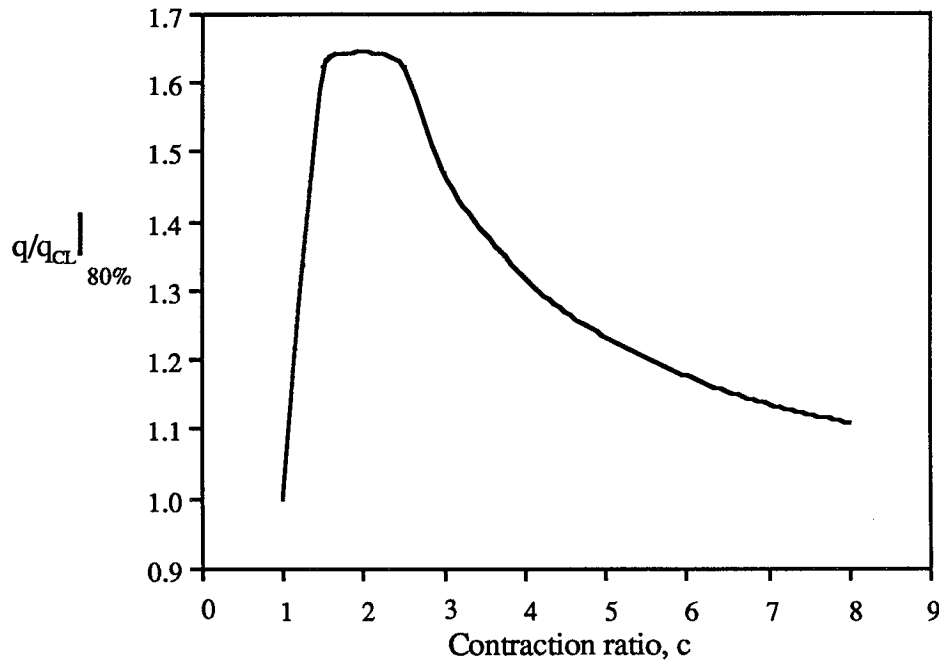


Figure 31. Effect of the contraction ratio on the magnitude of the test-section dynamic pressure nonuniformity. $x_m/L = 0.2$; $L/w_i = 0.5$; 5 screens

The effect of loss coefficient on three inlets with different contraction ratios is shown in figure 32. Contraction ratios of 1, 4, and 8 were chosen for this comparison. For these cases, $c = 1$ produces the least flow distortion and $c = 4$ the most. The $c = 1$ case is interesting in that the sense of the distortion is opposite to that of the other cases studied. That is, the flow near the walls is slower than the centerline flow except for the five-screen case which shows no distortion. This was the only geometry examined for which the addition of screens improved the velocity distribution. For this geometry, the flow distribution at the screen location is different from that generated by the larger contraction-ratio inlets. The velocity in the inlet is higher near the walls than at the center resulting in a larger pressure drop and lower dynamic pressure in the test section near the walls. The streamline patterns in figure 33 give an indication of the reason for the decrease in flow distortion with the addition of five screens. Compared to the no screen case, the streamlines for the five-screen calculation show the flow redirected more toward the center of the inlet producing a more uniform velocity distribution. The more uniform velocity passing through the screen produces in less flow distortion in the test section.

Constant width duct

The unique behavior of the unit contraction ratio geometry can be used to improve the performance of a wind tunnel inlet by attaching a constant area duct onto the inlet. The screens can then be positioned farther upstream of the start of the contraction in a region of more uniform flow. A sketch of the resulting inlet shape is shown in figure 34. A parametric study of this type of inlet was performed by varying the length of the duct as well as the screen position in the duct. The general geometry and definitions are shown in the figure.

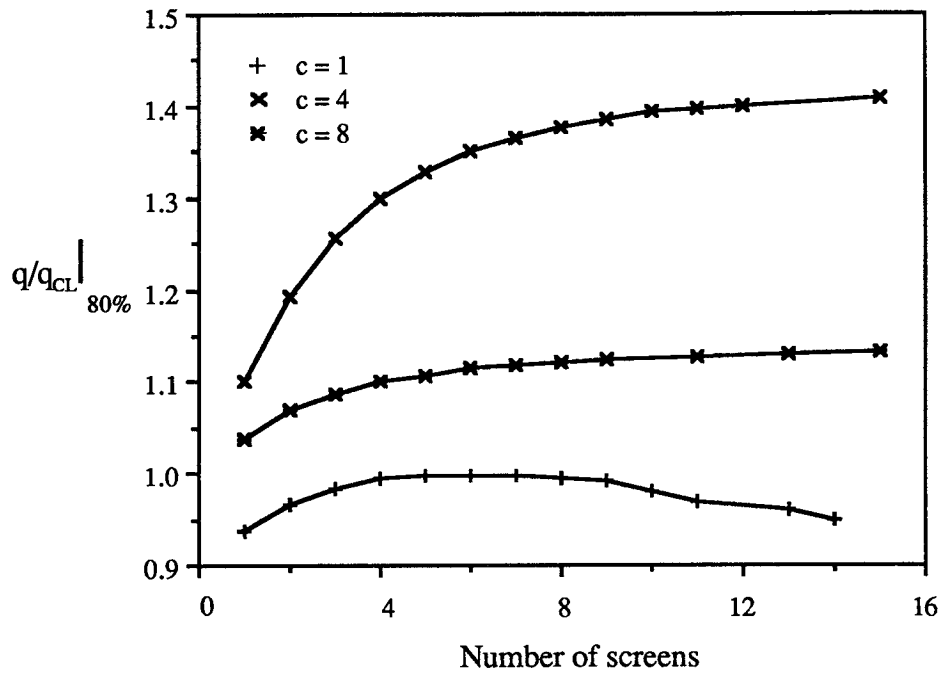


Figure 32. Effect of the contraction ratio and the number of screens on the magnitude of the test-section dynamic pressure nonuniformity. $x_m/L = 0.2$; $L/w_i = 0.5$

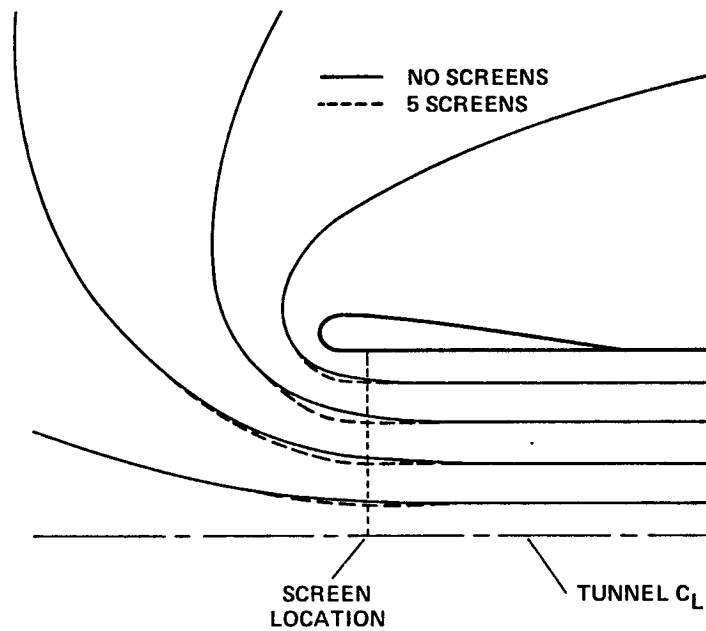


Figure 33. Effect of five screens on the calculated streamline paths for $c = 1.0$

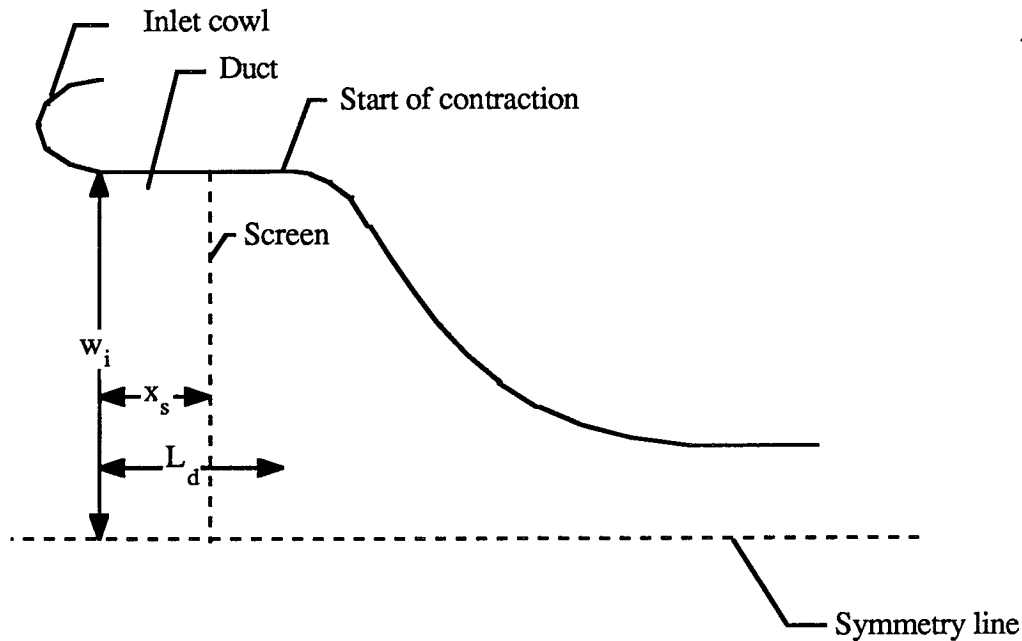


Figure 34. Geometry definitions for the inlet with a constant width duct upstream of the contraction

The effect of duct length is summarized in figure 35. Three different screen positions are shown in the figure; $x_s/L_d = 0, 0.5, \text{ and } 1.0$. The length of the duct has almost no effect when the screen is located immediately upstream of the contraction, $x_s/L_d = 1.0$. This position also gives the largest flow distortion. When the screen is moved to $x_s/L_d = 0.5$ or 0.0 the duct length has a noticeable effect. For $x_s/L_d = 0.0$ the distortion can be reduced to less than 1% if L_d/w_i is between 0.5 and 0.8. For longer ducts the distortion is increases again to greater than 1%. This tradeoff is caused by the interaction of the flow distributions induced by the flow around the cowl and by the contraction shape. When the duct is short, the flow through the screen (located just downstream of the cowl) is dominated by the contraction but is dominated by the cowl when the duct is long.

Another way to look at the effect of the duct is to keep the duct length constant and vary the screen position in the duct. The effect of this variation is shown in figure 36 for $L_d/w_i = 1.0$. There is almost no test-section dynamic pressure distortion as long as the screen is less than half-way from the cowl to the contraction. At $x_s/w_i = 0.5$ the distortion is approximately 1% and grows rapidly as x_s/L_d increases. These results indicate that some benefit may be found from the addition of a constant area section to an indraft wind tunnel inlet when the contraction ratio is smaller than desired as long as the screens are properly positioned in the duct. There are also implications for closed-circuit wind tunnels which employ anti-turbulence screens. These screens generally have a large total loss coefficient and can have an influence on the test-section flow uniformity if they are placed too close to the start of the contraction. The curve in figure 36 indicates that such screens should be placed at least 0.5 duct widths upstream of the start of the contraction for the geometry examined.

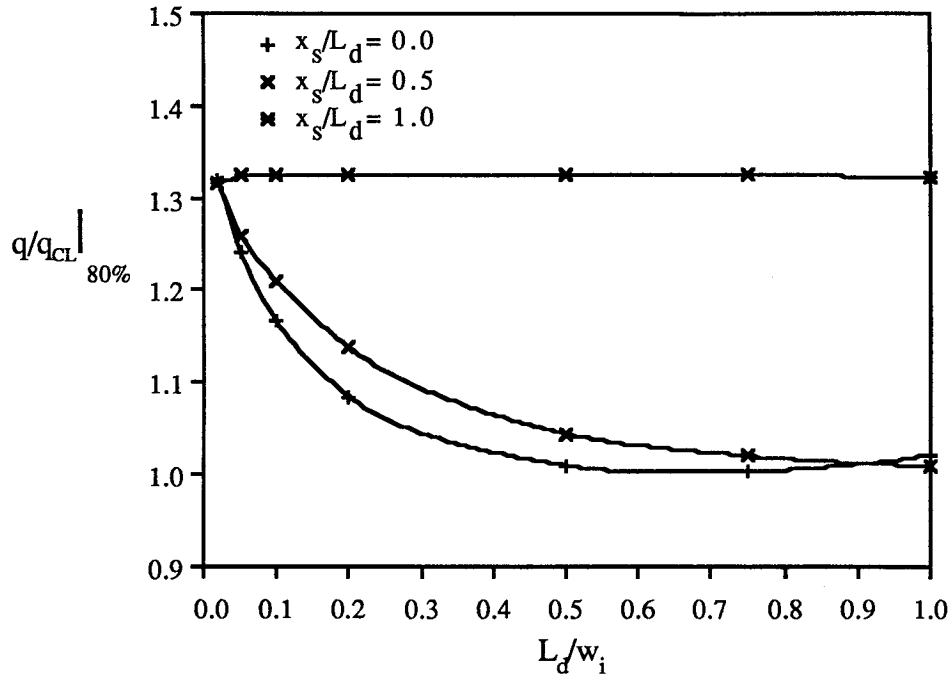


Figure 35. The effect of the upstream duct length, L_d/w_i , on the magnitude of the test-section dynamic pressure nonuniformity for various positions of the screen in the duct. $c = 4$; $x_m/L = 0.2$; five screens

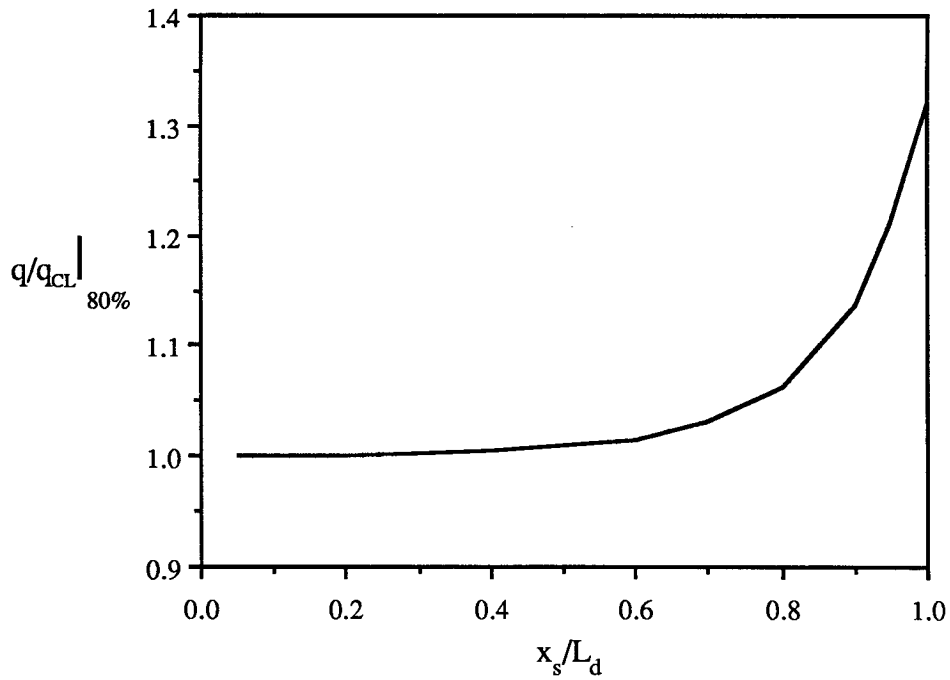


Figure 36. The effect of the position of the screen in the upstream duct on the magnitude of the test-section dynamic pressure nonuniformity. $c = 4$; $x_m/L = 0.2$; $L_d/w_i = 1.0$; five screens

Match point

The effect of the match point on the magnitude of the test-section dynamic pressure nonuniformity is summarized in figure 37 for $c = 4$ and 8 . The effect of moving the match point downstream is to reduce the amount of flow distortion at the screen location and, as a result, in the test section. This is in agreement with the results of references 15 and 16. Placing the match point near the beginning of the contraction results in rapid area change immediately upon entering the contraction. The rapid area change tends to slow the fluid near the walls and accelerate the fluid near the center. The net result when screens are placed in the inlet is a large variation in dynamic pressure in the test section. Moving the match point downstream reduces the inlet flow nonuniformity; the area change at the start is not as rapid so the flow is more uniform and the test-section dynamic pressure is more uniform as a result. This analysis does not include the effect of the match point on the wall boundary-layer thickness. Several researchers have shown that regions of high curvature near either end of the contraction result in thickened boundary layers, and if the curvature is too high, separation may occur. Careful attention must be paid to this particular effect in the design of any inlet or contraction.

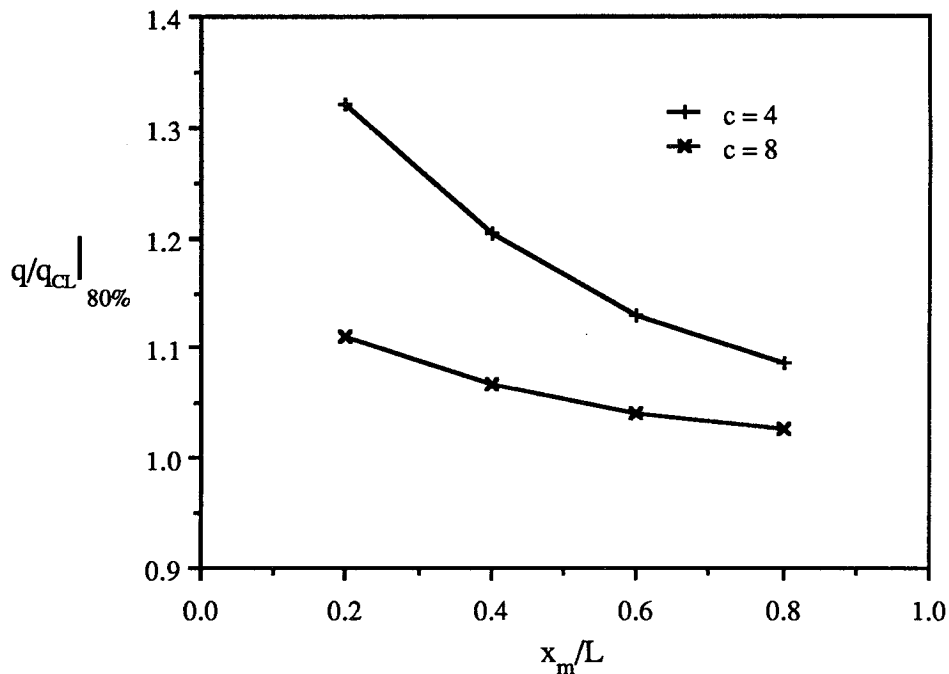


Figure 37. The effect of the match point, x_m/L , on the magnitude of the test-section dynamic pressure nonuniformity for $c = 4$ and $c = 8$. $L/w_i = 0.5$; five screens

Contraction length

The effect of contraction length on flow uniformity is shown in figure 38 for $c = 4$ and 8 . Longer inlets have less rapid area changes at the start for a given match point location, and therefore have a more uniform inlet flow distribution. This results in more uniform test-section dynamic pressure. The 8:1 contraction had less than 1% distortion in test section "q" when the length was twice the inlet width. It is often impractical to build inlets this long and a penalty arises from the additional boundary-layer growth which occurs. For this reason, very long inlets are not usually built.

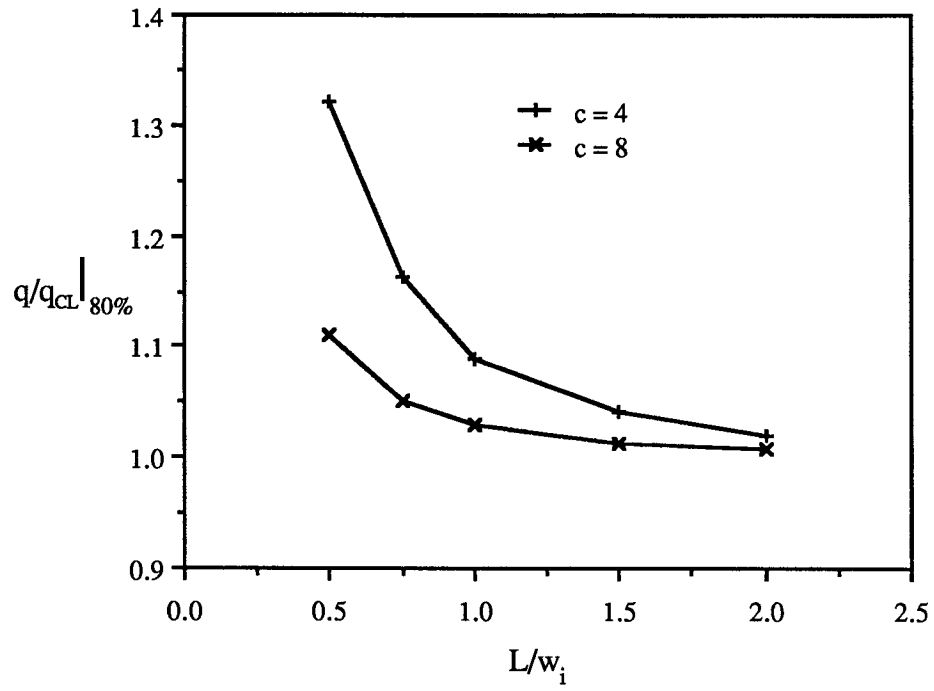


Figure 38. The effect of the inlet length, L/w_i , on the magnitude of the test-section dynamic pressure nonuniformity for $c = 4$ and $c = 8$. $x_m/L = 0.2$; five screens

CHAPTER 5. INLET CASCADE

In Chap. 4 it was shown that the turning of the flow by a screen located in an inlet can significantly modify the inlet velocity distribution. Flow turning may also be achieved by employing a cascade in the inlet, upstream of the required anti-turbulence screens. It should therefore be possible to manipulate the flow passing through the screen in order to obtain uniform test section velocity. The successful application of this concept could significantly reduce the size requirement for wind tunnel inlets since the nonuniform flow produced by a small inlet would be alleviated by the inlet cascade.

The cascade concept is shown in figure 39a. The flow direction at the inlet is shown both with and without the cascade present. The flow is redirected by the vanes to travel in a different direction downstream of the cascade than it would if the vanes were not present. In the example shown, the vanes redirect the flow toward the center of the inlet. To illustrate the concept the lift generating vanes in figure 39a can be represented by point vortices at the vane locations as shown in figure 39b. The net effect of the vanes in this particular example, is to slow the flow near the center of the inlet and accelerate it near the walls. This redistribution of the flow can have a large effect on the test-section flow uniformity if there is a screen located downstream of the cascade. By tailoring the cascade to provide uniform pressure drop through the screen across the width of the inlet, the test-section flow can be made uniform. To examine the practicality of the inlet cascade concept an analysis method was developed which could predict the performance of an inlet cascade. The details of the analysis method are presented in the next section and, somewhat more briefly, in Appendix B.

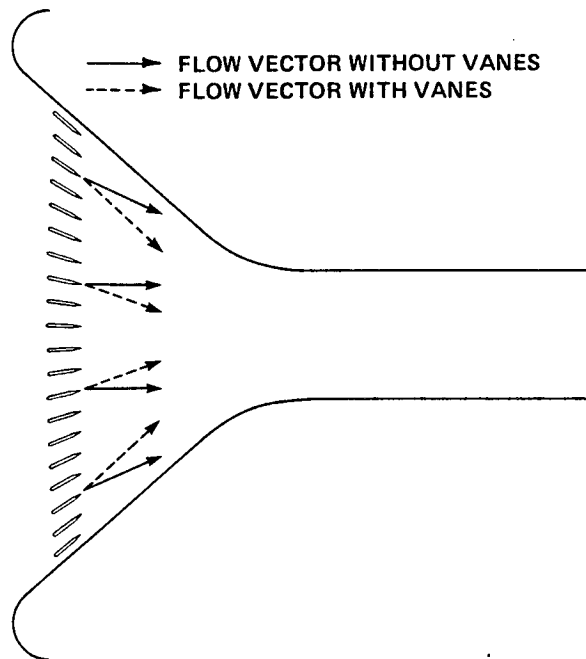


Figure 39a. Qualitative effect of a cascade on the direction of the flow in the inlet of an indraft wind tunnel

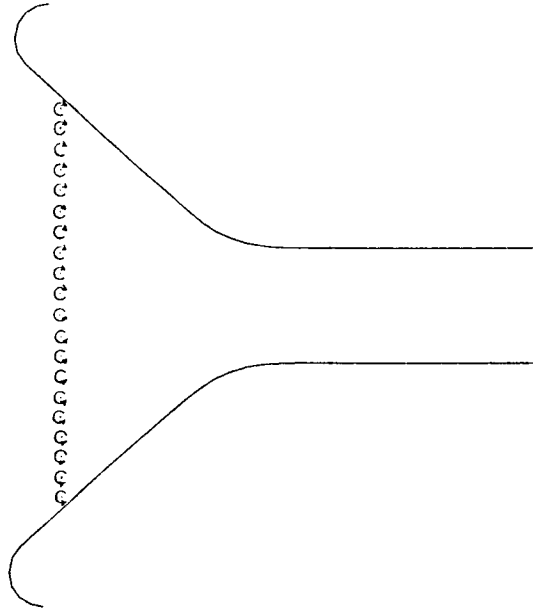


Figure 39b. Point vortex analogy for the vanes in an inlet cascade

Cascade Analysis

It is possible to use the analysis method presented Chap. 3 to calculate the performance of an inlet cascade. This would require that the cascade included as an actuator disk, similar to the way the screen was simulated. In such an approach the flow turning would take place at individual grid points in the calculation. The desired exit angle from the cascade would be specified. The proper stream function gradient imposed to accomplish the required turning is given by:

$$v = - \frac{\partial \Psi}{\partial x} = u \tan \theta$$

where θ is the desired outflow angle and v is the transverse velocity required to achieve the desired outflow angle. The cascade actuator disk would have to be placed one grid station upstream of the screen location so that the screen turning would also be included. The interaction of the two closely coupled actuator disks may prevent accurate prediction of the cascade performance. Due to this uncertainty an alternative approach was taken. In keeping with the simpler is better philosophy of computational aerodynamics a well-tested potential flow program was employed along with an empirical model of the screen effects.

Flow through cascades can be accurately modeled using panel methods. The theory of panel methods is well covered in the literature (refs. 24-26). Briefly, the basic idea is to model bodies by superposition of source and doublet distributions on the body surface. The singularity distribution results from the satisfaction of the zero normal flow boundary condition imposed on the body. In practice, the boundary condition is satisfied at a limited number of points on the body called control points. Each control point is associated with a panel of unknown singularity strength (source, doublet, or both). If there are n control points there are also n unknown singularity strength. The system of equations is solved to obtain the singularity strengths. Once the individual singularity strengths are known, the velocity at any point in the flowfield may be calculated by superposition.

In the present application, the panel method has a major drawback; it is a potential flow method and, as such, cannot model the rotational flow produced by a screen. An empirical model of the screen effects was therefore included in the calculations resulting in an accurate simulation of the entire flowfield.

Potential flow cascade calculation

A simple inlet cascade is shown in figure 40. The panel code HILIFT (ref. 25) was used to model the inlet and cascade. Flow through the tunnel is established by specifying a normal velocity on each of the panels which close off the downstream end of the test section. The normal velocity is obtained by the proper distribution of sinks on each of these panels. The free-stream velocity is set to zero so that only the induced flow of the sinks is present. This simulates the flow into an indraft tunnel located in quiescent surroundings. The velocity can be calculated at any point in the flow field. For the present work, the velocity of the flow at the screen location is of primary interest. The magnitude and direction of the flow at the points along the velocity survey line shown in figure 40 are used to predict the pressure drop induced by the screen.

The effectiveness of a cascade in redirecting the flow in the inlet is shown in the streamline plots of figure 41. Calculated streamline paths are shown for cases both with and without the inlet cascade. The effect of the cascade in this example is to accelerate the flow near the walls relative to the empty inlet flow.

Total pressure determination

The pressure drop at discrete points along the survey line is calculated using the method described in Chap. 3. Since the total pressure cannot vary in a potential flow calculation, the total pressure distribution determined at the screen location by (23) for the flow conditions determined by the panel code calculation is simply transformed to a test section coordinate system by conservation of mass. This is equivalent to the convection of total pressure which was included in the screen analysis of Chap. 3. The transformation is given by:

ORIGINAL PAGE IS
OF POOR QUALITY

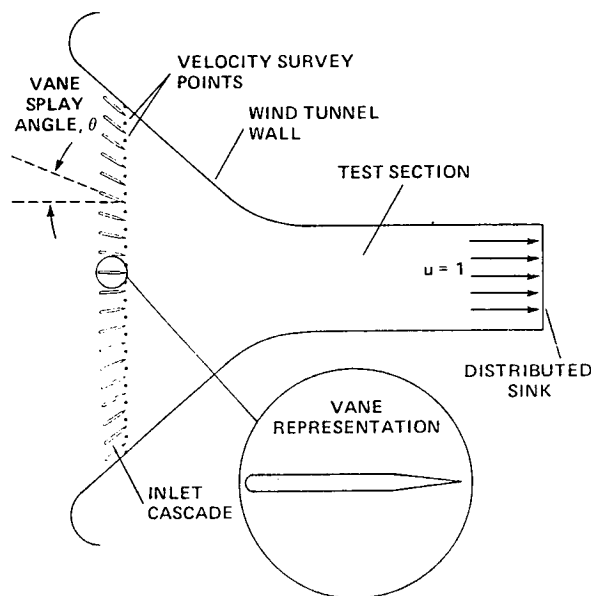


Figure 40. Geometry of the tunnel with an inlet cascade as modelled in the 2-D panel code calculation

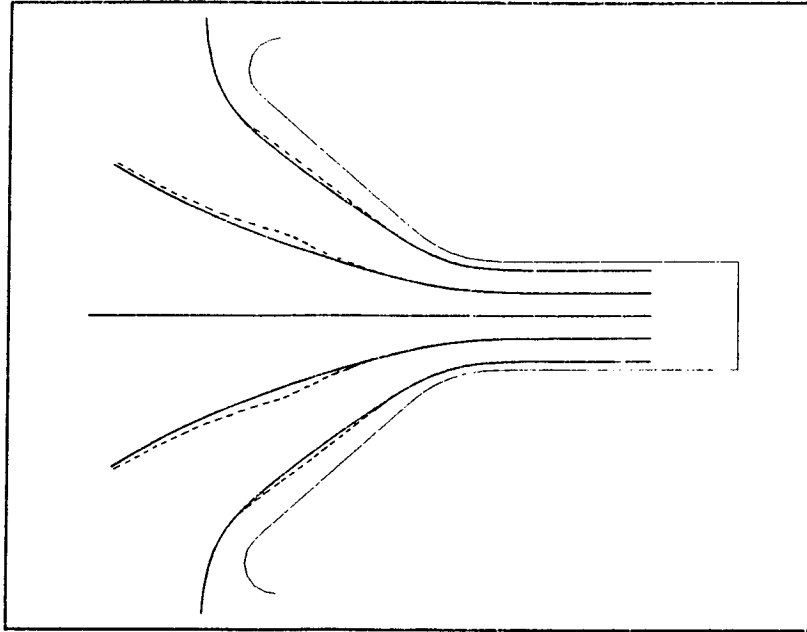


Figure 41. Comparison of the calculated streamline paths with and without the inlet cascade

$$c \int_{-0.5}^{\eta_i} u_i d\eta_i' = \int_{-0.5}^{\eta_{ts}} u_{ts} d\eta_{ts}'$$

where $\eta_i = \frac{y}{w_i}$

and $\eta_{ts} = \frac{y}{w_{ts}}$

The value of η_i is known from the location on the survey line. The total pressure at each of the η_i was then assigned to the corresponding η_{ts} value. In this transformation, the value of u_{ts} is a constant determined by the sink strength in the HILIFT calculation. This is not the case when the total pressure varies across the width of the test section. The error resulting from this assumption will be larger for cases with large variation in test-section total pressure than if the pressure drop through the screen is made uniform. Since the goal of the inlet design is to generate uniform test-section flow, the transformation is valid when the design goal is met. The integration was performed using the trapezoidal rule. After integrating to find all of the corresponding values of η_{ts} , a cumulative error of approximately 3% of the test-section width was found. Rather than using a more sophisticated integration scheme, the values of η_{ts} were simply rescaled to range from -0.5 to 0.5.

Simulation of screen turning

The screen itself was not simulated directly in the potential flow calculation so the turning effect of the screen had to be included in another manner. The simplest way to include screen turning was to deflect the trailing edge of each vane by the amount of screen turning expected for the particular onset angle and screen loss coefficient (ref. 49). Several methods have been proposed to empirically predict the turning angle of flow through screens (refs. 34, 42, and 47). Taylor and Batchelor (ref. 42) present

results from tests of various screens which indicates that the ratio ϕ/θ is constant for a screen of given loss coefficient. They present an empirical formula to calculate this constant as:

$$\frac{\phi}{\theta} = \frac{1.1}{\sqrt{1 + k_o}}$$

The angle ϕ is the outflow angle and θ is the onset angle. Both angles are measured with respect to the normal vector of the screen. This simple result makes the calculation of the screen-turning angle relatively easy if the constant of proportionality is known. For the screen used in the experimental work of the present study, (26) gives this ratio a value of 0.74. The experimental investigation described in reference 49 gives a value $\phi/\theta = 0.8$ which is in good agreement with the empirical equation. The turning angle is therefore taken to be 0.2 times the onset angle as indicated by the experimental data cited. The onset angle in the potential flow calculation was taken to be equal to the angle of the vane relative to the tunnel center-line (before the trailing-edge deflection). The panelled representation of a vane with and without trailing-edge deflection are shown in figure 42.

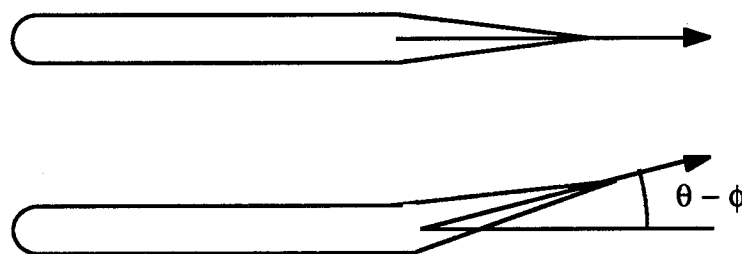


Figure 42. Details of the vane geometry in the potential flow calculation shown with and without trailing-edge deflection simulating screen turning

Effect of Kutta condition

The predicted dynamic pressure distributions from two calculations are shown in figure 43. The curve without symbols was generated using field velocities calculated at 100 points along a line located 2% of a vane chord downstream of the vane trailing edges.

The waviness in this curve is caused by the Kutta condition which is applied at airfoil trailing edges in the potential flow calculation in order to generate the correct lift. The condition specified in HILIFT is that the potential at the trailing edge is zero on both the upper and lower surfaces. This satisfies the condition of zero vorticity at the trailing edge. The predicted lift using this condition is quite accurate, however, the local velocity field is not the same as exists for a real airfoil. The potential-flow Kutta condition results in stagnation at the trailing-edge point. The calculated flow in the vicinity of the trailing edge is therefore different from that which exists in an actual flow where the trailing-edge condition is that the velocity on upper and lower surfaces are equal. The panel code, therefore, calculates lower velocities near the trailing edge than occur in real flows.

This low calculated velocity near the trailing edges of the vanes causes the local pressure drop through the screen to be underpredicted. The peaks in the dynamic pressure distribution of figure 43 then correspond to the low calculated velocity behind the trailing edge of each vane. A better prediction of the pressure drop would be obtained if some sort of average velocity between vane trailing edges was used in the estimate. A simpler solution is to use the predicted velocity at the midpoint between adjacent vanes. Using the midpoint velocity should not degrade the accuracy of the predicted test-section distributions. The curve with symbols in figure 43 shows the result of using only the mid-points in the analysis. The

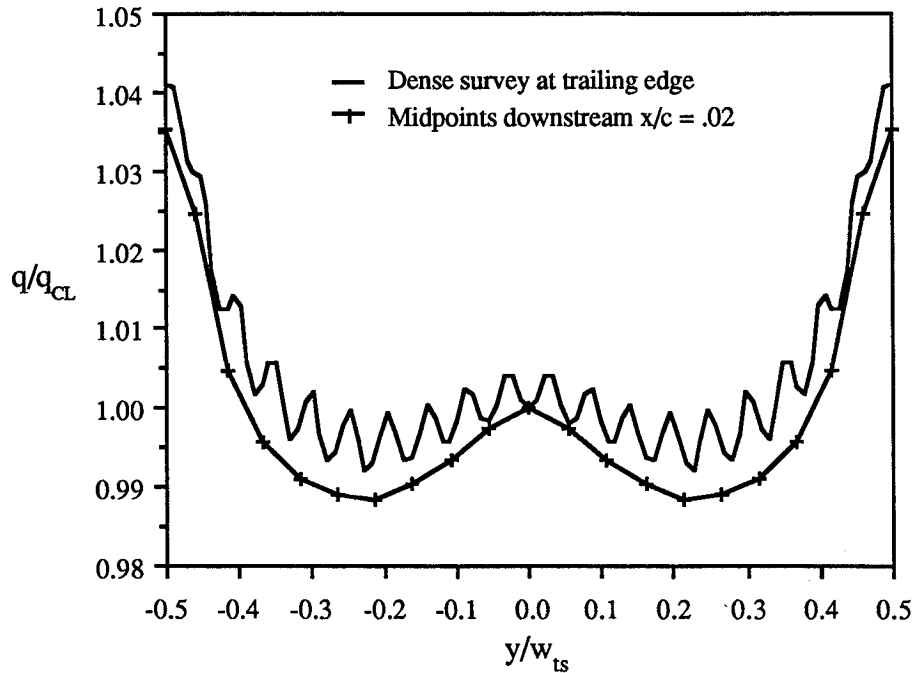


Figure 43. Demonstration of the effect of the potential flow Kutta condition on the calculated test-section dynamic pressure distribution

small change in the shape of the curve is due to repositioning the survey line to lie along the actual screen position which was along a line connecting the vane trailing edges.

Sample calculations

The primary variable which determines the cascade performance is the angle at which each of the vanes is set relative to the wind-tunnel centerline. This is referred to as the splay angle or splay distribution. With a little experience, it was possible to modify the splay distribution in such a way as to change the test section flow distribution in any desired manner. Three different splay distributions are shown in figure 44. The symbols represent the actual vane locations. Only the splay angles for positive values of y/w are shown. The curves are antisymmetric about $y/w_i = 0$. The curves were generated using a polynomial curve fit. Splay distributions were obtained by selecting up to six points through which the distribution was required to pass. This method of splay generation gave good control of the angle distribution and provided an automated means by which the splay angles could be supplied to the potential flow solver.

Calculated dynamic pressure distributions for the three splay distributions of figure 44 are shown in figure 45. The power of the cascade is apparent in the figure. By modifying the splay distribution almost any test-section dynamic pressure distribution could be obtained. Splay distribution "I" resulted in a predicted dynamic pressure distribution which varies less than 1% from the centerline value across more than 80% of the test-section width. Without the cascade the variation is approximately 10% from the centerline value over the same portion of the test section.

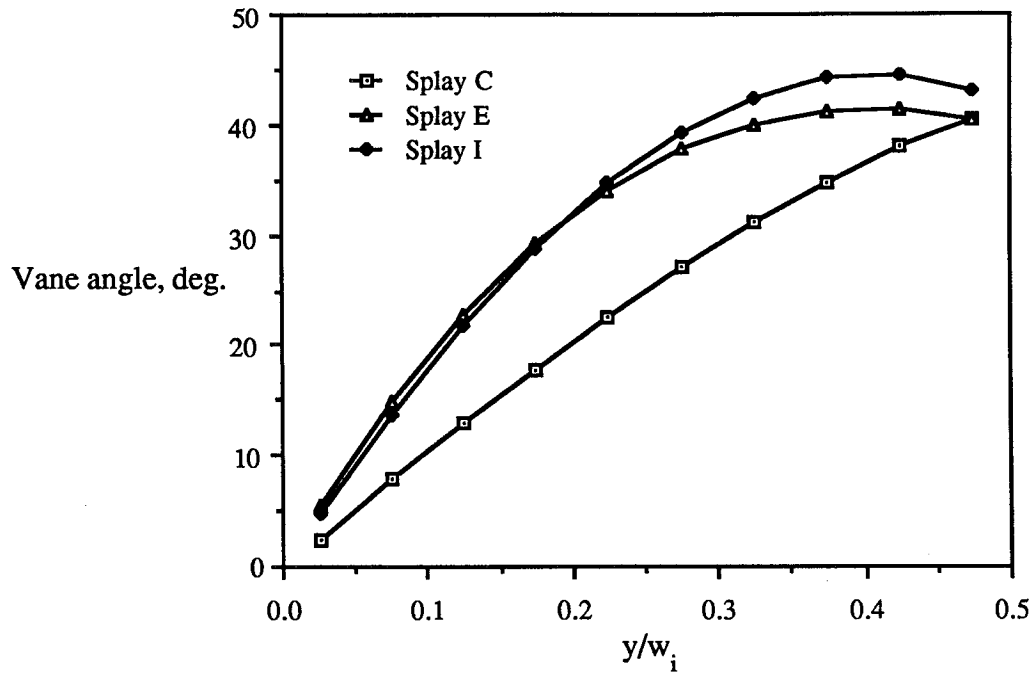


Figure 44. Comparison of several splay distributions used in both the numerical and experimental study of the inlet cascade

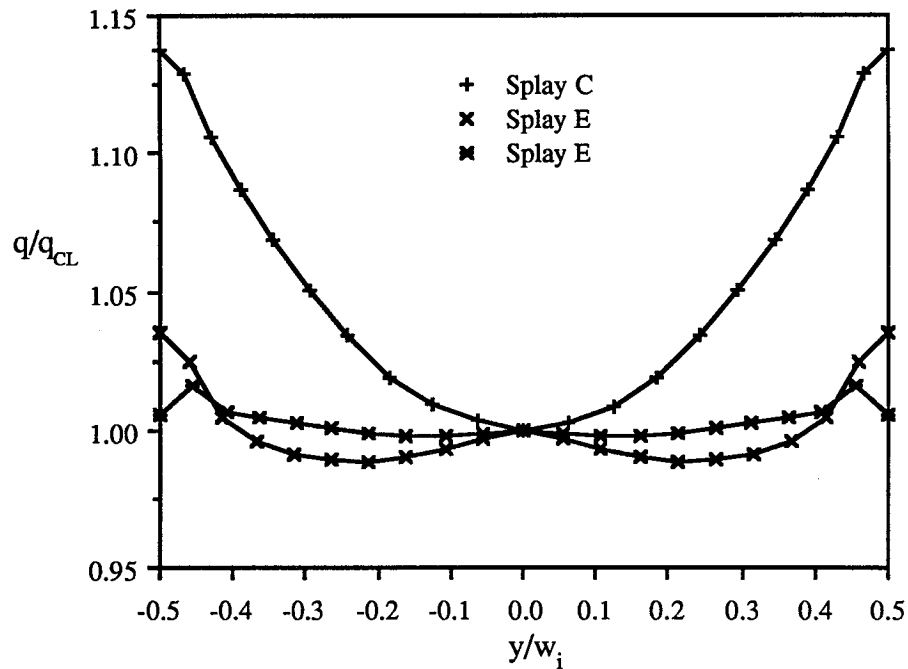


Figure 45. Effect of the vane splay distribution on the calculated test-section dynamic pressure distribution

The splay distribution labeled "C" in figure 44 was defined by positioning each vane at an angle equal to the angle of flow at the location of the vane trailing edge determined in a calculation which did not include the vanes. This case was used to examine the effect of including the actual cascade geometry in

the modeling. If the cascade were modeled as an actuator disk it would have no effect on the solution for splay distribution "C." When the cascade analysis was applied to the cases of no vanes and splay "C" a noticeable difference was found between the two solutions. Figure 46 shows the predicted test-section flow distributions for the two cases. The presence of the vanes increases the flow non-uniformity. It is apparent that the chord of the vanes has an effect in this case. Even though the trailing edges are pointed in the direction of the flow found in the no vane case, they still generate lift. Lift must be generated since the vanes are located in a region of curving flow. If the vanes are to carry no load and, hence, not change the results from the no vane calculation, each vane must be cambered to conform to the streamline which passes through its trailing-edge point in the no vane calculation. Since the vanes are uncambered they do generate a small amount of lift and therefore affect the flow distribution. It is, therefore, important to include the vanes in the modelling of an inlet cascade, particularly if the chord of the vanes is large compared to the radius of curvature of the streamlines entering the inlet.

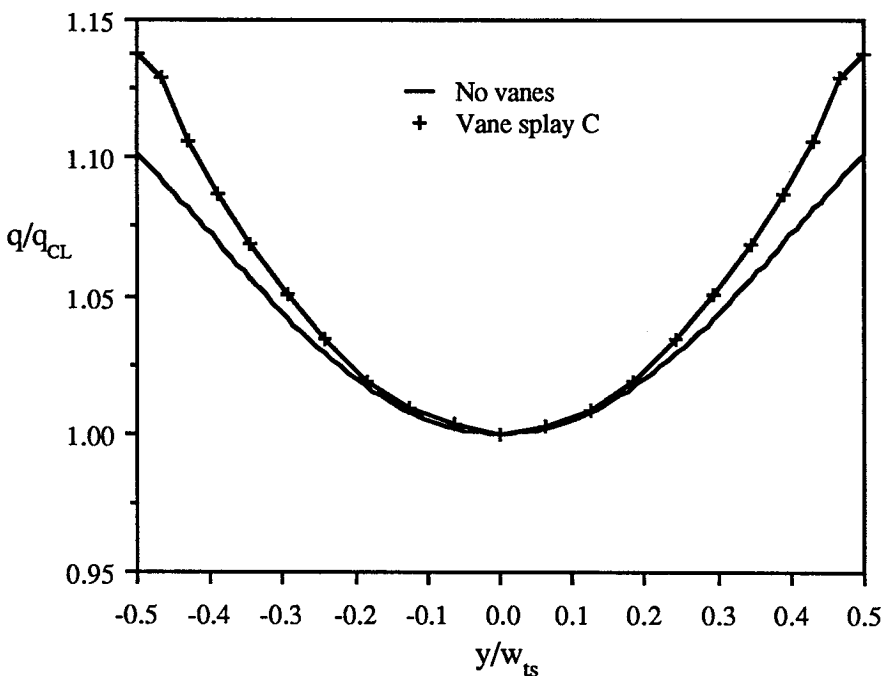


Figure 46. Comparison of the calculated dynamic pressure distributions for the cases of no vanes and vane splay "C."

Inlet Cascade Experiment

If the analysis method is to be used as a design tool it must be capable of accurately predicting actual test-section flow distributions. The test facility used in the inlet screen experiments described in Chap. 2 was modified to accept an inlet cascade with a single screen fastened to the trailing edges of the vanes. Photographs of the modified 2-D tunnel are shown in figures 47a, 47b, and 48. Figure 47a is a top view of the inlet without vanes. The shape of the inlet walls was changed from the matched cubic to a straight line tangent to the inlet cowl and the contraction near the entry to the test section. The cascade is easier to fit in an inlet of this shape than in a matched cubic type. This is the same geometry used in the analyses presented previously (see fig. 40). The inlet is shown in figure 47b with the vanes installed.

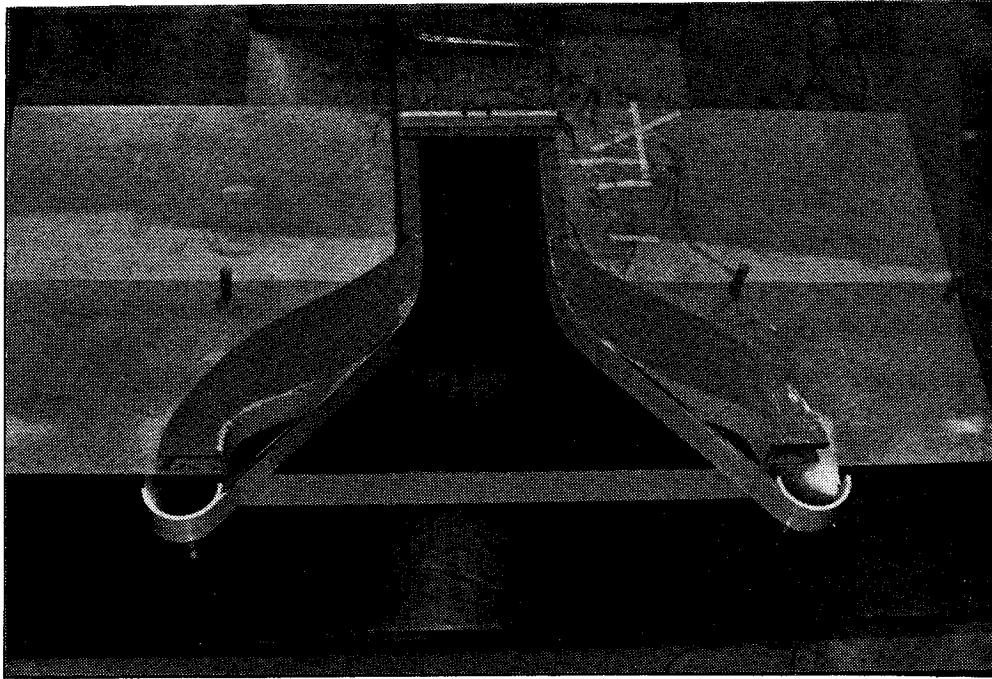


Figure 47a. Top view of the inlet showing the modified wall shape for the inlet cascade experiment

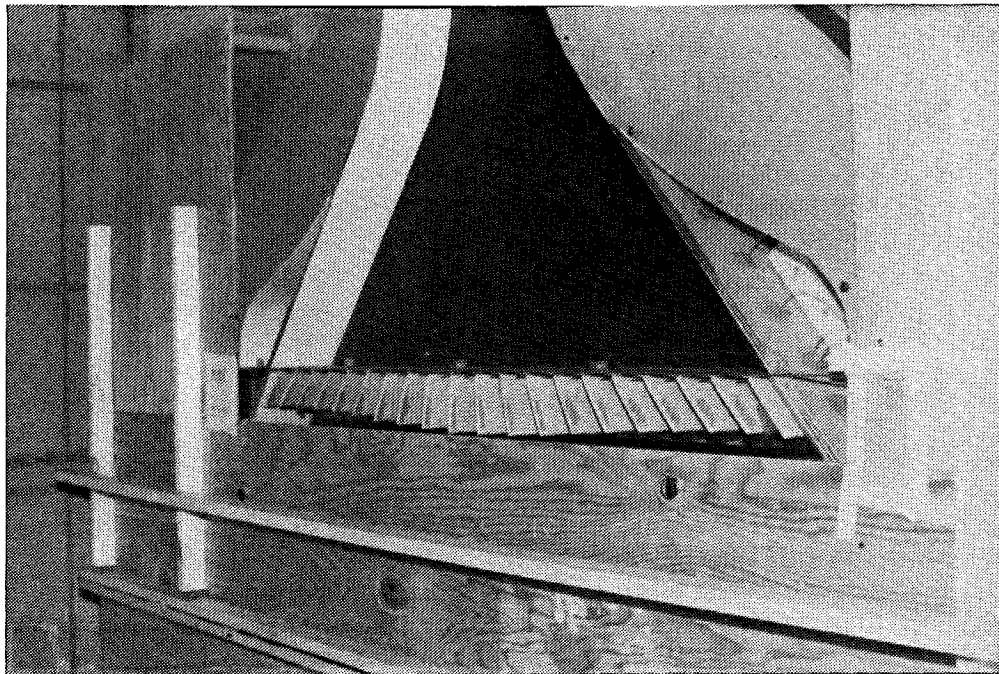


Figure 47b. Cascade installed in the inlet

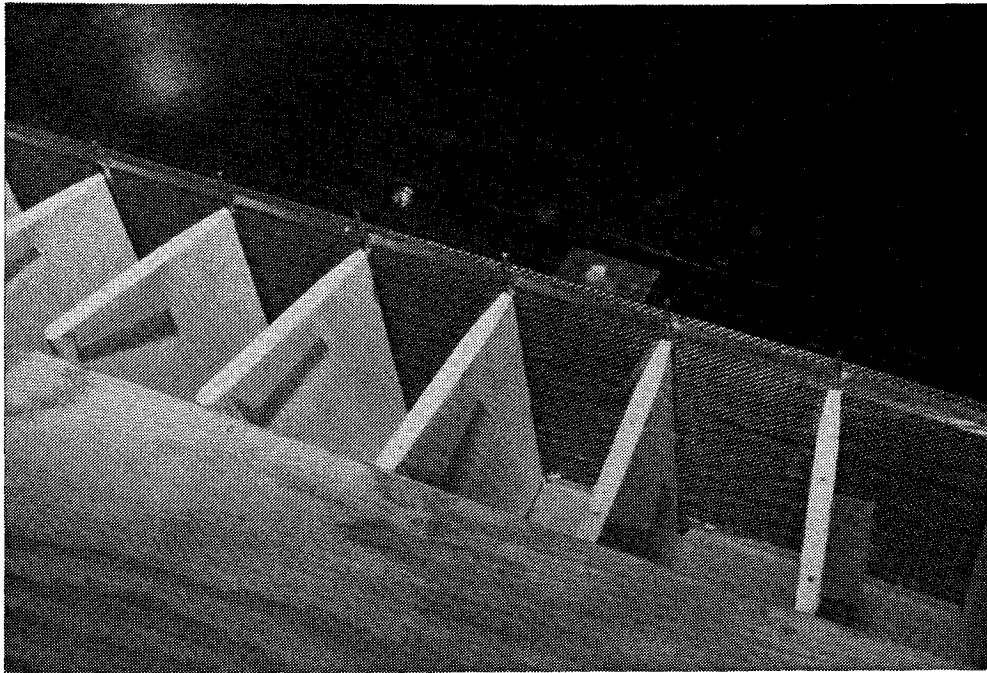


Figure 48. Details of vane installation showing the trailing edge pivots and the screen

Figure 48 shows the trailing edge of one of the vanes and the screen. The vanes are made of balsa wood and are pivoted at the trailing edge to allow easy adjustment of the splay angles. The pivot is provided by a 1/16 in. ID copper tube glued to the trailing edge. A pin passes through the plexiglas top and bottom plates of the tunnel and through the tube. The trailing edges are therefore rather blunt. This should pose no particular problem since only the outflow angle is important. The increase in drag caused by the blunt trailing edge should be negligible compared to the pressure drop of the screen. The tunnel was operated in exactly the same manner as during the previously described screen experiment. The data acquisition system from those tests was also used.

Comparison of Predictions and Experiment

The tunnel was tested with the screen but without the cascade to provide a simple test case for the analysis. A comparison of the predicted and measured test-section dynamic pressure distributions is shown in figure 49. A prediction from the screen analysis program is also presented. There is reasonably good agreement between all three distributions. The discrepancy between the cascade analysis and the screen analysis for $y/w_{ts} > .35$ is due to the lack of screen turning in the potential flow method since the vanes are not present. Near the tunnel centerline, the flow passes through the screen in a nearly perpendicular direction so there is no screen turning. When the vanes are present in the simulation, screen turning is modelled which improves the accuracy near the walls. The agreement with the experimental data is fairly good, however, particularly over the center 80% of the test section.

The cascade analysis was used to predict the performance of several splay distributions. Experimental results were also obtained for these distributions. Figures 50 - 52 present comparisons between the predicted and measured performance of the splay distributions in figure 44. The comparison is made for splay "C" in figure 50. In general the agreement is good particularly over the center 50% of the test section where the predicted and measured dynamic pressure ratios are within 0.5% of each other. The analysis, however, overpredicts the dynamic pressure near the edge of the boundary layer by approximately 3%. This is evidence of the inaccuracy of the transformation given in (25) since the flow is very nonuniform in the test section for this case. For splay distribution "E" in figure 51, the agreement is much

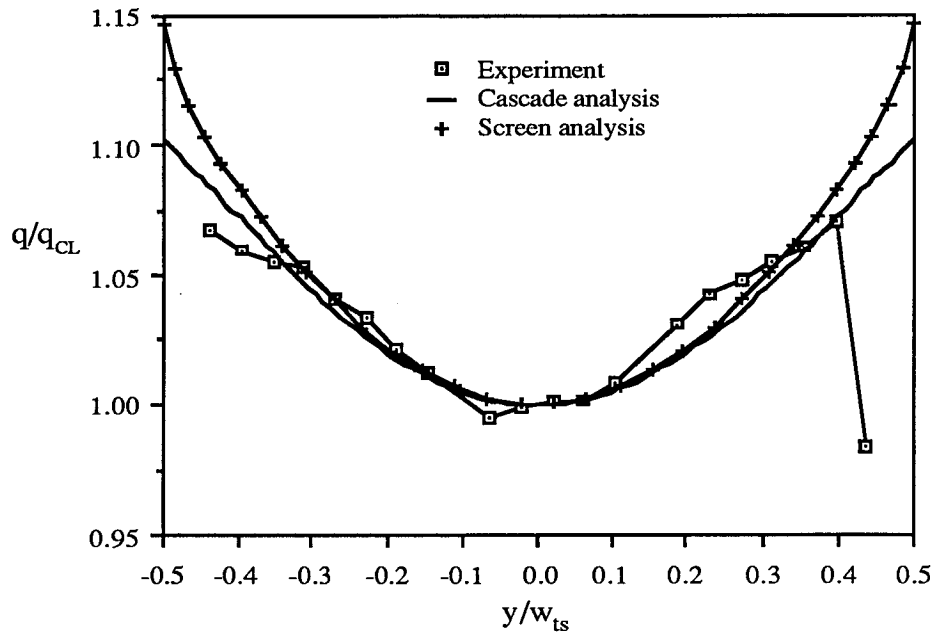


Figure 49. Comparison of the computational results with experimental measurements the test-section dynamic pressure distribution for the modified inlet shape with no vanes and one screen

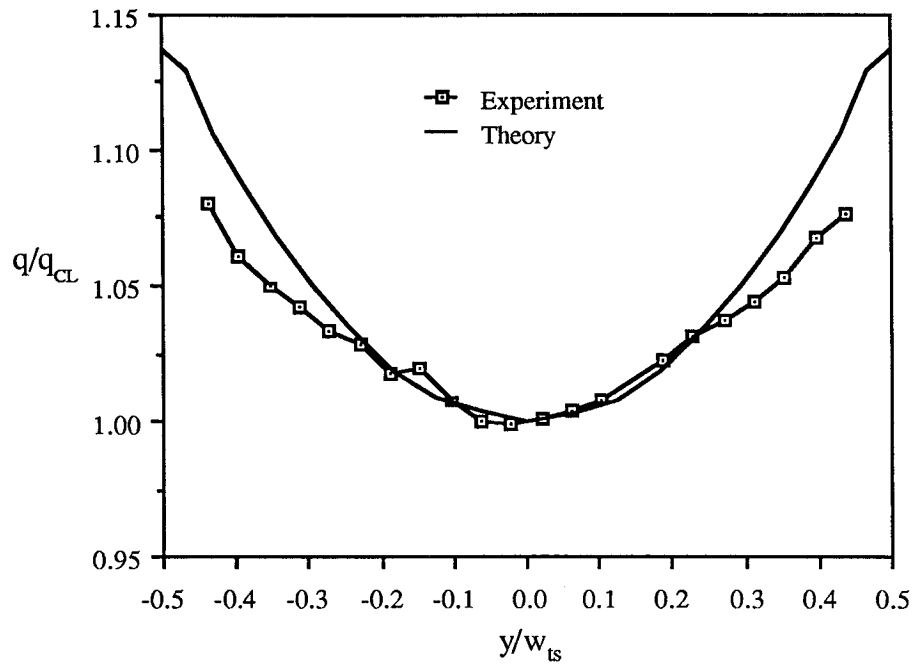


Figure 50. Comparison of the predicted and measured test-section dynamic pressure distributions for cascade splay configuration C

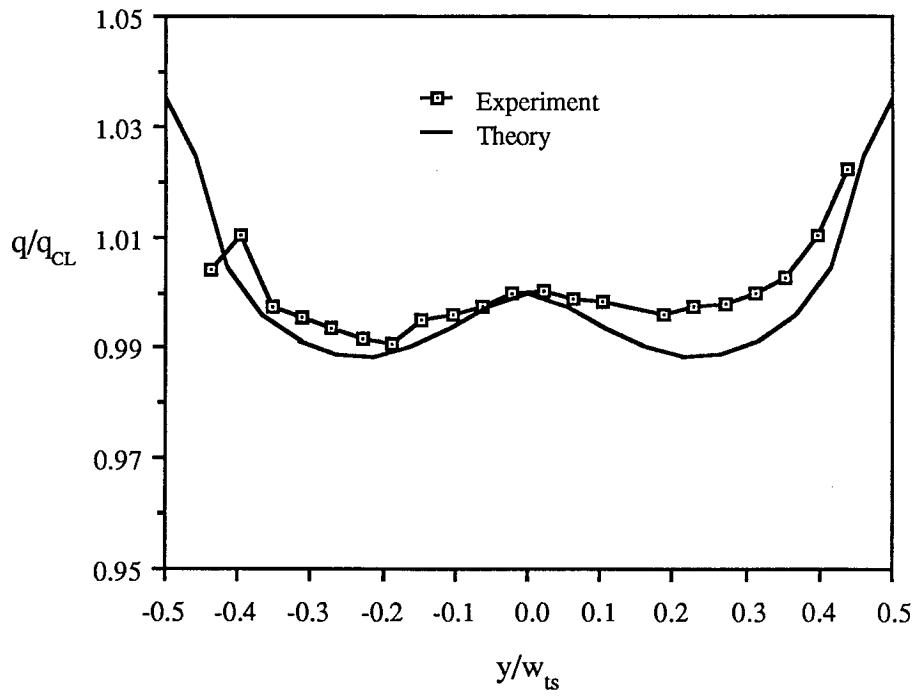


Figure 51. Comparison of the calculated and measured test-section dynamic pressure distributions for cascade splay configuration E

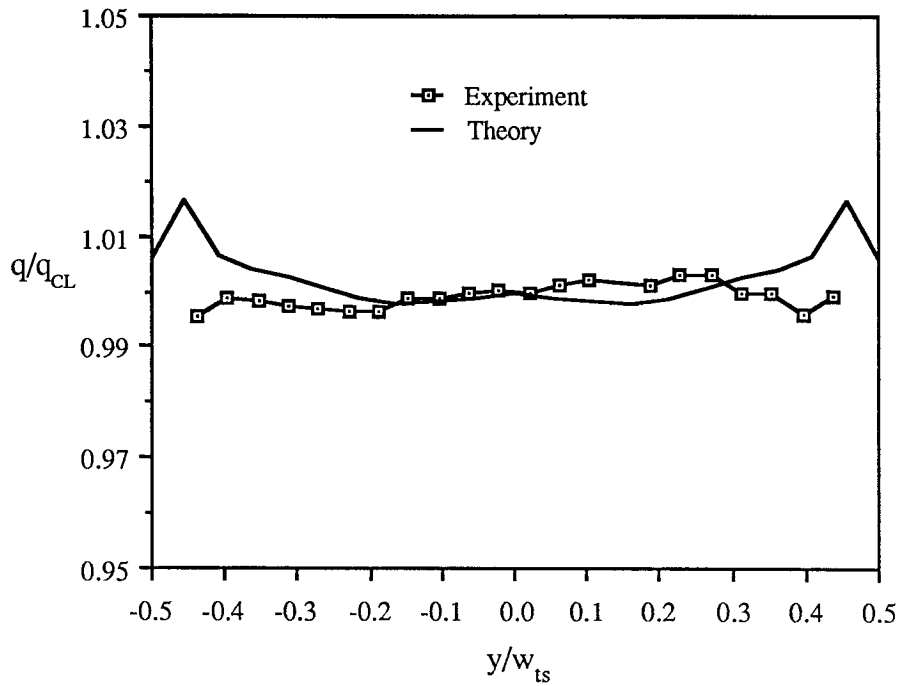


Figure 52. Comparison of the calculated and measured test-section dynamic pressure distributions for cascade splay configuration I

better since the flow is more uniform for this configuration (note the change in the vertical scale in relative to fig. 50). The difference between the prediction and measurements is no larger than 1% outside of the boundary layer. The asymmetry of the experimental data is also much more apparent for this configuration.

The use of splay distribution "I" (see fig. 44) was shown by the analysis to provide very nearly uniform test-section flow. The experimental data support this result with approximately 0.8% variation in dynamic pressure across 90% of the test section. It should be noted that the calculations shown were all performed prior to the wind-tunnel test. The experimental results were quite accurately predicted in all of the cases examined.

The slight asymmetry in the measured dynamic pressure was found to be due to a misalignment of the inlet relative to the tunnel centerline amounting to approximately 1°. When the misalignment is included in the analysis (referred to as splay distribution J) the calculated results are in much better agreement with the experimental data (fig. 53). Splay distribution J was generated by rotating each of the vanes so that they are in the same orientation relative to the wind-tunnel centerline as in the experiment. As a separate check, the 1° shift was also made to the experimental splay distribution and the results are plotted along with the splay "I" calculation in figure 54. The agreement in this case is also very good showing the sensitivity of both the analysis method and the inlet cascade to small changes in the splay distribution.

The effectiveness of the inlet cascade in improving the test-section flow uniformity of a poorly performing inlet is demonstrated in figure 55. The experimentally measured dynamic pressure distributions for the inlet without the cascade and with the cascade adjusted to splay distribution "J" are shown in the figure. In this particular example the dynamic pressure nonuniformity was reduced from approximately 7% to 1% over the center 80% of the test-section width. Further improvement could be achieved by refining the splay distribution and possibly by increasing the chord to gap ratio of the cascade to gain tighter control of the inlet flow distribution.

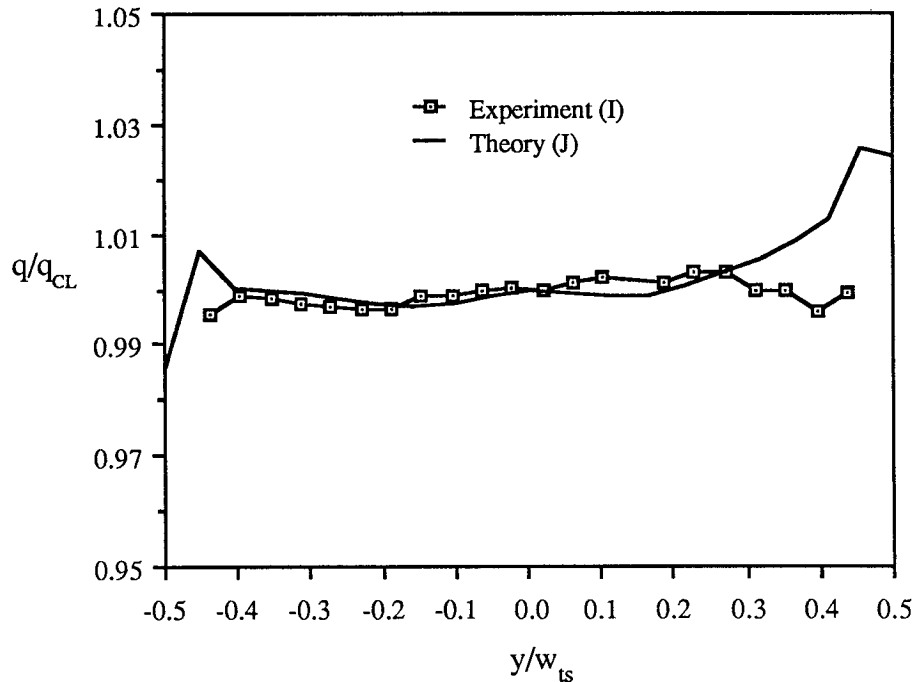


Figure 53. Comparison of the calculated and measured test-section dynamic pressure distributions with a 1° shift in the theoretical splay distribution

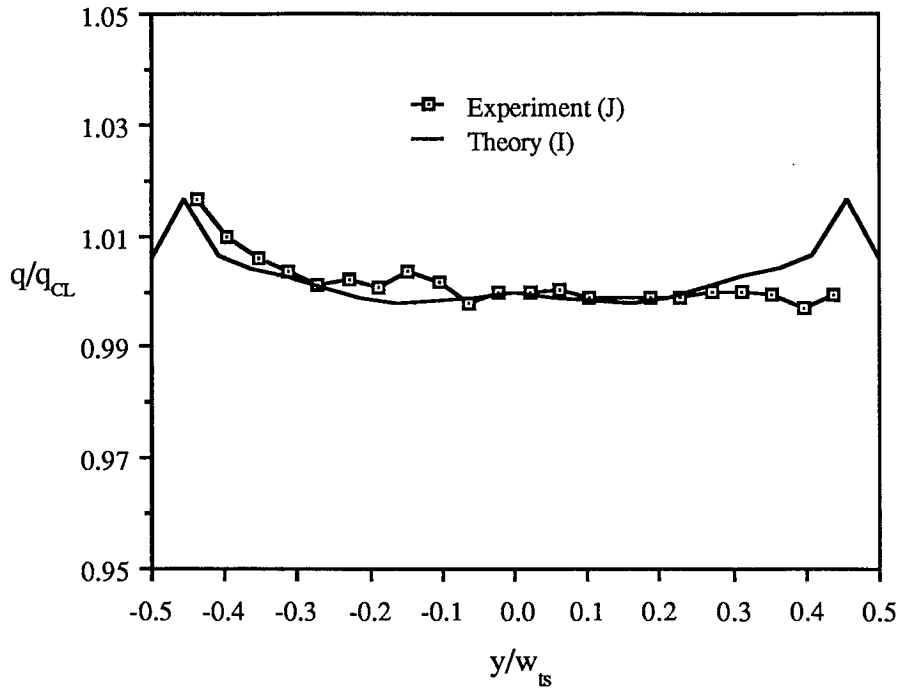


Figure 54. Comparison of the calculated and measured test-section dynamic pressure distributions with a 1° shift in the experimental splay distribution

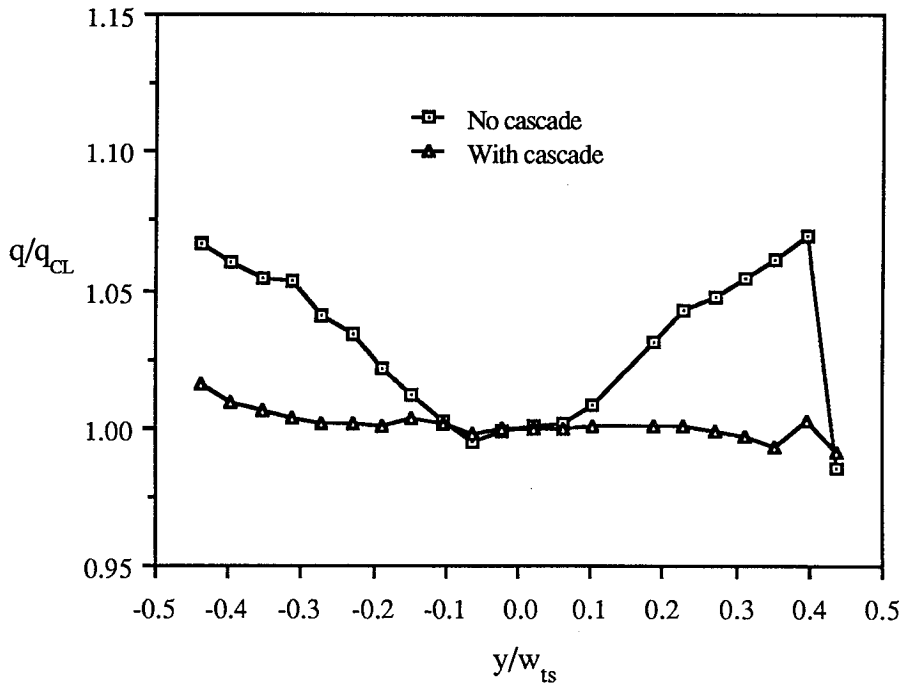


Figure 55. Improvement of the test-section dynamic pressure distribution by a properly tailored inlet cascade

Extension to Three-Dimensions

The analyses and experimental data presented so far are for a 2-D, idealized wind tunnel. Real wind tunnels, however, are almost always 3-D. The present cascade analysis can accurately predict the performance of a 3-D inlet when a rather simple correction is made to the calculated velocity distribution at the screen. This correction procedure is presented in reference 4 (Appendix B). In that report a 1/15-scale model of the 80- by 120- Foot Wind Tunnel at NASA Ames Research Center was modelled in the analysis as a simple horizontal cut through the tunnel. In choosing this representation, the horizontal contraction of the inlet is included in the analysis but the contraction in the vertical direction is ignored. Therefore, for a given test-section velocity, the calculated 2-D velocity at the screen location is higher than the actual value. If the predicted velocities are scaled by the ratio of the 2-D contraction ratio to the full 3-D contraction ratio, the predicted test-section dynamic pressure distribution is in good agreement with the measured distribution as shown in figure 56. The measurements shown were made along the mid-height of the test section.

A description of the inlet design selected for the 80- by 120-Foot Wind Tunnel is given in Appendix B. In this design, the inlet cascade is incorporated into a large honeycomb located at the front of the inlet. The vanes in the cascade are the vertical surfaces in the honeycomb and horizontal plates placed between the vanes at 22 levels complete the honeycomb. A screen with a loss coefficient of 1.7 is attached to the trailing edges of the vanes. The large honeycomb/screen combination is effective in preventing large, atmospheric turbulent structures from influencing the test-section flow. By properly tailoring the vane splay distribution the test-section flow can be made uniform. The application of this technology allowed the wind tunnel to achieve the desired flow quality with an inlet which is much smaller than would be required using a more conventional approach.

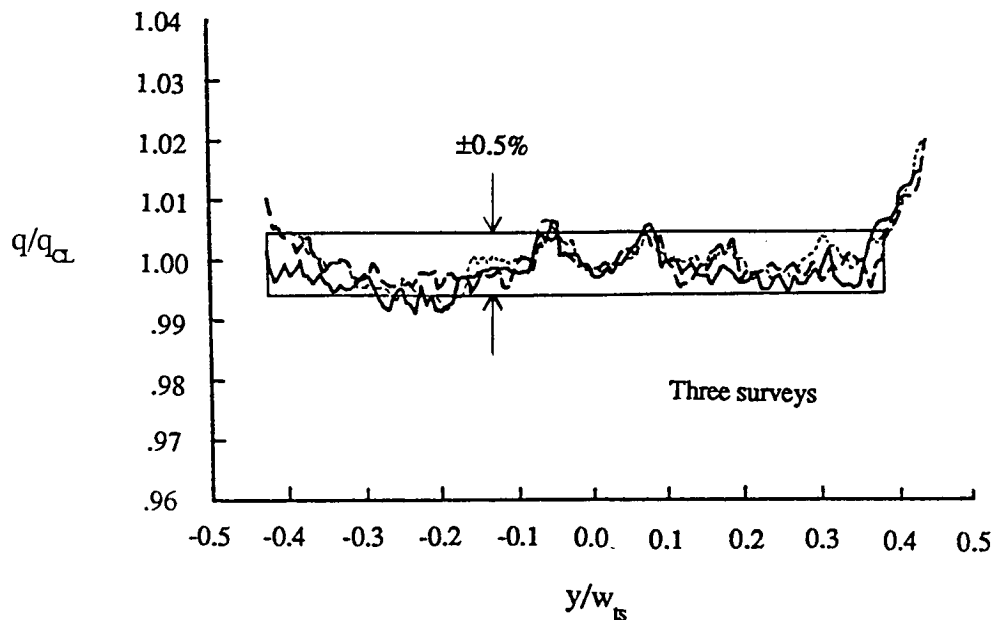


Figure 56. Dynamic pressure distribution in the test-section of a 1/15-scale model of the 80- by 120- Foot Wind Tunnel across the mid-height of the test section

CHAPTER 6. CONCLUDING REMARKS

The design of indraft wind tunnels is a complex task in that the inlet must perform several simultaneously, some of which interfere with one another. The contraction of the inlet accelerates the air to the test-section velocity allowing the anti-turbulence treatment to be placed in a region of relatively low velocity. Anti-turbulence devices include screens and honeycombs and can effectively isolate the test section from the effects of unsteady external flow conditions. A properly designed honeycomb/screen combination can provide acceptable levels of test-section turbulence and flow steadiness. This particular design problem has been adequately addressed in the literature. The interaction of the inlet geometry and the pressure drop induced by screens and honeycombs can cause the test-section flow to be nonuniform, particularly if the inlet has a low contraction ratio (less than about 8) and a short length to width ratio (less than 2). The objective of the present study was to investigate the fluid dynamics of an inlet with screens with the goal of developing an inlet design method for small inlets.

Before a design method could be developed, it was necessary to gain a better understanding of the flow through a screen located in an inlet. An experimental study was conducted to obtain information about the effect of screens on the flow uniformity for a short, low contraction ratio inlet. The experimental results indicate that the drag of the screen does not affect the flow distribution in the inlet directly. It was therefore not possible to generate uniform flow by simply adding more screens in the inlet. While the information obtained from these experiments did not provide a detailed picture of the flow mechanisms involved, it did generate an extensive data set which was useful in validating the computational methods developed.

The computational method uses the stream function, vorticity formulation of the incompressible Euler equation. In this analysis, the screen is modeled as an actuator disk with the pressure drop determined by an empirical formula. The screen analysis method can accurately calculate the test-section dynamic pressure distribution generated by screens in the inlet. The calculated distributions are in good agreement with the experimental data. Insight into the fluid dynamics of the overall flow field was also gained. In particular, it was found that the primary factor determining the distribution of the flow passing through a screen is the turning of the flow by the screen when the onset angle differs from the screen normal. Parametric geometry variations were performed which showed that uniform flow can be achieved if the screens are located appropriately in a constant-width duct upstream of the contracting section of the inlet. This approach has been used in several wind tunnels to date (e.g., refs. 5, 30). These designs were arrived at through experimentation rather than by analysis. The present analysis could be used to analyze this type of inlet design and eliminate a large amount of iterative experimentation.

The effectiveness of a variable loss coefficient screen in providing uniform test-section flow was examined. A technique was developed by which the the required loss coefficient distribution is found which includes the flow redistribution caused by the screen in the calculation. The loss distribution thus obtained was found to produce uniform test section flow. Unfortunately, the required loss coefficient near the sides of the inlet is too large to be practical for the inlet geometry examined (k_0 was as high as 70 in that region). Production of a continuously variable screen would also be impractical. Another calculation was made using a "stepped" loss distribution which could be produced by placing more layers of screen in the regions where a larger loss coefficient is called for. The resulting flow distribution was very nonuniform with the steps in loss coefficient plainly visible in the predicted dynamic pressure distributions. For the inlet geometry studied the graded screen approach is not feasible, however it may be useful for geometries which have smaller velocity gradients than the inlet of the present study.

The most promising concept for a small inlet providing uniform test-section flow is the addition of an inlet cascade. The idea is that a properly tailored cascade placed in the inlet is used to redistribute the flow passing through the screen. When properly designed, the pressure drop through the screen can be made constant across the width of the inlet, thus providing uniform test-section dynamic pressure. An analysis method was developed based on a 2-D panel code and an empirical pressure drop analysis. The method was used to determine the angle for each vane in a cascade, located just upstream of a screen, required to produce uniform-test section flow. An experiment that was performed using several vane splay angle distributions which had been examined computationally showed that the experimentally measured dynamic pressure distributions were accurately predicted by the computations. The analysis proved sensitive enough to determine the source of a slight asymmetry in the experimentally measured test-section dynamic pressure distributions. The asymmetry was found to be due to a 1° misalignment of the inlet with respect to the axis of the wind tunnel. The ability of the inlet cascade to produce any desired test-section flow distribution (within reason) makes it a good choice in the design of indraft wind tunnels.

A simple scaling of the velocities predicted by the 2-D panel code at the screen location was subsequently used to extend the analysis to 3-D. The scaling was introduced to account for the lack of contraction in the third dimension in the analysis. Including the correction in the analysis allowed the accurate prediction of the horizontal dynamic pressure distribution at the vertical centerline of a 1/15-scale model of the 80- by 120-Foot Wind Tunnel at NASA Ames Research Center. The analysis method was used to design the inlet for the full-scale facility (ref. 4). The inlet was found to produce sufficient isolation from external winds while maintaining uniform test-section flow.

The analysis methods presented in the present study could be extended to 3-D which would allow a more detailed examination of the effects of external wind on inlet performance. In addition, the ground boundary layer could be modeled by a proper distribution of total pressure in the far field which is a problem that cannot be addressed using the present analysis method.

The computational methods and design concepts developed in the present study can also be used in the design and analysis of closed-return wind tunnels. Screens are often placed in the settling chamber of these tunnels to reduce the turbulence intensity in the test section. If the screens are placed too close to the start of the contraction, nonuniform test-section flow can be produced. The minimum space between the contraction and the nearest screen can be determined using the screen analysis presented here. Screens are also used in closed-return wind tunnels to prevent separation in wide-angle diffusers which are often located upstream of the settling chamber. Coupling the screen analysis with a boundary layer calculation could provide a useful tool in the analysis of this type of flow.

REFERENCES

1. Dryden, H. L., and I. H. Abbott: The Design of Low-Turbulence Wind Tunnels. NACA Report 940, 1948.
2. Mehta, R. D., and P. Bradshaw: Design Rules for Small, Low-Speed Wind Tunnels. *Aeronautical Journal*, 83, No. 805, Nov. 1979, pp. 443-449.
3. Mehta, R. D.: The Aerodynamic Design of Blower Tunnels with Wide-Angle Diffusers. *Progress in Aerospace Sciences*, 18, 1977, p. 59.
4. Ross, J. C., L. E. Olson, J. M. Van Aken, and L. Meyn: A Novel Design Concept for Indraft Wind-Tunnel Inlets with Application to the National Full-Scale Aerodynamics Complex. AIAA paper No. 86-00147. Reno, Nev., Jan. 1986, and NASA TM 88226, 1986.
5. Krishnaswamy, I. N., S. M. Ramachandra, and V. Krishnamoorthy: Design and Characteristics of the 14' x 9' Open Circuit Wind Tunnel. *Proceedings of the Seminar on Aeronautical Sciences*, NAL, Bangalore, India, 1961.
6. Kirk, J. A.: Experience with a V/STOL Tunnel. *J. Royal Aero. Soc.* 71, No. 681, Sept. 1967, pp. 606-622.
7. Batchelor, G. K.: *The Theory of Homogeneous Turbulence*. Cambridge, England: Cambridge University Press, 1970.
8. Tsien, H. S.: On the Design of the Contraction Cone for a Wind Tunnel. *J. Aero.Sci.*, 10, 1943, pp. 68-70.
9. Smith, R. J., and C. T. Wang: Contracting Cones Giving Uniform Throat Speeds. *J. Aero.Sci.*, 11, 1944, pp. 356-360.
10. Libby, P. A., and H. R. Reiss: The Design of Two-Dimensional Contraction Sections *Quarterly of Applied Math.*, 9, 1951, pp. 95-98.
11. Goldstein, S.: Notes on the Design of Converging Channels. Technical Report R. & M. No. 2643, March 1945.
12. Cheers, F.: Note on Wind-Tunnel Contractions. Technical Report R. & M. No. 2137, 1945.
13. Barger, R. L., and J. T. Bowen: A Generalized Theory for the Design of Contraction Cones and Other Low-Speed Ducts. NASA TN D-6962, 1972.
14. Rouse, H., and M. M. Hassan: Cavitation-Free Inlets and Contractions. *Mech. Eng.*, 71, No. 3, 1949, pp. 213-216.
15. Morel, T.: Comprehensive Design of Axisymmetric Wind Tunnel Contractions. ASME paper 75-FE-17. Minneapolis, Minn., May 1975.

16. Morel, T.: Design of Two-Dimensional Wind Tunnel Contractions. ASME paper 76-WA/FE-4. New York, N. Y., Dec. 1976.
17. Stratford, B. S.: The Prediction of Separation of the Turbulent Boundary Layer. *J.Fluid Mech.*, vol. 5, pt. 1, 1959, pp. 1-16.
18. Chmielewski, G. E.: Boundary-Layer Considerations in the Design of Aerodynamic Contractions. *J. Aircraft*, vol. 11, no. 5, August 1974, pp. 435-438.
19. Borger, G. G.: The Optimization of Wind Tunnel Contractions for the Subsonic Range (translation of "Optimierung von Windkanalduesen fur den Unterschallbereich"). Doctoral dissertation. Ruhr-Universitat, 1973. (Also NASA TT F-16899, March 1976.)
20. Mikhail, M. N.: Optimum Design of Wind Tunnel Contractions. *AIAA J.*, vol. 17, no. 5, May 1979, pp. 471-477.
21. Downie, J. H., R. Jordinson, and F. H. Barnes: On the Design of Three-Dimensional Wind Tunnel Contractions. *Aero.Quarterly*, vol. 88, no. 877, 1984, pp. 287-295.
22. Batill, S. M., and J. J. Hoffman: Aerodynamic Design of High Contraction Ratio, Subsonic Wind Tunnel Inlets. AIAA paper No. 84-0416. Reno, Nev., Jan. 1984.
23. Batill, S. M., M. J. Caylor, and J. J. Hoffman: An Experimental and Analytic Study of the Flow in Subsonic Wind Tunnel Inlets. AFWAL-TR-83-3109, Oct. 1983.
24. Hess, J. L., and A. M. O. Smith: Calculation of Potential Flow about Arbitrary Bodies. *Prog. Aero.Sci.*, vol. 8, 1967, pp. 1-138.
25. Olson, L. E., W. D. James, and P. R. McGowan: Theroretical and Experimental Study of the Drag of Single- and Multi-Element Airfoils. *J.Aircraft*, vol. 16, no. 7, 1979), pp. 462-469.
26. Maskew, B.: Program VSAERO - A Computer Program for Calculating the Non-Linear Aerodynamic Characteristics of Arbitrary Configurations. NASA CR-166476, 1982.
27. Kaul, U. K., J. C. Ross, and J. L. Jacock: A Numerical Simulation of the NFAC (National Full-Scale Aerodynamics Complex) Open Return Wind Tunnel Inlet Flow. AIAA paper No. 85-0437. Reno, Nev. Jan. 1985.
28. Emslie, K.: The VSTOL Test Facility. British Aircraft Corporation Report AX. 286, July, 1963.
29. Leef, C. R., and R. G. Hendry: Development of a Nonrecirculating Wind-Tunnel Configuration Insensitive to External Winds. *J. Aircraft*, vol. 6, no. 3, 1969, pp. 221-227.
30. Breunlin, D. C., and N. B. Sargent: Effect of Transient Winds on the Flow Quality of an Open-Circuit Wind-Tunnel Model. NASA TM X-2538, April 1972.
31. Mort, K. W., W. T. Eckert, and M. W. Kelly: The Steady-State Flow Quality of an Open Return Wind Tunnel Model. *Canadian Aero. Space J.* vol. 18, no. 9, 1972, pp. 285-289.

32. Eckert , W. T., and K. W. Mort: Earth Winds, Flow Quality, and the Minimum-Protection Inlet Treatment for the NASA Ames 80- by 120- Foot Wind Tunnel Nonreturn Circuit. NASA TM 78600, 1978.
33. Mueller, T. J.: Smoke Visualization of Subsonic and Supersonic Flows (The legacy of F. N. M. Brown). AFOSR Report No. TR-78-1262, 1978. (Notre Dame University Report No. UNDAS TN-3412-1, 1978.)
34. Horlock, J. H.: *Actuator Disk Theory*. London, England: McGraw-Hill International Book Company, 1978.
35. van Aken, J. M.: Experimental Investigation of Several Inlet Flow-Control Cascades for the NFAC 80- by 120-Foot Indraft Wind Tunnel. University of Kansas Center for Research, Inc. Report No. CRINC 6900-1, 1986.
36. van Aken, J. M., and N. M. Scheller: Experimental Investigation of Inlet Flow-Control Cascades for the NFAC 80- by 120-Foot Indraft Wind Tunnel. AIAA paper No. 88-0054, Reno, Nev., 1988.
37. Mehta, R. D.: Turbulent Flow through Screens. AIAA paper No. 84-0538. Reno, Nev., Jan. 1984.
38. Chaterjian, N. M.: The Numerical Simulation of Steady Transonic Rotational Flow using a Dual Potential Formulation. Ph.D. Dissertation, Stanford University, Stanford, California, 1984.
39. Chaderjian, N. M., and J. L. Steger: The Numerical Simulation of Steady Transonic Rotational Flow using a Dual Potential Formulation. AIAA paper No. 85-0368, Reno, Nev., Jan. 1985.
40. Collar, A. R.: The Effect of a Gauze on the Velocity Distribution in a Uniform Duct. RAE R.&M. 1867, Feb. 1939.
41. Derbunovich, G. I., A. S. Zemskaya, YE. U. Repik , and YU. P. Sosedko: Optimum Wire Screens for Control of Turbulence in Wind Tunnels. *Fluid Mechanics-Soviet Research*, vol. 10, no. 5, 1981, pp. 136-147.
42. Taylor, G. I., and G. K. Batchelor: The Effect of Wire Gauze on Small Disturbances in a Uniform Stream. *Quar.J.Mech.Appl. Math.* vol. 2, pt. 1, 1948, pp. 1-29.
43. Schubauer, G. B., W. G. Spangenberg, and P. S. Klebanoff: Aerodynamic Characteristics of Damping Screens. NACA TN 2001, 1950.
44. Wieghardt, K. E. G.: On the Resistance of Screens. *Aero.Quar.*, vol. 4, Feb. 1953, pp. 186-192.
45. Annand, W. J. D.: The Resistance to Airflow of Wire Gauzes. *J.Royal Aeronautical Society*, vol. 57, March 1953, pp. 141-146.
46. Anon.: Pressure Drop in Ducts across Round-Wire Gauzes Normal to the Flow. Engineering Sciences Data Unit Item No. 72009, 1972.

47. Reynolds, A. J.: Flow Deflection by Gauze Screens. *J.Mech.Eng. Sci.*, vol. 11, no. 3, Mar. 1969, pp. 290-295.
48. Laws, E. M., and J. L. Livesey: Flow through Screens. In *Annual Review of Fluid Mechanics*, vol. I. Ed. M. van Dyke, J. V. Wehausen, and J. L. Lumley. Palo Alto, Calif.: Annual Reviews, Inc., 1978, pp. 247-266.

APPENDIX A: DESCRIPTION OF DATA ACQUISITION SYSTEM

The data acquisition and reduction for the experiments was performed automatically during by a Zenith PC-100 microcomputer equipped with a MetraByte DASH-8 input/output card. A schematic of the overall system is shown in figure 57. The I/O card has eight analog inputs, a 4-bit digital input, and a 4-bit digital output. One of the analog inputs was used for the signal from the ± 1 psi pressure transducer. The pressure transducer signal was filtered and amplified by a Vishay signal conditioning amplifier. A Scanivalve™ scanning pressure switching device was used to measure the pressure at all of the ports on the model using a single transducer. During the tests the static pressure was measured at 20 points along one wall of the inlet and contraction and on all four walls in the test section. In addition 24 total pressures were measured across the test section using the rake shown in figure 6 of Chap. 2.

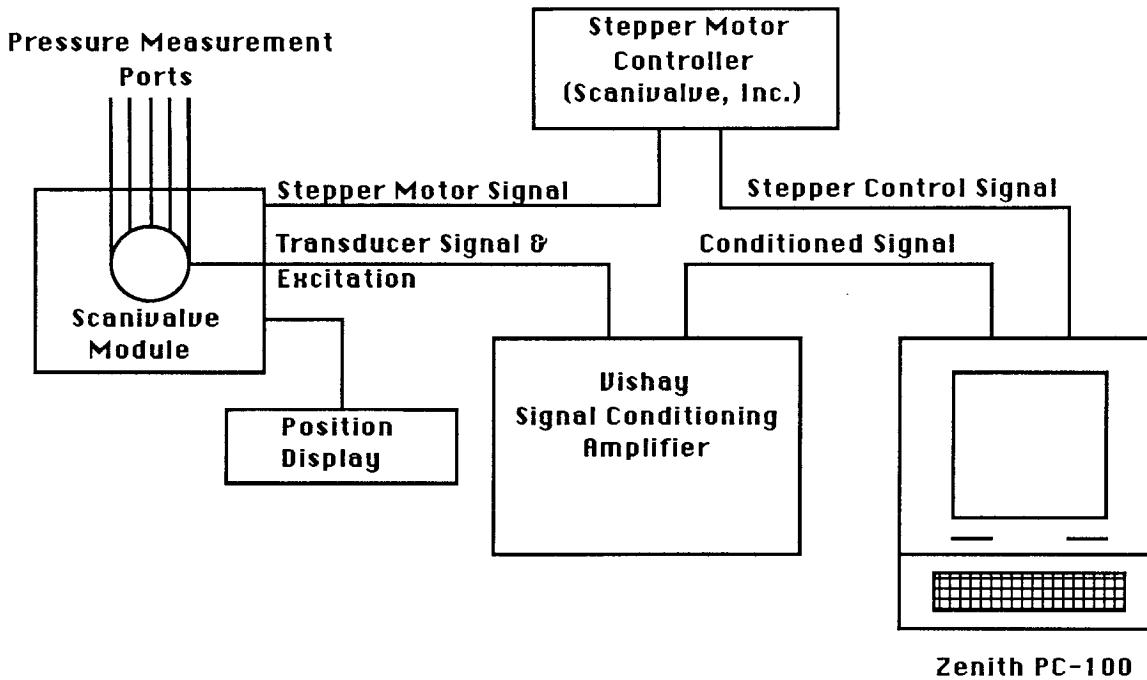


Figure 57. Schematic of data acquisition system

The data acquisition process is as follows. Upon initiation of a cycle, the computer reads a preset number of samples of the signal from the transducer through the A/D converter. These samples were averaged and the result stored. A command is then sent by the computer to the stepper motor controller to step the Scanivalve to the next port. This process was repeated until all of the desired pressure data were recorded. The first, 24th, and 48th ports all measured the test section static pressure. After a complete cycle, these three pressures are compared and if they differ by more than 1% the entire cycle of data is discarded. This is to assure that all the pressures were measured for the same test section conditions since a complete cycle through the 48 ports required approximately 5 min. A total of 200 samples were taken at every port to obtain a good average. The data were saved on disks for subsequent analysis and plotting.



Report Documentation Page

1. Report No. NASA TM-100050	2. Government Accession No.	3. Recipient's Catalog No.	
4. Title and Subtitle Theoretical and Experimental Study of Flow-Control Devices for Inlets of Indraft Wind Tunnels		5. Report Date September 1989	6. Performing Organization Code
		8. Performing Organization Report No. A-88040	
7. Author(s) James C. Ross		10. Work Unit No. 505-60-21	11. Contract or Grant No.
		13. Type of Report and Period Covered Technical Memorandum	
9. Performing Organization Name and Address Ames Research Center Moffett Field, CA 94035		14. Sponsoring Agency Code	
		12. Sponsoring Agency Name and Address National Aeronautics and Space Administration Washington, DC 20546-0001	
15. Supplementary Notes Point of Contact: James C. Ross, Ames Research Center, MS 247-2, Moffett Field, CA 94035 (415) 694-6722 or FTS 464-6722			
16. Abstract The design of closed-circuit wind tunnels has historically been performed using "rules of thumb" which have evolved over the years into a body of useful guidelines. The development of indraft wind tunnels, however, has not been as well documented. The design of indraft wind tunnels is therefore generally performed using a more intuitive approach, often resulting in a facility with disappointing flow quality. The primary problem is a lack of understanding of the flow in the inlet as it passes through the required antiturbulence treatment. For wind tunnels which employ large-contraction-ratio inlets, this lack of understanding is not serious since the relatively low velocity of the flow through the inlet treatment reduces the sensitivity to improper inlet design. When designing a small-contraction-ratio inlet, much more careful design is needed in order to reduce the flow distortions generated by the inlet treatment. As part of the National Full-Scale Aerodynamics Complex Modification Project, two-dimensional computational methods were developed which account for the effect of both inlet screens and guide vanes on the test-section velocity distribution. Comparisons with experimental data are presented which indicate that the methods accurately compute the flow distortions generated by a screen in a nonuniform velocity field. The use of inlet guide vanes to eliminate the screen-induced distortion is also demonstrated both computationally and experimentally. Extension of the results to three dimensions is demonstrated and a successful wind tunnel design is presented.			
17. Key Words (Suggested by Author(s)) Wind tunnel Wind tunnel inlet Inlet vanes Screens		18. Distribution Statement Unclassified-Unlimited Subject Category - 09	
19. Security Classif. (of this report) Unclassified	20. Security Classif. (of this page) Unclassified	21. No. of Pages 74	22. Price A04

